# Dynamic Simulation of Energy Management Control Functions in VAV-HVAC Systems

**Wen Zhen Huang**

**A Thesis**

**In**

**Department of Building, Civil & Environmental Engineering**

**Presented in Partial Fulfillment of the Requirements**

**For the Degree of Master of Applied Science at**

**Concordia University**

**Montreal, Quebec, Canada**

**November 2003**

*Your file Votre référence*
*ISBN: 0-612-91043-1*
*Our file Notre référence*
*ISBN: 0-612-91043-1*

# ABSTRACT

## Dynamic Simulation of Energy Management Control Functions in VAV-HVAC Systems

**Wen Zhen Huang**

Energy Management Control Systems (EMCS) in buildings can help reduce the energy consumption while maintaining satisfactory occupant environment. The energy management control strategies have to be developed taking into consideration the thermal behavior of buildings and the thermal, operational characteristics of mechanical systems in buildings.

In this thesis, improved EMC algorithms are developed and implemented in a variable air volume HVAC (VAV-HVAC) system. Firstly, HVAC system component dynamic models are developed. Then, several individual improved EMC functions (outdoor air economical cycle, programmed start time, programmed stop time, reset supply air temperature setpoint, occupied time control strategies) are developed and evaluated. Finally, real-time simulations are carried out, in which the results of implementing above improved EMC functions are compared with those of conventional EMC functions. This comparison reveals that the HVAC system with each independent improved function can save 7% to 12% energy. Simulation results also show that a

VAV-HVAC system employing all EMC algorithms can save between 14% to 15% energy during summer and winter operation. An optimization methodology to compute optimal setpoints is proposed. These optimal setpoints were used as tracking signals to PI and adaptive control strategies developed in this thesis. The use of optimal setpoints resulted in 17% energy savings.

A real-time supervisory EMC platform is developed in which the developed EMC algorithms are embedded. Simulation results showing the typical operation of a VAV-HVAC system under supervisory EMC system are presented.

# ACKNOWLEDGEMENTS

I would like to take this opportunity to express my sincere gratitude to my supervisor, Dr. M. Zaheer-uddin for his initiating this project, and his invaluable guidance, encouragement and suggestions in all phases of this research work. Also, I am thankful for financial assistance.

My thanks are also to the members of staff in Center for Building Studies for their collaboration, support, and help whenever I needed.

My thanks also go to my colleagues, for their helpful discussion and suggestions in my study.

I would like to dedicate this thesis to my husband Zhigang Tang and lovely son, Haowei Tang for their patience, encouragement, and moral support during my whole studies.

## Table of Contents

## List of Figures

## List of Tables

# Nomenclature

| | |
|---|---|
| $A$ | face air area ($m^2$) |
| $a_0$, $a_1$, $a_2$, $a_3$ | constant |
| $A_a$, $A_w$,$A_{hp}$, | coefficient |
| $A_{it}$ | inside area of tube per unit length(m) |
| $A_o$ | total area of coil per unit length (m) |
| $b_1$, $b_2$ | constant |
| $B_a$,$B_w$,$B_{hp}$ | coefficient |
| $c_{fin}$ | specific heat of fin(J/kg.K) |
| $C_i$ | thermal capacity of node i(J/K) |
| $c_{p,a}$ | specific heat of air at constant pressure(J/kg.K) |
| $c_t$ | specific heat of tube(J/kg.K) |
| $c_w$ | specific heat of water (J/kg.K) |
| $C_z$ | zone thermal capacity (J/K) |
| $E_{daily}$ | daily energy consumption (w) |
| $h_c$ | heat transfer coefficient between air and tube($W/m^2K$) |
| $h_{it}$ | heat transfer coefficient between water and tube($W/m^2K$) |
| $h_{lim}$ | high limit |
| $h_t$ | air-side heat transfer coefficient ($W/m^2K$) |
| $i$ | node or enthalpy (kj/kg) |
| $i_m$ | mixed air enthalpy (kj/kg) |
| $i_o$, $H_{out}$ | outdoor air enthalpy (kj/kg) |
| $i_s$ | supply air enthalpy(kj/kg) |
| $i_z$,$H_{in}$ | zone air enthalpy (kj/kg) |
| $k$ | variable coefficiency |
| $k_{ia}$, $k_{iw}$,$k_{ihp}$ | integral gain |
| $k_{pa}$, $k_{pw}$,$k_{php}$ | proportional gain |
| $L_c$ | length of cooling coil (m) |
| $l_{lim}$ | low limit |
| $M_a$ | mass flow rate of air (kg/s) |
| $M_{amax}$ | maximum mass flow rate of air (kg/s) |
| $m_{fin}$ | mass of fin material per unit length(kg/m) |
| $m_t$ | mass of tube material per unit length(kg/m) |
| $M_w$ | mass flow rate of water (kg/s) |
| $m_w$ | mass of water per unit length(kg/m) |
| $M_{wmax}$ | maximum mass flow rate of water (kg/s) |
| $P$ | fan pressure (kpa) |
| $P_{coil}$ | coil power (kw) |
| $P_{fan}$ | fan power (kw) |
| $P_{heatpump}$ | heat pump power (kw) |

| | |
|---|---|
| $Q$ | fan delivery air volume($m^3/s$) |
| $q_{c,s}$ | cooling coil sensible load (w) |
| $q_{env}$ | building envelop load (w) |
| $q_{int}$ | zone internal gain (w) |
| $q_s$, $q_{sei}$ | zone sensible load/ non-ventilation sensible load (w) |
| $q_{s,max}$, $q_{s,peak}$ | maximum zone sensible load (w) |
| $q_{s,oa}$ | outdoor air sensible load (w) |
| $q_{sol}$ | solar heat gain (w) |
| $q_{s,s}$ | system sensible load (w) |
| $q_t$ | zone total load (w) |
| $R_{i,j}$ | thermal resistance($m^2/w$) |
| $T$ | time(s) or temperature(℃) |
| $T_{a,s}$, $t_{a,s}$, $t_s$, $t_a$ | supply air temperature(℃) |
| $T_{aset}$, $t_{aset}$ | supply air temperature setpoint(℃) |
| $t_h$ | high time value(h) |
| $T_h$ | expected maximum value (℃) |
| $t_l$ | low time value(h) |
| $T_l$ | expected minimum value (℃) |
| $T_m$, $t_m$ | mixing air temperature (℃) |
| $T_o$, $T_{out}$, $t_o$, $t_{oa}$ | outdoor air temperature (℃) |
| $t_{o,mean}$ | mean outdoor air(℃) |
| $T_{start}$ | start-lead-time (s) |
| $T_{stop}$ | stop-lead-time (s) |
| $T_t$,$T_{ta}$, tta | tube temperature(℃) |
| $T_w$ | average water temperature (℃) |
| $T_{wr}$,$t_{wr}$ | return water temperature(℃) |
| $T_{ws}$,$t_{ws}$ | supply water temperature(℃) |
| $T_{wset}$, $t_{wset}$ | supply water temperature setpoint (℃) |
| $T_z$,$t_z$,Tin | zone air temperature(℃) |
| $t_{zf}$ | final zone temperature (℃) |
| $t_{zin}$ | initial zone temperature (℃) |
| $T_{zset}$, $t_{zse}$, $t_{z,set}$ | zone temperature setpoint (℃) |
| $U_{fan}$ | fan motor input (w) |
| $u_{hp}$ | output of heat pump's controller |
| $U_{hpmax}$ | heat pump maximum input |
| $u_{sa}$ | output of damper's controller |
| $u_{sw}$ | output of valve's controller |
| $v_m$ | medium value |
| $V_z$ | zone volume ($m^3$) |
| x, $x_v$, ra | outdoor air ratio |
| $\alpha_z$ | heat loss factor of zone |

# Abbreviations

| | |
|---|---|
| AHU | Air Handling Unit |
| ASAT | alternative supply air temperature strategy |
| BC | base case |
| BFGS | Broyden Fletcher Goldfarb Shanno |
| COAR | constant outdoor air ratio |
| COP | coefficient of performance |
| $COP_{max}$ | maximum coefficient of performance |
| CSATS | constant supply air temperature strategy |
| DEC | daily energy consumption (W) |
| EB | energy balance |
| EBEC | enthalpy-based-economy cycle |
| EMC | energy management control |
| EMCS | energy management control system |
| ENC | enthalpy cycle subroutine |
| ETC | equivalent thermal capacity |
| ISATS | improved supply air temperature strategy |
| LSATS | linear supply air temperature strategy |
| NC | night cycle subroutine |
| OA | outdoor air or outdoor air ratio |
| $OA_{min}$ | minimum outdoor air ratio |
| OAR | outdoor air ratio |
| OC | on-off control |
| OPC | occupied time cycle |
| PBC | proportional band control |
| PI | proportional –plus-integral |
| RA | return air |
| RWT | return water temperature (℃) |
| SA | supply air |
| SAT | supply air temperature (℃) |
| SNC | summer night cycle |
| SPC | stop time cycle |
| STC | start time cycle |
| SWT | supply water temperature (℃) |
| TBEC | temperature-based-economy cycle |
| VOAR | variable outdoor air ratio |
| WNC | winter night cycle |

# Greek letters

| | |
|---|---|
| $\alpha$ | coefficient |
| $\gamma$ | ratio of specific heats $C_p/C_v$ |
| $\eta$ | fan efficiency |
| $\eta_s$ | efficiency of fins in sensible heat transfer |
| $\eta_{s,ov}$ | overall efficiency of fins in sensible heat transfer |
| $\rho_a$ | density of air ($kg/m^3$) |
| $\rho_w$ | density of water ($kg/m^3$) |

# Chapter 1 Introduction

## 1.1 Introduction

Dynamic models of HVAC systems and components describe the thermal, hydraulic, environmental and mechanical characteristics. They are the basis for practical applications in testing, commissioning and evaluating HVAC systems' operating features, control strategies, control program implementation and energy performance in energy management control systems (EMCS).

Numerous publications have emphasized on dynamic modeling and simulation of HVAC systems. Zaheer-uddin and Zheng (1994b) developed a system-level transient model of a two-zone VAV system. There are computer software packages available such as TRNSYS, DOE-2, BLAST, HVACSIM$^+$, EnergyPlus, etc., which are useful to simulate HVAC systems.

Energy Management Control Systems (EMCS) in North America are also known as Building Energy Management Systems (BEMS) in Europe. In buildings, it is reported, that HVAC systems consumed around 50% of total building energy [Payne 1984]. Therefore, HVAC systems if properly operated, tend to offer the most energy saving opportunities. EMCS can help improve the energy efficiency of HVAC systems in buildings and maintain good thermal environment. This can be achieved by incorporating several improved EMC functions and performing real-time adjustments to the HVAC systems.

Many different types of EMC systems from comprehensive and integrated devices to independent local controllers are feasible. Generally, there are some common strategies used to reduce energy consumption in buildings. There are: programmed start/stop; optimal start/stop; duty cycling; load reset; electric demand limiting; adaptive control; chiller optimization; boiler optimization; optimal energy sourcing, etc. [Payne 1984].

Most published papers have focused on implementing one EMC function each time with optimal control algorithms; however, these studies have paid little attention to integrating several individual EMC functions into one system. Zaheer-uddin et al. (2001) and Wang (1999) demonstrated implementation of three EMC functions such as the system pressure reset, supply air temperature (SAT), and outdoor air (OA) volume control in the operation of HVAC systems.

The advanced optimization and control techniques published in the literature are useful research based methods. However, they are too complex and their reliability is not very well proven for implementation on existing commercially available EMC systems installed in most modern buildings. Another observation concerning the existing EMC systems reveals that they are mostly heuristic and use empirical methods. Although they are simple for real time implementation, their effectiveness in achieving energy efficiency is not verified. These observations point out to the need for systematically examining the existing energy management control functions and improving them wherever feasible. This is the motivating factor in understanding this research work. The improvements undertaken in this thesis are by no means optimal. A guideline was adapted in the analysis

and development of improved EMC functions that is to keep their structure simple and compatible with the existing EMC functions so that future implementation is easy and realizable.

To this end, the following methodology is used to analyze and develop EMC functions. First, a dynamic model of a VAV-HVAC system is developed with a view to use it as a simulation platform for assessing the performance of EMC functions. Second, individual energy management functions are critically analyzed and improved versions are proposed. Finally, these EMC functions were implemented in VAV-HVAC system model and simulation runs were made to assess their operating performance. Therefore the specific objectives of this thesis based on the above stated goals are summarized in the following.

The thesis is organized as follows. A study of literature is conducted in chapter 2. A single zone VAV-HVAC system model useful for simulating the operation of EMC functions is developed in chapter 3. The individual EMC functions are very important in the overall performance of the HVAC system. Many researchers have evaluated system energy consumption utilizing outdoor air (OA) economizer cycle strategy in on-off control mode or proportional only control or proportional integral (PI) control. Although PI control can obtain good result, selecting control parameters may be complex. In this thesis several different OA economizer strategies based on full component models are developed in chapter 4. An equivalent thermal capacity method used to develop start/stop-lead-time technique is demonstrated in chapter 5. In chapter 6, two supply air

temperature (SAT) reset schemes based on predictive OA temperature and room load are demonstrated, and compared with other normal schemes. In addition, the single-zone VAV system simulation is implemented using three closed-loops (dampers, valve and heat-pump) by two control strategies PI and adaptive control during occupied time. The individual EMC functions are integrated in a real-time system. Flowcharts describing the overall EMC system are presented in chapter 7. Finally, the conclusions are summarized in chapter 8.

## 1.2 Objectives

This thesis will focus on the development and application of EMC functions in a single-zone VAV system in an office building. The main objectives are:

1. To develop, adapt and modify if necessary the appropriate HVAC system component models and build an overall dynamic model of a VAV system.
2. To analyze and develop individual energy management control (EMC) functions. These are:
   - i) Temperature based economy cycle
   - ii) Enthalpy based economy cycle
   - iii) Programmed start/stop algorithms
   - iv) Predictive supply air temperature reset algorithm
   - v) Occupied period control strategies
     --PI control strategy
     --Adaptive control strategy.
3. To implement these EMC functions in a VAV system used in an office building

and assess their individual performance;

4. To determine optimal setpoints for the VAV system using steady state optimization method.
5. To implement all EMC functions developed in this thesis in a VAV-HVAC system and assess overall operating performance of the system and EMC functions during typical daily operation.
6. To develop a $C^{++}$ program incorporating all the EMC functions and test to verify its simulated real-time operation.

## 1.3 Contributions

The contributions of this thesis are mainly in the area of analysis and development of several energy management control functions. Some specific contributions are:

1. Development of improved EMC functions by incorporating such features as predictive techniques to enhance their performance.
2. Developed a steady state optimization technique to compute optimal setpoints for the VAV system operation.
3. Proposed an adaptive control algorithm for regulating the HVAC thermal process.
4. Development of a $C^{++}$ program in which all EMC functions are embedded. This $C^{++}$ program is intended as a part of development effort in building a real-time stand-alone energy management control system.

# Chapter 2 Literature review

## 2.1 Introduction

Methods for reducing energy consumption in buildings and improving indoor environment have been studied by several researchers since the energy crisis of 1970s. The published papers in this area appropriate to the present study have been reviewed in this chapter.

Accordingly, this literature review is grouped in three parts. In section 2, component and system models are reviewed. Energy Management Control (EMC) algorithms are examined in section 3 and EMC simulation and control strategies are reviewed in section 4.

## 2.2 Modeling

Many researchers have studied, developed, and perfected dynamic models of HVAC systems during last four decades. Generally, HVAC system models can be grouped in two classes: steady state models and transient models; each of them contains both empirical and theoretical models.

Empirical models employed the concept of "black box" either based on physical laws or ignoring physical laws (Yuill and Wray 1990). One major function of the empirical models is that they can forecast the equipment performance in the particular

circumstances such as the operating environments and within the available range of the test data, in which the models could be derived. Another goal is that their simplicities make them suitable in adaptive control modeling. However, any changes, for example, the performance outside the test data, or for the similar equipment operating in different environment, can result the models unsuitable.

In contrast, theoretical models are based on fundamental physical laws, which are general principles of thermodynamics, heat, mass and momentum. Energy, momentum and mass balance equations describing the thermal process in HVAC systems are used to predict the variation in temperature, pressure, and fluid flow rates. Therefore, these models are suitable to predict the equipment performance within wide range of operating conditions.

In addition, steady state model analyze the system stability while neglecting the influence of the transient variables. The dynamic models reflect the transient responses, which are useful to investigate the system operational features and to explore control strategies.

### 2.2.1 Component models

HVAC system components models include cooling/heating source models such as chiller/boiler model, cooling/heating coil model, duct & fan model, and zone model. Properly integrated these models can simulate the overall performance of different HVAC system configurations.

#### 2.2.1.1 Coil model

Cooling coil is a key element of most HVAC systems because it is the core component which is connected to the primary plant (chiller or heat pump) and the secondary air distribution systems. Furthermore, its dynamic characteristics are the most influential in air system and space thermal performance. Therefore, many researchers have studied its dynamic performance. A steady-state model of cooling and dehumidifying coil was developed by Khan (1994), in which he employed NTU method. He also estimated the performance of the cooling coil under partial load conditions by using his model.

Most dynamic models used differential equations to describe the characteristics of coil. For example, Elmahdy (1975) developed transient models of cooling and dehumidifying coil by treating the air, water, and tube temperature and humidity ratio as dependent variables of the time and space, but he only studied the static performance of the coil.

Zaheer-uddin and Zheng (1994b) developed a dynamic model of a cooling and dehumidifying coil. The model developed was based on a typical counter-cross-flow coil with continuous plate-fins on tube. They treated the heat transfer coefficients on air-side and water-side as a function of temperature and flow field characteristics. The coil efficiencies are variable; consequently, the models are particularly suitable to analyze the performance of the variable air volume and water flow rate systems.

### 2.2.1.2 Chiller and storage tank model

In most of cooling systems, chillers are required to provide chilled water to the cooling coil, in which heat and mass exchange occurs between water and air. Accordingly, cooling towers are needed to reject heat from the condenser of a chiller to the ambient environment. Typically, the cooling resource system composes chillers, cooling towers and cold-water pumps and chilled water pumps as well as distribution and connection piping. Wong and Wang (1989) presented a simple transient model to describe the characteristics of the evaporator and condenser. Also, they illustrated that the static operating feature of the chiller like temperature, pressure, fluid flow, heat transfer, and power inputs were impacted by operating factors.

Zaheer-uddin and Goh (1991) developed a heat pump and storage tank model based on heat balance principles. It described the situation of the heating case, and is very useful in analyzing the performance of heating system. Also, it is the basis to develop cooling system model.

### 2.2.1.3 Zone model

Zone model is used to represent the thermal behavior of the buildings, so it is another important component model of building-HVAC systems. Basically, These models are based on energy balance principle.

Zaheer-uddin (1986) developed and validated a detailed model of a single zone and subsequently modified to take into account the latent loads. Later, Goh (1990) derived a simple sensible load equation representing the dynamic characteristics of a zone, which

used the concept of equivalent thermal capacity of building envelope.

On the other hand, Athienitis (1994) modeled the room with resistance-capacitance (RC) elements, described the heat transfer between building shell and space air by thermal network method, and coupled the effect of solar radiation with radiant, conductive, and convective heat transfer in detail. He built a set of energy balance equations at each node, solved them using explicit finite difference method in MathCAD program. A typical energy balance equation is applied for each node as follows:

$$T_{i,p+1} = \frac{\Delta t}{C_i}(q_i + \sum_j \frac{T_{j,p} - T_{i,p}}{R_{i,j}}) + T_{i,p}$$

Where subscript i indicate the node for which energy balance is written and j for all nodes connected to node i, while p is the time interval; $q_i$ represents a heat sources at node i such as solar radiation. T, C, R represents temperature, thermal capacity and thermal resistance respectively. The critical time step (t) is selected based on the following condition for numerical stability (Holman 1986).

$$\Delta t \leq \min(\frac{C_i}{\sum_j \frac{1}{R_{i,j}}})$$

### 2.2.1.4. Ductwork and fan model

Grot and Harrje (1981) developed a ductwork model by neglecting the storage effects and axial wall conduction but assuming forced convection as the main heat transfer mechanism. Pinnella (1986) illustrated a motor model representing the torque

balance on the axis of the motor by assuming the fan operating in steady state.

### 2.2.2 Overall models

Component models individually describe the thermal behavior, while, from the point of view of the system, the interaction occurring between them should be taken into account. A system-level model is required to include a complete set of HVAC component models and the dynamic model of the building.

Stoecker (1976) evaluated the steady state operating performance of an HVAC system by modeling the system with polynomial expressions, and he showed how the coefficients of the polynomials can be extracted using the experimental on-site data.

Mehta (1984) presented a dynamic model by coupling the HVAC system and the heating/cooling loads, and this method had been successfully validated through experiment by Metha and Wood (1980).

The two most popular building energy simulation programs such as DOE-2 (1981), BLAST (1979) and the newest program EnergyPlus adapted from the former two programs can calculate the hourly energy consumption and energy cost of a commercial or residential building given information about the climate, building's construction, operation, utility rate schedule and HVAC equipment, as well as may be suitable to simulate the quasi-dynamic-type operation of building systems for designing large buildings, but they didn't take the control strategies into account.

The TRANSYS (Klein et al 1983) program primarily applied in simulating solar

energy systems. It has a modular structure that allows the interconnection among system components in any desired manner, iterates by substitution to solve the system equations about component models and their interconnections. The newest version of TRANSYS is capable of involving heating/cooling plants after undergoing many revisions.

The HVACSIM$^{+}$(Clark et al. 1985) program is a research tool to study the dynamic interactions among the building, HVAC and control systems. It solves the system equations by advanced nonlinear equation solution techniques and also uses a modular method, similar to the one adapted in TRNSYS.

However, those programs were used to simulate the different building (dynamic) and system configurations (steady state, or quasi-dynamic) and to study the influence of building and system operation on energy consumption. They are not intended and therefore not suitable in the analysis and design of HVAC control system.

Zheng (1997) presented a dynamic system-level model of a multi-zone VAV system using both bottom-up and top-down methods. The model developed is very useful to study the interaction between the building heating/cooling load, VAV system, and control system with multi variables such as air flow rate, water flow rate and system pressure, and several setpoints, as well as to simulate the performance of various energy management and control strategies.

## 2.3 EMC algorithms

Generally, Energy Management Control Systems (EMCS) are classified in four level architectures, and they can achieve several functions, whose major objectives are that reasonable energy can be effectively utilized without sacrificing the occupant comfort environment as well as systems can be conveniently operated and maintained. This literature survey focuses on outdoor air (OA) economizer cycle, optimum start-stop, duty cycle control, night cycle and night purge (night ventilation), and load reset strategies.

### 2.3.1 OA economizer cycle

OA economy cycle is widely used to save energy in HVAC systems, when the external climatic conditions and interior environment strongly favour its application. Basically, an economy cycle involves bringing proper OA to satisfy all or a portion of the building's cooling requirements in order to use "free" cooling when the OA temperature (enthalpy) is less than that of the return air from the space. Generally, there are two types of economy cycles, namely, temperature-based economizer cycle (TBEC) and enthalpy-based economizer cycle (EBEC).

The utilization of TBEC can be a cost-effective energy conservation measure, relying on the climatic conditions and the type of mechanical systems. When OA temperature falls down below the design supply temperature, cooler OA is then drawn into the system and used to reduce space temperature. An EBEC is similar to a TBEC, except it measures total heat content of air. OA is used for cooling when its enthalpy is

less than that of the return air.

Earlier papers on this subject included comparison of economizer control and ensuring energy savings. For example, Spitler et al. (1987) reported the potential energy savings for two prototypical buildings in five locations, which represented typical climatic conditions, using TBEC and EBEC. The simulation was done using BLAST program. They recommended TBEC, which had potential energy savings up to 30% in most climates possibly except of hot, humid climate. Also, they offered the guidelines for the use of TBEC or EBEC. However, their study didn't discuss the implementation of TBEC/EBEC in real systems.

In the last 10 years, researchers have paid close attention to air distribution system arrangements and dampers' control strategies in bringing outdoor air in buildings. Avery (1986) presented the interaction among four control loops, such as pressure loop, temperature loop and mass flow loop, and their influence on the stability and economy of the system depending on different arrangement of supply air, return air and relief air system. He estimated 4.25% energy savings by using relief fan instead of return fan. His analysis didn't cover the OA mass flow rate as a function of the outdoor and indoor conditions.

Elovitz (1995) analyzed six existing approaches to achieve minimum OA control in VAV systems based on the pressure distribution in the ductwork. The author stated variety of strategies could be used to maintain the desired minimum OA amount by designers, but particular attention should be paid to keep the proper pressure relationships among

OA, supply air and recirculated air in the application. However, energy consumption and OA economizer cycle weren't addressed in his investigation.

Seem et al. (1998) demonstrated a new volume matching control method to control the return fan, which linked the position of the recirculation air damper and the exhaust air damper, but OA damper fully opened during occupied time. They stated that this new method could prevent air from entering AHUs through the exhaust air outlet using simulation, laboratory, and field results. In contrast, they argued that in the traditional method, in which OA, recirculated and relief dampers are coupled, may cause poor performance. However, the study didn't address the prediction OA flow rate and energy consumption.

Most recently, Krakow et al. (2000) demonstrated control strategies concerning OA, supply and return dampers by analytical and experimental investigations, pointed out that economizers with linear dampers required less power and less fan speed variation than that with nonlinear dampers; the strategy of coupling OA and recirculated dampers with supply damper fully open during operation consumed slightly less fan power than the strategy involving coupling between all three dampers.

Moreover, OA airflow rate control strategies have been studied by several researchers. Janu et al. (1995a, 1995b) presented an online outdoor airflow measurement and control strategy. They treated carbon dioxide ($CO_2$) as a feedback tracer gas signal and developed a novel method to measure OA flow rate based on tracer gas concentration balance. Further, the control strategy that integrated multiple requirements for providing

OA (ensuring adequate ventilation, meeting space pressurization requirements, and satisfying economizer control) was described in their report. Nevertheless, energy consumption analysis weren't addressed.

Ke et al. (1997a) demonstrated the simulation results and analysis of utilizing eight ventilation control strategies in VAV systems of multiple space in a college library; the research involved the indoor air quality (IAQ) and annual energy consumption by introducing GMSE conception (generalized multiple spaces equation) to correct the ratio of OA to the total primary supply air. They pointed out that no control strategies could satisfy the OA requirements without tempering at the terminal boxes. They pointed out that the method of fixed OA percentage had the worst IAQ; and fixed minimum OA rate strategy consumed the most energy. The most economical control and better IAQ was achieved in the strategy which employed both optimized reset supply air temperature (SAT) and supply airflow rate.

Rock et al. (1998) presented the performance of four ventilation schemes for a typical small office building with a single-zone constant-air-volume (CAV) HVAC system in ten U.S. cities. The simulation results of energy consumption and cost displayed that the difference between fixed OA rate, temperature-based economizer, enthalpy-based economizer and artificial neural network (ANN) demand-controlled ventilation (DCV) were insignificant. The selection among these strategies wasn't clear because the decision strongly depended on the climate, economic and building type and use. The limitation was that these research could be quite different when applied to VAV

systems.

Brandemuehl et al. (1999) investigated the energy use associated with different combinations of demand-controlled ventilation and economizer strategies in CAV system for four different types of building. They pointed out that the savings in heating could be more significant than that in cooling. Significantly greater savings were possible for the buildings with large variability in occupancy and high internal gains. However, for the office buildings, the savings were not obvious since the occupancy and internal gains were almost fixed.

### 2.3.2 Start/stop strategies

Optimum start and stop is one of the most commonly used EMC function. In most buildings, several zones/spaces are not occupied 24-hour-a-day; therefore, determining the start/stop time is the most important function for both saving energy and satisfying comfort conditions. Traditionally, the system is operated on a fixed schedule independent of the weather and zone conditions. The system is restarted prior to occupancy to cool down the space by the first person to arrive. On the other hand, the optimized start/stop function of the system automatically starts and stops the system to minimize the energy required to provide the desired environmental conditions during occupied hours. The function automatically estimates the thermal inertia of the structure, the capacity of the system to either increase or reduce the temperature in the facility start-up and shutdown times, and weather conditions to accurately determine the minimum hours of operation of

the HVAC system to satisfy the thermal requirements of the buildings. (Payne 1984)

Liu et al. (2002) reported their study on start/stop time in VAV-HVAC system. In the article, they addressed the energy saving control of HVAC system. They predicted the start time using back propagation (BP) neutral works and stop time by the way of penalty function. They pointed out that "the preparation period $T_{op}$ is mainly determined by outdoor temperature $x_1$, initial indoor temperature $x_2$, volume of rooms $x_3$ and the power capability of the air conditioner $x_4$." In addition, they pointed out that the predicted previous turning off period is affected by "the power of air conditioner, the heat emission of the office facilities and occupants, the volume of the building, the present temperature etc. as well as some indeterminate factors." However, they did not describe the detail mathematical model of the start time, also did not mention the effect caused by the system thermal capacity on start and stop time as well as effect of the desired final temperature on the turning off period.

In a recent paper, Yang et al. (2003) presented the application of artificial neural network (ANN) approach for determining optimal start time in heating systems. The detailed relationships between inputs and outputs didn't need to be known, but an input and output architecture and a various of factors of ANN model must be carefully decided. The limitation of such studies is the accuracy of the data used to train the neural networks.

### 2.3.3 Duty cycling

Duty cycling function is applied to HVAC systems. It is based on the theory that HVAC systems seldom operate at peak output. Therefore, the main idea is shutting down the system for predetermined short periods of time during normal operating hours. Accordingly, if a system is shut down for a short period of time, it still has enough capacity to overcome the slight temperature drift, which may occur during shutdown. "Although the interruption does not reduce total cooling load, it does reduce the net auxiliary loads, such as the energy required to operate the fans and pumps. It also reduce the outdoor air cooling loads since the outdoor air intake damper is closed while an air handling unit is off."(Payne 1984)

Zaheer-uddin and Zheng (1994a) presented typical daily performance of multi-zone VAV heating system. Both off normal operation and duty cycling processes were simulated. They combined the duty cycling of Chiller and PI control strategy to regulate the airflow rates during occupied time. The simulation results showed that both comfort and energy reduction could be achieved using these schemes.

On the other hand, duty cycling function has found less usage. Instead load reset strategy is preferred. However, duty cycling is still practiced in constant volume systems, and in single zone fan systems. (John et al. 1993)

### 2.3.4 Night cycle and night purge (Night ventilation)

Night cycle and night purge are ventilation strategies to maintain space conditions

during the unoccupied period and, in the cooling season, by the use of OA at night when it is a valid source of cooling. The night cycle algorithm cycles the fan on as necessary to maintain a low limit in the winter and high limit in the summer. The night purge program compares space conditions such as temperature and the moisture content to OA condition and uses OA to do free cooling when necessary and possible. (John et al. 1993)

Birtles and Kolokotronic, Perera (1996) investigated the night ventilation and cooling in UK office buildings during summer period from June to September. They presented that thermal mass of the building could use the cool night air to discard the most or entire of the heat absorbed during the day.

Geros et al. (1999) pointed out that three main parameters strongly impacted the efficiency of night ventilation through the numerous of experimental and theoretical studies. The lower outdoor temperature, the higher airflow rate during nighttime, and the thermal capacity of the buildings, the more effective was the night ventilation. In addition, the internal air distribution and the outdoor temperature amplitude also were important to influence the benefit due to the night ventilation. Night ventilation could significantly contribute both decreasing the room temperature and saving systems' energy.

Kolokotroni et al.(1999) demonstrated that natural night ventilation could result modest energy benefits in the typically constructed air-conditioned buildings in UK. Further, night ventilation with optimizing some parameters of buildings would obtain more energy benefit. Also, the buildings having exposed envelops with bigger thermal capacity would save more energy.

Kolokotroni (2001) stated the predicted effectiveness of night ventilation, of about 5% energy savings in typical buildings and up to 40% in buildings optimized for maximum benefit in cooling case from natural night ventilation. Mechanical night ventilation may not offer energy savings due to the energy required for running the fan for a long period during nighttime. These results are based on the predictions of the simplified thermal and ventilation model in U.K. office buildings in hot climate.

In addition, AboulNaga and Abdrabboh (2000) stated an effective approach to improve night ventilation in low-rise buildings from the point of view of building construction. They depicted that in hot-arid climate, combining wall-roof solar chimney could increase induced ACH (air change per hour) thereby reducing indoor air temperature. This concept is worth exploring since by incorporating mechanical systems and building construction features, improved EMC functions can be designed.

### 2.3.5 Load reset

The load reset is another common EMC function, which is simply resetting the supply temperature to a more moderate value that just satisfies the greatest demand zone. The most typical applications are the supply air temperature (SAT) reset and supply water temperature reset. The energy savings may be from the decreased energy needed to provide cooling and/or heating. However, the ventilation consequences and penalty resulting from increased fan power may occur. Ventilation is impacted since changes in the SAT setpoint change the primary airflow rate and the operation of economizer cycles,

i.e. the distribution of fresh outdoor air (OA). These changes may result in extra energy demand and ventilation inefficiency if the reset criterion is not appropriate.

Ke et al.(1997b) described a method to determine the SAT setpoint based on optimization principles in VAV systems. Simulation results showed that it could simultaneously reduce energy consumption and meet ventilation requirements.

## 2.4 EMC simulation and control strategies

EMC simulation often related to control strategies because the cooling and heating loads of building vary along with the period of the day and the period of the year. In order to provide comfort, the capacity of the HVAC system equipment must be adjusted according to those loads. Generally, there are many control schemes: bang-bang (on/off) control, PID (proportional-plus-integral-plus-derivative) control, artificial neural network (ANN) control, adaptive control, optimal control, etc. Traditional control methodology like on-off still remains popular today in practice due to its simplicity. Different energy effects may be impacted by various control strategies.

Firstly, optimal control is utilized in HVAC system mainly for the combination of minimizing the energy use without sacrificing the thermal comfort of the occupancy. Typically, The cost function used to find the optimal control strategy consists of two terms, which are the energy conservation of components within the system and the penalty terms to enforce the system constraints or to maintain system variables near

setpoint values. Several studies related to optimal control in HVAC system appeared in literature.

Mumma and Bolin (1994) stated a real-time, on-line optimal control method to minimize the energy consumption and satisfy ventilation requirements according to ASHRAE standard-62 for multi-zone VAV system. They searched the optimal solution for distributing the OA to each zone, simultaneously meeting the OA requirement in the critical zone and avoiding to delivery too much OA to the zone which needed less OA volume.

Wang (1999) simulated the operating characteristics and energy performance of a VAV-HVAC system under three on-line optimized EMC strategies such as VAV static pressure setpoint, AHU outlet air temperature setpoint and outdoor ventilation air flow setpoint at four different climatic conditions (sunny summer, cloudy summer, spring and winter) in Hong Kong. The savings by employing three strategies was 7.37% in sunny summer, and 37.98% in winter comparing with three constant setpoints.

Zaheer-uddin and Zheng (2001) illustrated multistage optimal operating strategies in single zone heating system. They simulated three EMC functions. The methodology addresses the need to combine time scheduled building operation and optimization by way of formulating and solving the multistage optimization problem.

Jin et al. (2001) demonstrated an on-line optimal strategy to optimize and reset setpoints for EMCS using genetic algorithms (GA) method based on the technique of parameter identification and self-tuning. The objective function considered both indoor

thermal comfort and energy consumption based on dynamic zone model and static cooling coil model. The simulation results revealed that optimal strategy could use less energy to maintain space comfort compared with constant setpoints.

Further, adaptive control has recently attracted increasing attention in HVAC applications. It is because that adaptive control is capable of compensating for uncertain parameters, nonlinear and dynamic variation of the system, long-term or seasonal changes in the operation of the process, and non-stationary disturbances acting on the process (Brandt,1986).

Chen and Lee (1990) demonstrated an adaptive robust control scheme to control zone temperature and humidity ratio of a single zone HVAC system. The approach was designed based on the nominal portion of uncertain system and certain functional properties of the uncertainty bound.

Piao et al. (1998) described a simple fuzzy adaptive control method to control zone temperature for a single zone heating system. They accomplished the control actions by a low cost and distributed hardware, also compared with PID and fuzzy-PID control. The simulation result revealed that the direct adaptive control based on fuzzy sliding mode control had better performance in the application in a swimming room.

Zhang (2001) illustrated an augmented constant gain control (ACGC) and variable gain control (VGC) to control zone temperature for radiant floor heating system. In fact, the VGC is a kind of adaptive control.

In addition, there also are some articles discussing the comparative performance

using various control schemes.

Mutammara et al. (1990) addressed the energy consumption estimates of three EMC functions, such as economy cycle, PI control and cold deck reset using five types of control strategies (economy no PI, PI no economy, PI with economy, PI with economy and cold deck reset) at five different locations using BLAST program. They pointed out that a simple economy cycle with PI control cooling coil and outdoor/return dampers can obtain low energy consumption in most of climate except hot, humid ones. Cold deck reset can also add to help energy savings.

Virk et al. (1991) stated EMCS performance through comparison of predictive on/off with conventional on/off and PI control. The simulations showed that both predicted on/off and PI approaches could result better performance than conventional on/off, and the former was superior to the latter with appropriate implementation hardware.

Recently, Rabie et al. (2002) presented an EMC function similar to the demand-side management in a telecommunications environment. He offered some guidelines for evaluating cost-effective energy configurations, schedules and tariffs.

Although modern control schemes due to the digital control techniques prevailing in some applications in HVAC systems, PID controllers continue to be popular in various applications. Until now, PID control has been the most successful and widely used technique in industrial applications because PID controllers are usually simple, and reliable for field operators in the process industries.

## 2.5 Summary

The follow issues were identified from the literature review:

1. A numerous articles describing EMC functions emphasized on one EMC function (OA cycle, start/stop, night ventilation) at a time; only a few articles involved in the use of three EMC functions.
2. Most of them presented the strategies intended for the design rather than operation and control studies.
3. Most studies didn't focus on implementation aspects of EMC strategies on existing hardware from the point of view of simplicity and ease of implementation. For example, most optimal control and ANN based schemes cannot be implemented on existing commercially available EMC hardware.

Accordingly, a major focus of this thesis is to keep the structure and computational requirement of developed EMC functions simple and compatible with the hardware platforms of commercially available EMC systems in buildings. This objective was the motivating factor in developing simple and yet improved energy management control strategies presented in this thesis.

# Chapter 3 Dynamic model of a VAV-HVAC system

In order to investigate the EMCS performance, appropriate dynamic models of the HVAC system have to be developed. This chapter is organized in three sections, which include sections consisting of single zone system model, two-zone system model, and transient responses simulation results.

## 3.1 Single zone system overall model

Single zone system model contains zone model, coil model, heat pump and tank model, heat pump model, and fan-motor model. The diagram is shown in Figure3.1. A portion of room return air (RA) is exhausted (Exhausted Air, EA) and the rest is mixed with outdoor air (OA). The mixed air is cooled in cooling coil (CC) and circulated via fan, duct, and VAV box arrangement shown in Figure 3.1. In response to demand for cooling from the zone thermostat, volume flow rate of supply air (SA) is varied by modulating the damper by the controller C1, similarly controller C2 maintains supply air temperature near its setpoint value by modulating the chilled water valve. The temperature of chilled water is varied by modulating the capacity of the heat pump using a third controller C3. Also, the OA is controlled by modulating the outdoor air damper by controller C4. In practice, a single controller is used to modulate both outdoor air, recirculated air dampers leaving exhausted air damper open at some fixed position. Alternate strategies are also used in many HVAC systems.

In order to implement the EMC control functions, the controller C1, thru C4 are used as open-loop controllers or as closed loop feedback controllers as required. They are also in communication with a supervisory control as shown in Figure 3.1. In the following a dynamic model of single zone VAV system will be developed. The developed model will be used to simulate several EMC functions.

### 3.1.1 Zone model

By neglecting the heat gains from the ducts and using energy balance principle a simple sensible load equation representing the dynamic characteristics of a zone can be written as (Goh, 1990)

$$\frac{dT_z}{dt} = \frac{1}{\rho_a c_{p,a} V_z}\{M_a c_{p,a}(T_{a,s} - T_z) + q_s + \alpha_z(T_o - T_z)\} \tag{3.1}$$

Where $T_z$, $T_{a,s}$, $T_o$ are the temperature of zone, SA and OA; $V_z$ is the volume of the zone; $\rho_a$ ,$C_{p,a}$ and $M_a$ are the density, specific heat and mass flow of air; $q_s$ the zone non-ventilation sensible cooling load; $\alpha_z = \frac{V_z c_{p,a} ACH}{3600}$, is the OA heat transfer factor and ACH is air changes per hour. This equation means that the rate of change in zone temperature is equal to zone transient load, (which includes building envelop load $q_{env}$, solar heat gain $q_{sol}$, and internal gains $q_{int}$), OA infiltration load $\alpha_z(T_o-T_z)$ and the rate of heat supplied or extracted by the HVAC system $M_a C_{p,a}(T_z-T_s)$.

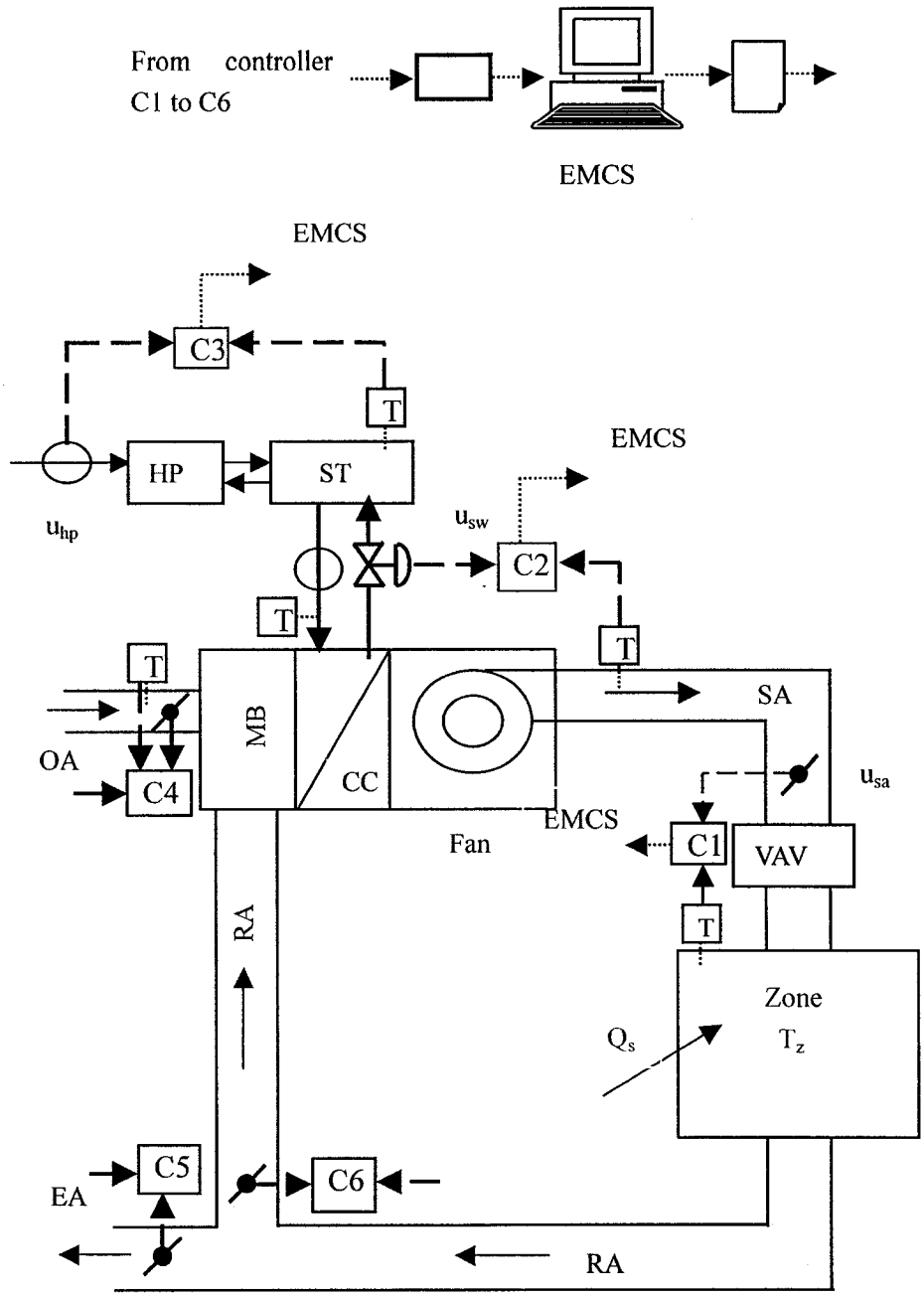


Figure 3.1 Schematic diagram of a single-zone VAV system

### 3.1.2 Cooling coil models

The cooling coil is a crucial element in most HVAC systems; moreover, it plays the most important bridge role between the primary plant (chiller or heat pump) and secondary air distribution system. As the matter of fact, its dynamic characteristic is dominant in the influence of air system. Therefore, several models have been developed in the literature to study its transient response characteristics.

In this study, we have adapted the transient cooling coil model developed by Zaheer-uddin and Zheng (1994b). The modeled cooling coil is a typical counter-cross flow type with continuous plate-fins on tubes. This model has capability to perform different coil configurations such as varying the number of rows of tubes and the number of fins per inch of tube. Since these models take into account the effect of variable airflow rates in the coil that occur in response to variation in fan speed, it is particularly suitable to perform simulation of VAV-HVAC systems. The air and water conditions out of coil are described by the following equations by knowing the conditions of air and water entering the coil.

Air-side

$$\frac{dT_a}{dt} = -\frac{h_t \eta_{s,ov} A_o}{\rho c_v A}(\bar{T}_a - \bar{T}_t) - \frac{\gamma M_a}{\rho A L_c}(T_a - T_{a,in}) \qquad (3.2)$$

Water-side

$$\frac{dT_{wr}}{dt} = \frac{h_{it} A_{it}}{m_w c_w}(\bar{T}_t - \bar{T}_w) + \frac{M_w}{m_w L_c}(T_{ws} - T_{wr}) \qquad (3.3)$$

Tube-temperature

$$\frac{d\overline{T_t}}{dt} = \frac{1-\eta_s}{\eta_s + \frac{m_t c_t}{m_{fin} c_{fin}}}\{\frac{\gamma M_a}{\rho A L_c}(T_a - T_{a,in}) - \frac{h_{it} A_{it}}{m_{fin} c_{fin}(1-\eta_s)}(\overline{T}_t - \overline{T}_w) +$$

$$(\frac{\eta_{s,ov} h_c A_o}{\rho c_v A} + \frac{\eta_{s,ov} h_c A_o}{m_{fin} c_{fin}(1-\eta_s)})(\overline{T}_a - \overline{T}_t)\} \quad (3.4)$$

$$T_{a,in} = xT_o + (1-x)T_z \quad (3.5)$$

$T_a$ is the temperature of air leaving the coil; $T_{a,in}$ is the temperature of air entering the coil. $T_{ws}$, $T_{wr}$ are the temperature of supply and return water; $T_a$, $T_w$, $T_t$ respectively are the mean bulk temperatures of air, water and tube within the coil.

These equations are obtained by energy balance principles. Equation (3.2) describes that the rate of change of air temperature varies with energy supplied to the air by virtue of heat transfer between air and tube, which is proportional to the term $(\overline{T_a} - \overline{T_t})$. Similarly, Equation (3.3) describes that the water temperature variation are due to heat transfer between tube temperature and chilled water temperature $(\overline{T_w} - \overline{T_t})$. Equation (3.4) similarly shows the energy balance between air and tube on one side and tube and water temperature on the other side giving rise to rate of changes in tube temperature.

There are three different methods to calculate $T_a$, $T_w$, $\overline{T_a}$, $\overline{T_w}$. In this thesis, the coil of interest is counter-cross-flow configuration; hence, we take the weighted average approach as shown below.

$$\overline{T}_a = \frac{M_a c_{pa} T_{a,in} + M_w c_w T_a}{M_a c_{pa} + M_w c_w} \quad (3.6)$$

$$\overline{T}_w = \frac{M_a c_{pa} T_{wr} + M_w c_w T_{ws}}{M_a c_{pa} + M_w c_w} \quad (3.7)$$

### 3.1.3 Heat pump and storage tank model

The heat pump and storage tank model describes the energy balance between the chiller energy input, the storage energy in the tank, and the heat gain via return water from the coil and from the surrounding space. By identifying the energy flows to and from the storage tank, we can express the energy balance using following equation(Zheng, 1997):

$$\frac{dT_{ws}}{dt} = \frac{1}{\rho_w c_w V_{\tan k}}[-M_w c_w (T_{ws} - T_{wr}) + U_{hp} U_{hp\max} COP + \alpha_h (T_{\infty,t} - T_{ws})] \quad (3.8)$$

Where $T_{ws}$, $T_{wr}$ represents supply and return water temperature; $\rho_w$, $C_w$ and $M_w$ the density, specific heat and mass flow of water. $U_{hp}$, $U_{hpmax}$ are normal capacity and maximum capacity of heat pump. COP is the coefficient of performance of heat pump, and it is given by equation (3.9). $T_{\infty,t}$ is the temperature of mechanical room. $\alpha_h$ is the heat transfer factor.

### 3.1.4 Heat pump COP model

In order to calculate the coefficient of performance of the heat pump in the cooling process, an empirical equation is used as given below

$$COP = a_0 COP_{\max} + a_1 T_{ws} + a_2 T_{ws}^{\ 2} \quad (3.9)$$

This is an approximate equation which assumes that COP is mainly affected by supply water temperature (SWT) $T_{ws}$, and other factors are neglected. Where $COP_{max}$ is the maximum coefficient of performance of heat pump; $a_0$, $a_1$, $a_2$ are constant coefficients.

At the same time, one restriction should be added. That is, the calculation of COP should not be greater than its maximum value.

### 3.1.5 Fan-Motor model

The relationship between motor input power and the fan delivered air volume; the fan pressure is of interest. They can be described as below using fan laws.

$$U_{fan} = \frac{Q\Delta P}{\eta} \tag{3.10}$$

Where $U_{fan}$ =fan motor input power kw,

Q = fan delivery air volume $m^3/s$,

P= fan pressure kpa,

η = fan efficiency.

## 3.2 Two-zone overall model

A schematic diagram of two-zone VAV system is shown in Figure 3.2. The addition of second zone with its VAV box and controller is the only difference compared to the single zone VAV system discussed in previous section. The model equations remain the same as those described in section 3.1 with the exception of the two separate equations for predicting respectively zone 1 and zone 2 temperatures. The zone model equations are described below.

$$\frac{dT_{z1}}{dt} = \frac{1}{\rho_a c_{p,a} v_{z1}} \{M_{a1} c_{p,a} (T_{a,s} - T_{z1}) + q_{s1} + \alpha_{z1} (T_o - T_{z1})\} \tag{3.11}$$

$$\frac{dT_{z2}}{dt} = \frac{1}{\rho_a c_{p,a} v_{z2}} \{M_{a2} c_{p,a} (T_{a,s} - T_{z2}) + q_{s2} + \alpha_{z2} (T_o - T_{z2})\} \tag{3.12}$$

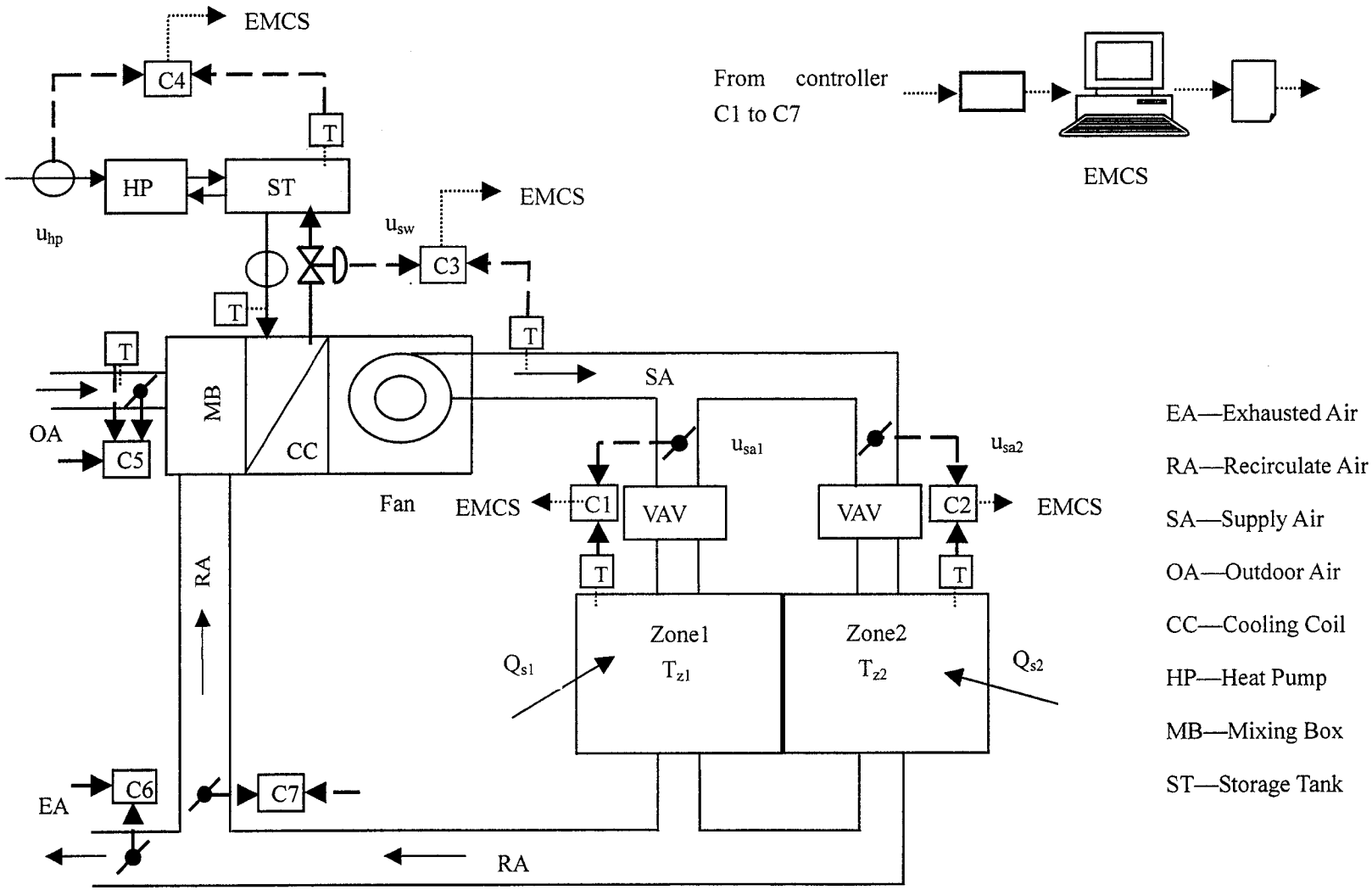


Figure 3.2 Schematic diagram of a two-zone VAV system

## 3.3 Simulation results

In this section, simulation results showing the open loop thermal responses of systems are given. The design parameters used in the simulations are summarized in Table 3.1. The design parameters were chosen using steady state design methods and sizing calculations corresponding to a 2-Ton VAV-HVAC system.

### 3.3.1 Single zone simulation results

The considered single zone model is an office room, which is located in the second floor in Thermal Environment and Control Laboratory in the Department of Building, Civil and Environmental Engineering at the Concordia University. It has one south-facing external wall with double-glazing window and other three walls are facing the interior environment. The length of zone is 6.6m; the width is 3m; and the depth is 2.8m. The floor area is 19.8m$^2$. The window is 1.8m for height, 2.4m for width. The single zone system parameters are given in Table3.2. The outdoor air temperature $t_o$ is assumed to be 30℃(86F), and OA flow rate $x_v$ is the 15% of the total air flow rate.

Equations (3.1) to (3.9) were solved using Matlab simulation software package. The single-zone VAV-HVAC system's open-loop transient responses are shown in Figures 3.3, and 3.4. Figure 3.3 depicts the responses of zone temperature and SAT; Figure 3.4 shows the transient responses of water temperature $t_{wr}$, $t_{ws}$, tube temperature $t_{ta}$, and COP of heat pump. The transient responses are summarized in Table 3.3, where the time constant is the time at which the function value reaches 66.6% of final value. Table 3.3 reveals that

zone temperature $t_z$ has the biggest time constant and SAT has the smallest one, which is slightly greater than that of water temperature $t_{wr}$, $t_{ws}$. This is easily verified because zone has the biggest thermal capacity while the thermal capacity of air is the smallest one. Therefore, zone responses are slow, while the coil responses are fast. Thus the VAV-HVAC system can be characterized as a two-time constant system.

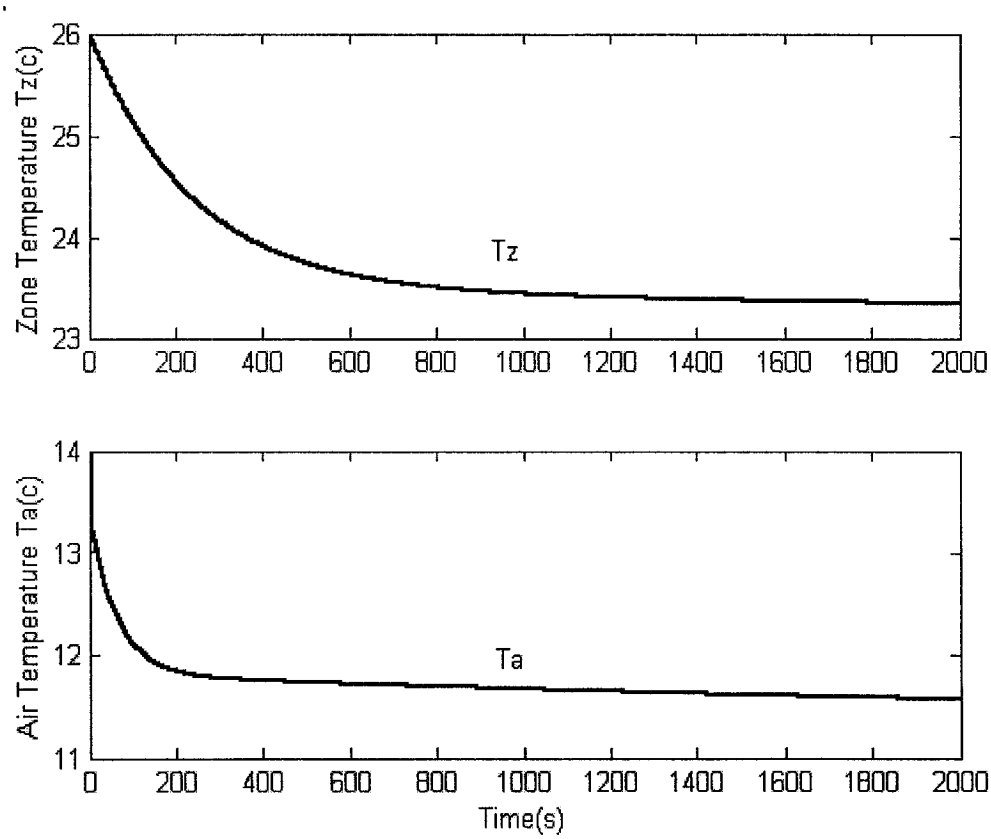


Figure 3.3 Zone temperature and SAT profiles of single zone simulation

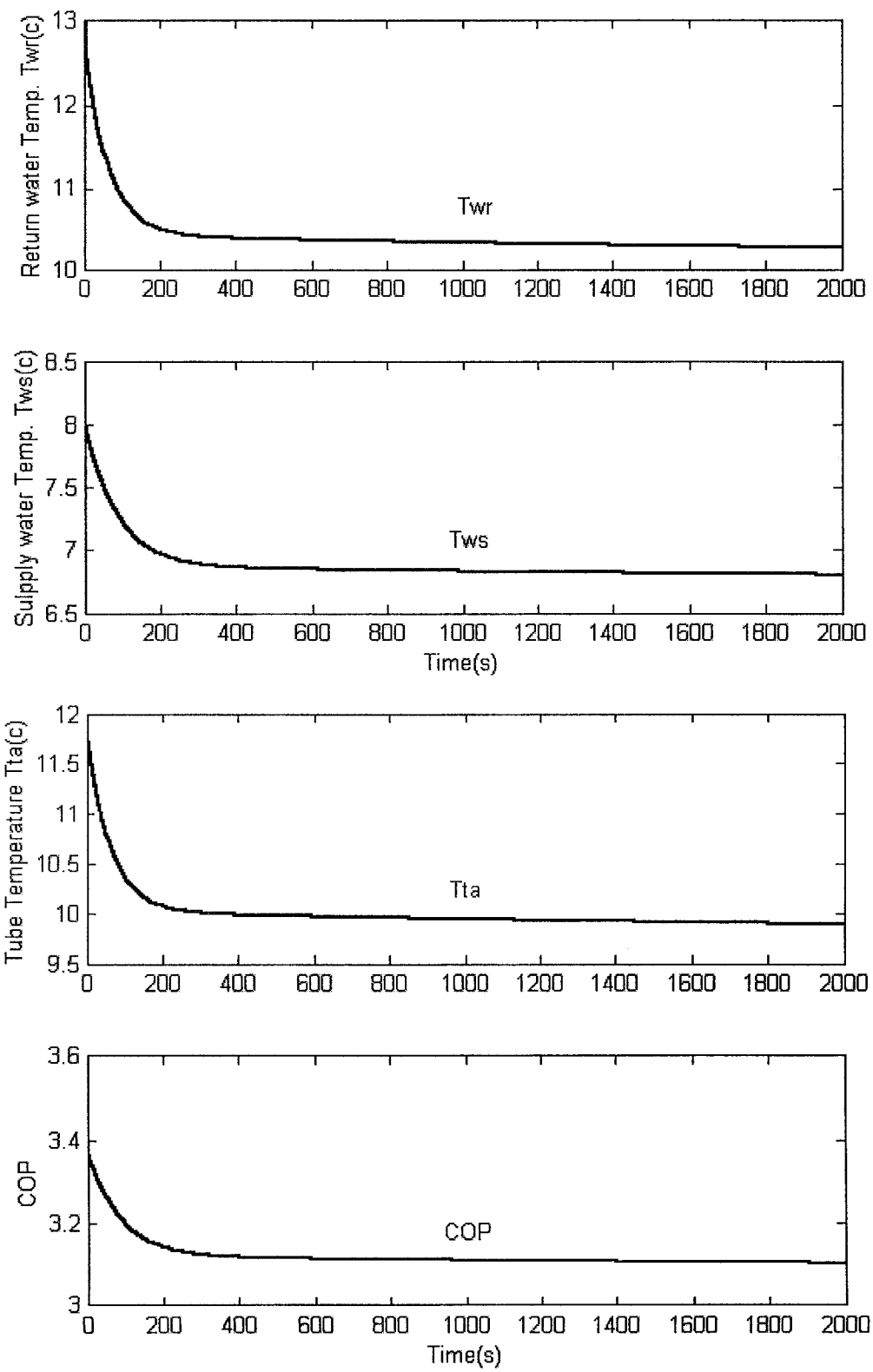


Figure 3.4 Water, tube temperature and COP profiles of single zone simulation

Table 3.1 Design parameters used in simulations

| Item | Symbol | Magnitude and Unit |
|---|---|---|
| **Cooling coil** | | |
| Face air area | A | $0.2787m^2$ ($432in^2$) |
| Total heat transfer area | $A_{total}$ | $48.8697m^2$ ($75748.035in^2$) |
| Primary heat transfer area | $A_{fin}$ | $47.1668m^2$ ($73108.54in^2$) |
| Width of coil | WC | 0.6096m (24in) |
| Height of coil | HC | 0.4572m (18in) |
| Depth of coil | LC | 0.2032m (8in) |
| Tube outer diameter | d | 0.0159m (0.626in) |
| Tube inner diameter | din | 0.0146m (0.575in) |
| Number of fin per unit length | nf | 472.44/m (12/in) |
| Number of rows | nr | 4 |
| Number of tubes per row | ntpr | 14 |
| Mass of fin material per unit length | $m_{fin}$ | 55.4858kg/m ($3.1076lb/in^2$) |
| Mass of tube material per unit length | $m_t$ | 44.5845kg/m ($2.4970lb/in^2$) |
| Specific heat of fin | $c_{fin}$ | 896J/kg-K (0.214Btu/lbm-F) |
| Specific heat of tube | ct | 385J/kg-K (0.0804Btu/lbm-F) |
| **Heat-pump and storage tank** | | |
| Maximum heat-pump input | $U_{hpmax}$ | 5000W (6.7Hp) |
| Tank Volume | $V_{tank}$ | $0.347m^3$ ($12.26ft^3$) |
| Maximum water mass flow rate | $M_{wmax}$ | 0.3774kg/s (6GPM) |
| Maximum COP | $COP_{max}$ | 3.5 |

Table 3.2 Zone system parameters

| Item | Symbol | Magnitude and Unit |
|---|---|---|
| **Single zone system** | | |
| Zone volume | V | $55.44m^3$ ($1958ft^3$) |
| Maximum supply air mass flow rate | $M_{amax}$ | 0.283kg/s (600CFM) |
| Zonal sensible load | $q_s$ | 3080W (10512Btu/h) |
| **Two-zone system** | | |
| Zone 1 volume | $V_1$ | $27.72m^3$ ($979ft^3$) |
| Maximum supply air mass flow rate | $M_{a1max}$ | $0.11m^3/s$ (233CFM) |
| Zonal sensible load | $q_{s1}$ | 1280w (4368Btu/h) |
| Zone 2 volume | $V_2$ | $27.72m^3$ ($979ft^3$) |
| Maximum supply air mass flow rate | $M_{a2max}$ | $0.173m^3/s$ (367CFM) |
| Zonal sensible load | $q_{s2}$ | 1800W (63576Btu/h) |

Table 3.3 Single-zone transient response feature

| Item | Initial value | Final value | Time constant (s) | Steady state time (s) |
|---|---|---|---|---|
| $T_z$ | 26℃ | 23.3℃ | 290 | 700 |
| $T_a$ | 14℃ | 11.6℃ | 60 | 180 |
| $T_{wr}$ | 13℃ | 10.2℃ | 80 | 180 |
| $T_{ws}$ | 8℃ | 6.8℃ | 110 | 180 |
| $T_{ta}$ | 12℃ | 9.9℃ | 80 | 180 |
| COP | 3.375 | 3.15 | 110 | 180 |

### 3.3.2. Two-zone simulation results

The design parameters of two-zone system are given in Table 3.2. Each zone dimensions are 3.3m in length, 3m in width, and 2.8m in depth, and the floor area is 9.9m$^2$. The window dimensions are 1.8m in height, 1.2m in width.

The open-loop simulation results shown in Figures 3.5 and 3.6 and the simulation performance summarize in Table 3.4. From the figures and the table, we can see that zone temperatures response with the biggest time constants and longest steady state times while coil responses are the faster and storage tank responses are in the middle. Moreover, the time constant of zone temperature in zone 1 differs from in zone 2 since they have different final values. Compared with the responses in single zone system, the responses are almost the same in two-zone system except some difference in storage tank. This is because the arrangement of cooling loads and supply air mass flow rates in zone 1 and zone 2 increase their response times.

Table 3.4 Two-zone transient response feature

| Item | Initial value | Final value | Time constant (s) | Steady state time (s) |
|---|---|---|---|---|
| $T_{z1}$ | 26℃ | 22.5℃ | 280 | 900 |
| $T_{z2}$ | 26℃ | 23.5℃ | 300 | 700 |
| $T_a$ | 14℃ | 11.2℃ | 40 | 220 |
| $T_{wr}$ | 13℃ | 10.℃ | 60 | 200 |
| $T_{ws}$ | 6.5℃ | 7.4℃ | 180 | 600 |
| $T_{ta}$ | 12℃ | 9.6℃ | 70 | 200 |
| **COP** | 3.05 | 3.21 | 200 | 600 |

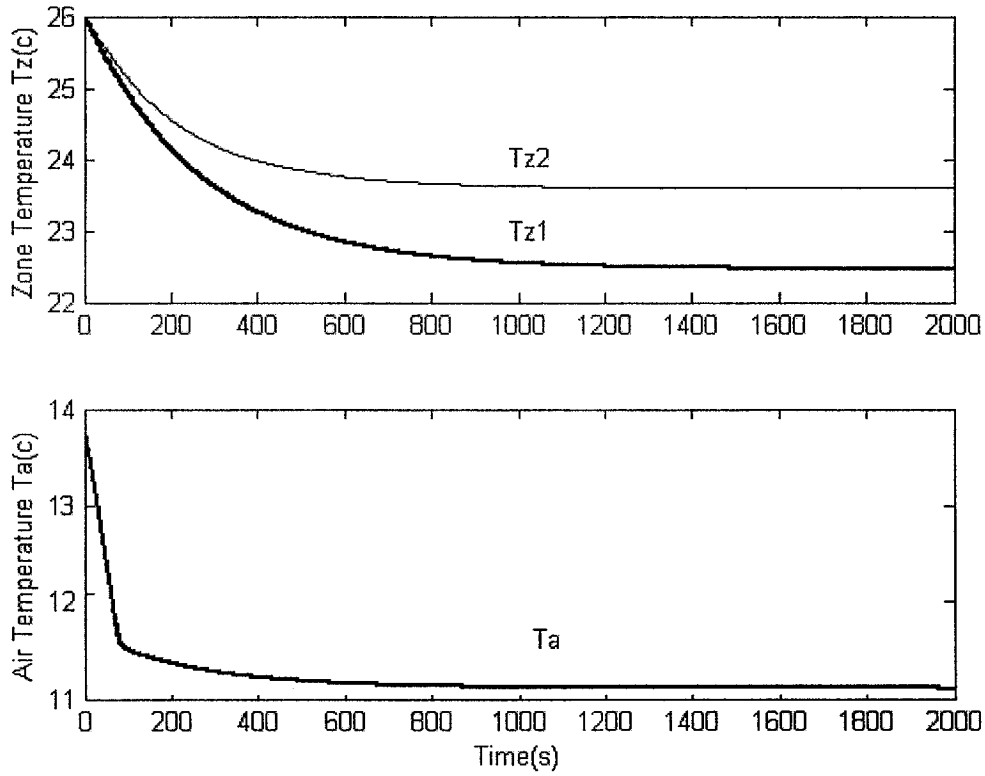


Figure 3.5 Zone temperatures and SAT responses of two zone simulation

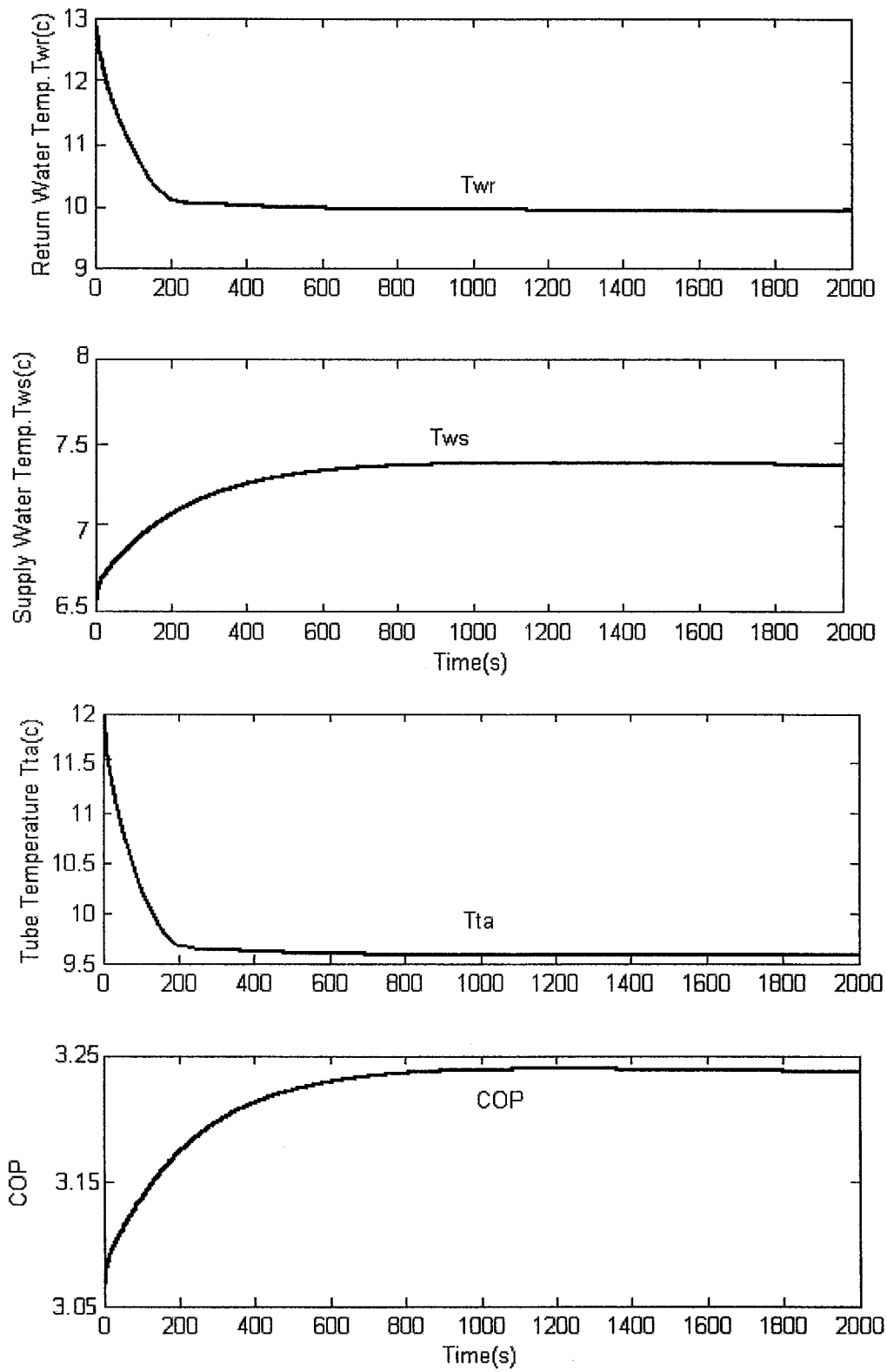


Figure 3.6 Water temperature and COP responses of two-zone simulation

# Chapter 4 EMC algorithm: OA economy cycle

The utilization of outdoor economizer cycle is a popular method of saving energy in HVAC systems. Two strategies commonly used are Temperature–Based economizer cycle (TBEC) and Enthalpy-Based economizer cycle (EBEC). This chapter emphasizes on daily energy consumption as the basis for the analysis and comparison between different strategies, by defining two performance measures constant outdoor air ratio (COAR) and variable outdoor air ratio (VOAR). Both steady state and dynamic analysis have been carried out and the results are given in this chapter.

## 4.1 Temperature-based economy cycle in Steady-State

In an optimally operated HVAC system, the rate of change in cooling load is continuously balanced by the heat extraction rates in the cooling coil. Assuming the cooling load is the sensible, the rate of heat transferred in the cooling coil is

$$q_{c,s} = m_a c_{p,a}(t_m - t_s) \qquad (4.1)$$

From this equation, it is clear that the most savings in energy ($q_{c,s}$=0) occur when mixed-air temperature ($t_m$) equals SAT ($t_s$). In other words, the closer $t_m$ is to $t_s$, the more energy is saved. The system sensible cooling load $q_{s,s}$ consists of two parts: zone non-ventilation sensible load $q_{sei}$ (including building envelope load $q_{env}$, solar radiant load $q_{sol}$, and internal gains $q_{ints}$-occupants, light and electric appliance load), OA sensible load $q_{s,oa}$ and the load due to air infiltration in the zone is neglected. That is

$$q_{s,s} = q_{sei} + q_{s,oa} \qquad (4.2)$$

Where $q_{sei} = q_{env} + q_{sol} + q_{\text{int}\,s}$, and $q_{s,oa} = x_v m_a c_{p,a}(t_o - t_z)$.

Under equilibrium conditions, zone sensible cooling load actually equals to supply air sensible load. That is $q_{sei} = m_a c_{p,a}(t_z - t_s)$. To maintain zone air temperature close to setpoint, sensible cooling provided by the coil must be equal to the HVAC system's cooling requirement. That is, $q_{s,s} = q_{c,s}$. Therefore, an energy balance equation describing the temperature based economy cycle (TEBC) can be written as

$$x_v m_a c_{p,a}(t_o - t_z) + m_a c_{p,a}(t_z - t_s) = m_a c_{p,a}(t_m - t_s) \qquad (4.3)$$

## 4.2 Enthalpy-based economy cycle in steady state

Using the same analogy as in TBEC model, an enthalpy based economy cycle EBEC model is given by $q_t + x_v m_a(i_o - i_z) = m_a(i_m - i_s)$ or

$$x_v m_a(i_o - i_z) + m_a(i_z - i_s) = m_a(i_m - i_s) \qquad (4.4)$$

Where the enthalpy of air is computed from

$$i = 1.01t + d(2500 + 1.84t) \qquad \text{kJ/kg}$$

Where t is temperature, in ℃, d is specific humidity (g/kg) of dry air.

## 4.3 Outdoor air ratio (OAR)

In this section, we define a temperature based OAR ($x_v$) as a function of zone temperature $t_z$, supply air temperature $t_s$, and OA temperature $t_o$. Likewise, zone enthalpy ($i_z$), SA enthalpy ($i_s$), and OA enthalpy ($i_o$) will be used to define an enthalpy based OAR.

### 4.3.1 Temperature based OAR

From equation (4.3), when OA temperature is higher than zone air temperature, the outdoor air ratio OAR $x_v$ is set to minimum. Consequently, right side of the equation gives the cooling coil load with minimum outdoor air ratio $x_v$. On the other hand, when OA temperature is equal to or lower than $t_z$, colder OA can offer the greatest free cooling. From equation (4.3), we can get

$$x_v = \frac{t_z - t_s}{t_z - t_o} \qquad (4.5)$$

This is the relationship equation between OA ratio (OAR) and OA temperature. If $x_v>1$, we let $x_v=1$; while if $x_v<0.2$, we can set the minimum air flow needed such as $x_v=0.2$. This equation is suitable when OA temperature is between 6℃ (supply water temperature) and 24℃ zone setpoint temperature. In all other cases, minimum OAR is appropriate. Figure 4.1 illustrates the relationship between $x_v$ and variable $t_o$ as in equation (4.5) for different SAT.

### 4.3.2 Enthalpy based OAR

Extending the above analysis to the enthalpy balance equation (4.4), we see that most energy savings result when the mixed-air enthalpy ($i_m$) equals SA enthalpy ($i_s$). When OA enthalpy is higher than zone air enthalpy, we can let OAR the minimum. When OA enthalpy is equal to or lower than zone air enthalpy, the cooling coil load is equal zero ( $i_m=i_s$), That is:

$$x_v = \frac{i_z - i_s}{i_z - i_o} \qquad (4.6)$$

This is the relationship between OAR and OA enthalpy. The curve showing this functional relation is depicted in Figure 4.2.

In addition, it should be noted that in the above analysis (both temperature and enthalpy based cycles), energy consumption of supply air fan and return air fan and water pump are neglected. The outdoor air ratio equation (4.5) and (4.6) can be corrected to include the effect of pumping energy as shown below. Let $q_f$ and $q_p$ are the energy required to operate the fan(s) and pump(s). The energy balance equation (4.3) can be rewritten as

$$x_v m_a c_{p,a}(t_o - t_z) + m_a c_{p,a}(t_z - t_s) + q_f + q_p = m_a c_{p,a}(t_m - t_s).$$

We can define $m_a c_{p,a}(\hat{t}_z - t_s) = m_a c_{p,a}(t_z - t_s) + q_f + q_p$.

Where $\hat{t}_z$ is new zone temp-setpiont, which can be obtained from

$$\hat{t}_z = t_z + \frac{q_f + q_p}{m_a c_{p,a}}.$$

By substituting for $t_z$ in equation (4.5) for $x_v$, the corrected outdoor air ratio is

$$\hat{x}_v = \frac{\hat{t}_z - t_s}{\hat{t}_z - t_o}$$

Similarly, the corrected enthalpy based OAR equation can be derived which is given by $\hat{x}_v = \frac{\hat{i}_z - i_s}{\hat{i}_z - i_o}$

Note that in the following results are based on outdoor air ratios which do not include corrections for pumping power.

### 4.3.3 Results

In the simulation runs conducted it was assumed that when OA temperature $t_o$ (enthalpy $i_o$) is higher than zone air temperature $t_o$ (enthalpy $i_o$) or lower than 42.8F(6℃)(or 10kj/kgdry), the OAR set to minimum. Figure 4.1 illustrates a series of OAR profiles with $t_s$ equals to 15.6℃, 14.4℃, and 12.8℃ when zone temperature is held constant at 24℃. Figure 4.2 describes the OAR trend as a function of OA enthalpy. From these figures, we can see that when OA temperature (enthalpy) is between $t_z(i_z)$ and 42.8F(6℃)(10kj/kgdry), OA volume is increasing with the OA temperature (enthalpy). Particularly, in TBEC, the OAR varies with the different supply air temperature. The higher the SAT, the lower OAR at a certain zone temperature (see Figure4.1, $x_v$ (24℃/15.6℃)< $x_v$ (24℃/14.4℃)< $x_v$ (24℃/12.8℃)).

## 4.4 Steady state zone temperature model

In section 4.1, it was shown how the outdoor air ratio $x_v$ varies with OA temperature $t_o$ when zone temperature is held constant. In this section, we show how zone temperature $t_z$ is affected by OAR $x_v$, OA temperature $t_o$ and zone load $q_{sei}$.

Starting from the previous equation (4.3), we assume that the coil shuts down during the unoccupied cycle (18:00-08:00). In this event, the right side of the equation equals to zero, $m_a c_{p,a}(t_m - t_s) = 0$, then we have $x_v m_a c_{p,a}(t_o - t_z) + m_a c_{p,a}(t_z - t_s) = 0$. Therefore, the zone temperature $t_z$ can be predicted from

$$t_z = t_o + \frac{q_{sei}}{x_v m_a c_{p,a}} \qquad (4.7)$$

Figure 4.3 displays daily zone temperature profile subject to a sinusoidal variations in OA temperature $t_o$ curve (with mean value equals to 25℃, and amplitude equals to 10 ℃). The zone temperature $t_z$ is assumed to be constant at 24℃ during occupied period (08:00-18:00). Figure 4.4 depicts the same result in 3-dimentional graph with zone temperature and outdoor air ratios during a 24-hour daily operation.

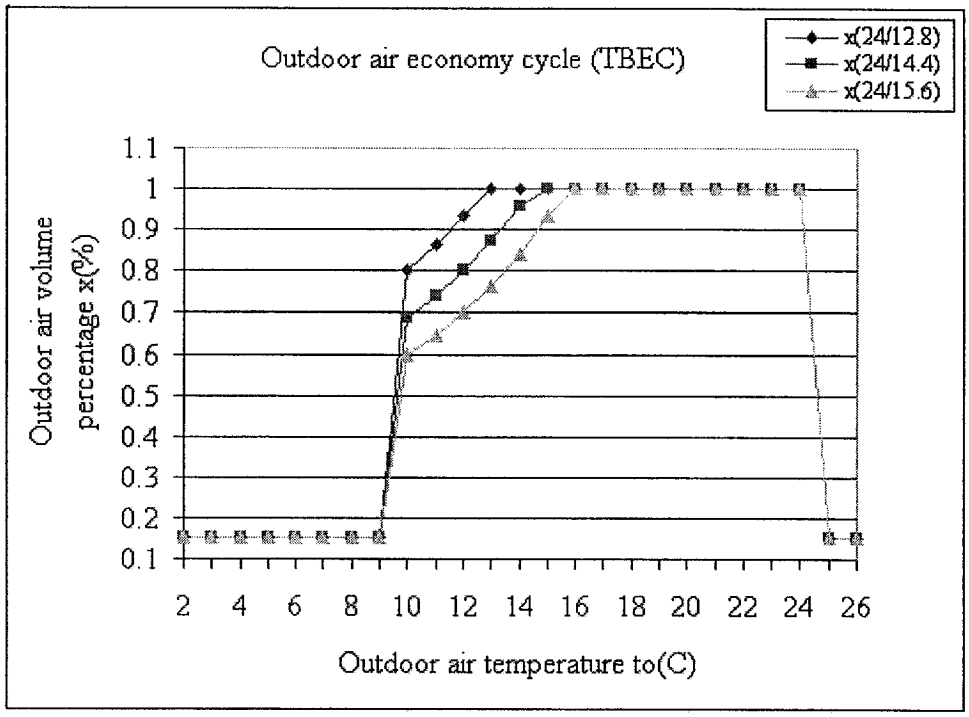


Figure 4.1 Relationship between OA ratio and OA temperature

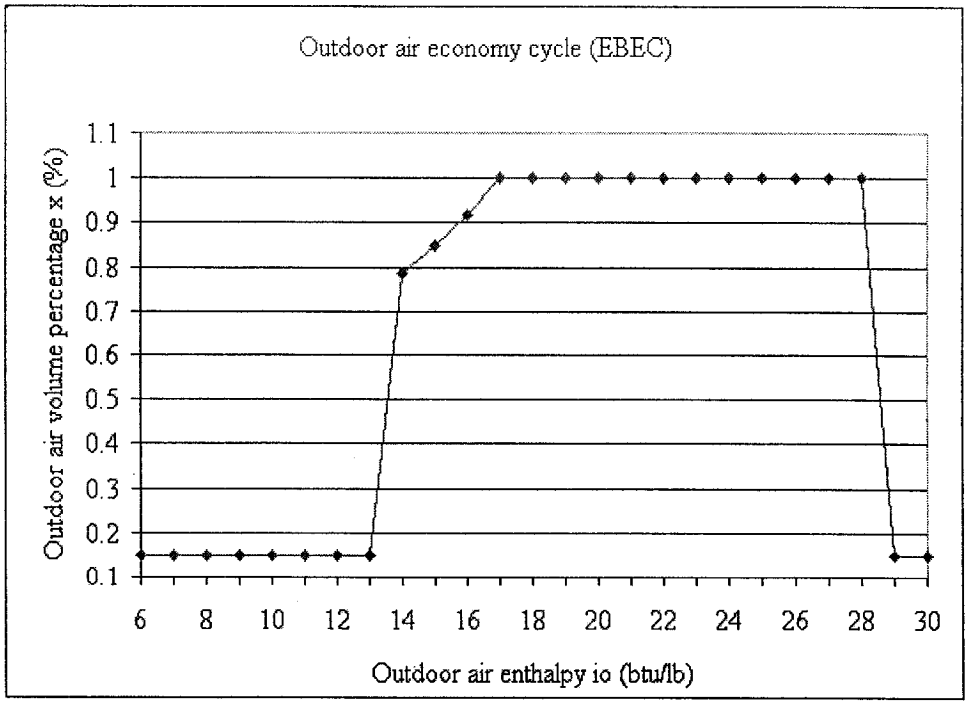


Figure 4.2 Relationship between OA ratio and OA enthalpy

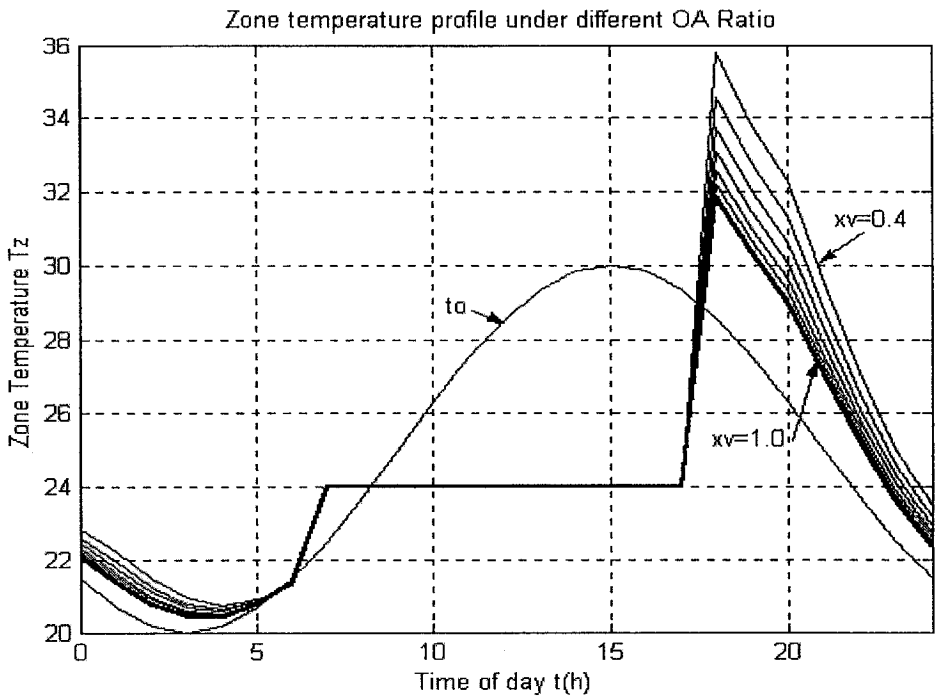


Figure 4.3 Zone temperature profile under different OAR in August

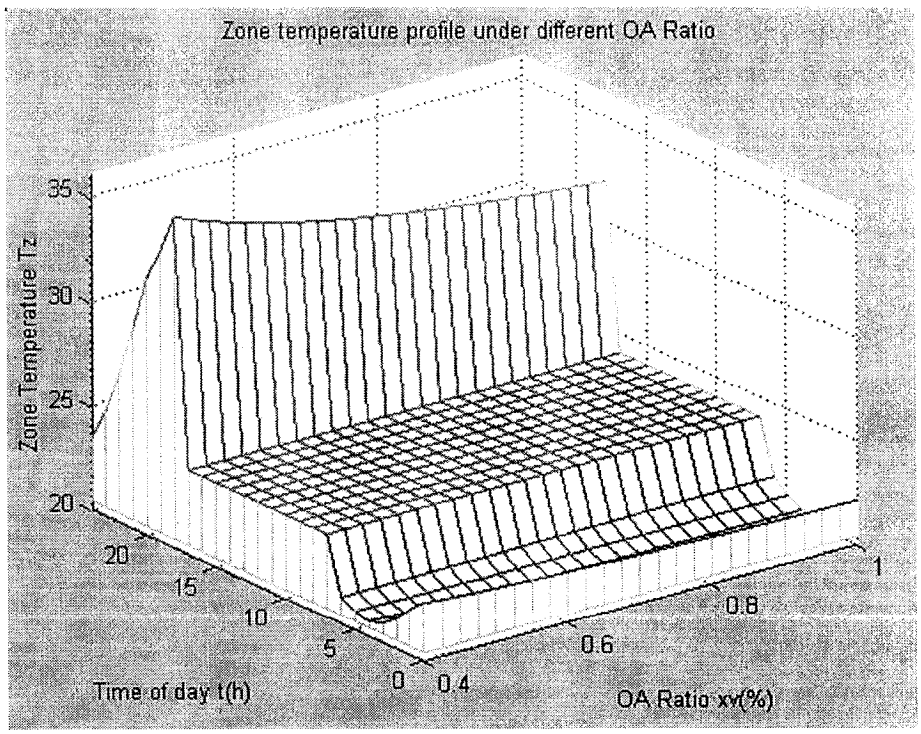


Figure 4.4 Zone temperature profile under different OAR in August

## 4.5 Steady state analysis of daily energy consumption

Daily energy consumption analysis is an important issue in evaluating the performance of HVAC systems. In order to do a systematic analysis, comparisons were made of daily energy consumption between steady state and dynamic outdoor air strategies. To this end, a constant outdoor air ratio (COAR) strategy is defined in which outdoor air is kept at its minimum value throughout the day.

### 4.5.1 Daily energy consumption with COAR strategy under steady state conditions

Daily energy consumption of HVAC systems strongly depends on how the system is operated. We assume that the system turns on during the occupancy period and turns off in the unoccupied time. Accordingly, different indoor temperature setpoint should be defined. Zone temperature is maintained constant at 24℃ in order to satisfy indoor comfort conditions during occupied period, while it is allowed float during unoccupied periods. The OAR is kept constant at 0.2 throughout the day.

The predicted hourly power includes two parts, fan power ($P_{fan}$) and coil power ($P_{coil}$). The sum of these two is the daily energy consumption ($E_{daily}$). That is

$P_{hourly} = P_{fan} + P_{coil}$ or

$$E_{daily} = \int_0^8 (P_{hourly})dt + \int_8^{18} (P_{hourly})dt + \int_{18}^{24} (P_{hourly})dt \qquad (4.8)$$

The typical daily operation was simulated consisting of three stage operation as

defined below.

Stage 1: unoccupied period (00:00 - 08:00), $t_z$ predicted by using equation (4.7), $P_{coil} = 0$, and $P_{fan} = a_1 r_a^3 + a_2 r_a^2 + a_3 r_a + a_4$ (4.9)

Where $a_1$, $a_2$, $a_3$, $a_4$ are coefficients, and $r_a$ is the ratio of actual mass flow rate of air to maximum mass flow rate of air.

Stage2: occupied period (08:00 - 18:00), $t_z$=24℃, $P_{fan}$ computed from equation (4.9), and $P_{coil} = q_{s,oa} + q_{sei}$. (4.10)

Stage3: unoccupied period (18:00 - 24:00), $t_z$, $P_{fan}$, $P_{coil}$ are the same as in stage1.

### 4.5.2 Daily energy consumption on three typical days using COAR strategy

Daily energy consumption was computed using COAR strategy on three typical days, in August, October and May. The daily OA temperature $t_o$ (℃) profiles of three days are depicted in Figure 4.5. The predicted power profiles are depicted in Figure 4.6, 4.7, 4.8. The results summarized in Table 4.1.

Figures 4.7 and 4.8 show that the power is small before 10 o'clock in May and before 11 o'clock in October. The reason is that only fan power is accounted for during this time with no heating or very little heating. Zone temperature is lower than 24℃ before 08:00 so that some heat is in need to bring zone temperature to 24℃ at occupied time. With zone heat gain gradually increasing, cooling coil turns on to cool the zone. Only zone cooling power is considered in this simulation.

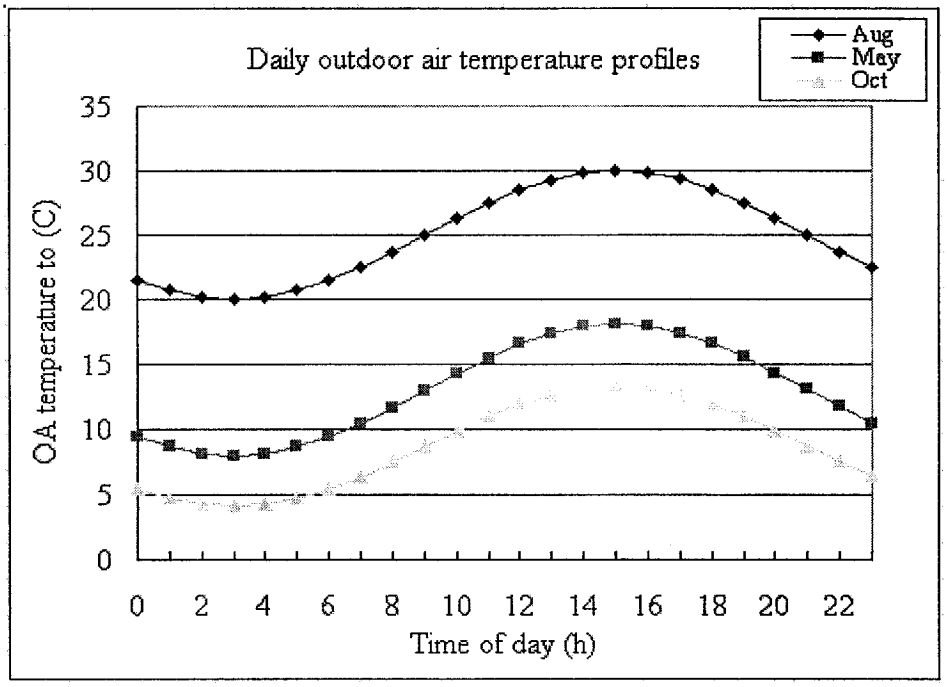


Figure 4.5 Typical daily outdoor air temperature profiles

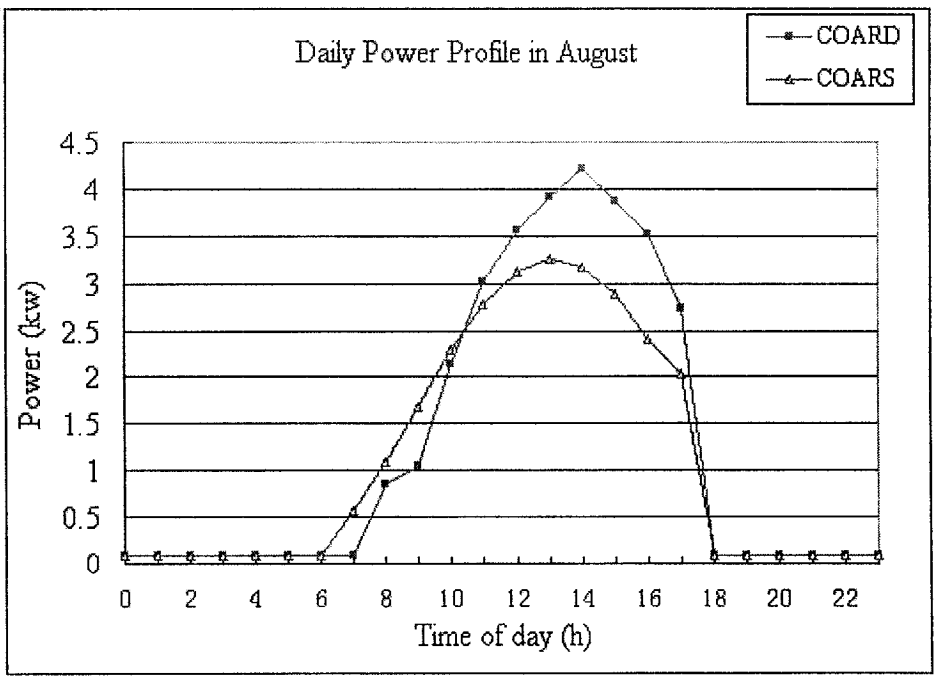


Figure 4.6 COAR daily power profile in August
(COARS=Steady state, COARD=Dynamic)

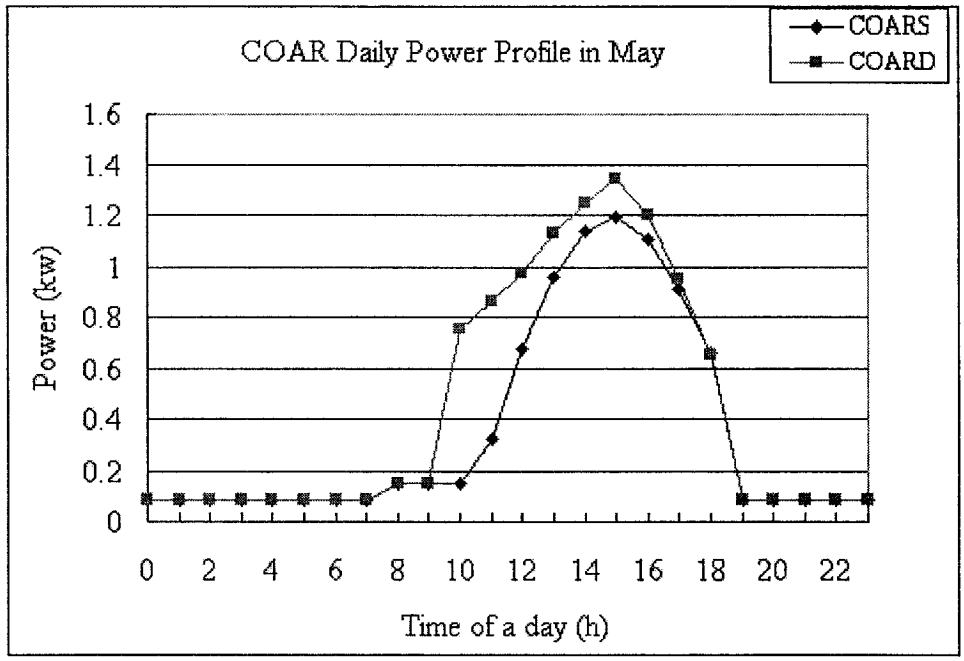


Figure 4.7 COAR daily power profile in May
(COARS=Steady state, COARD=Dynamic)

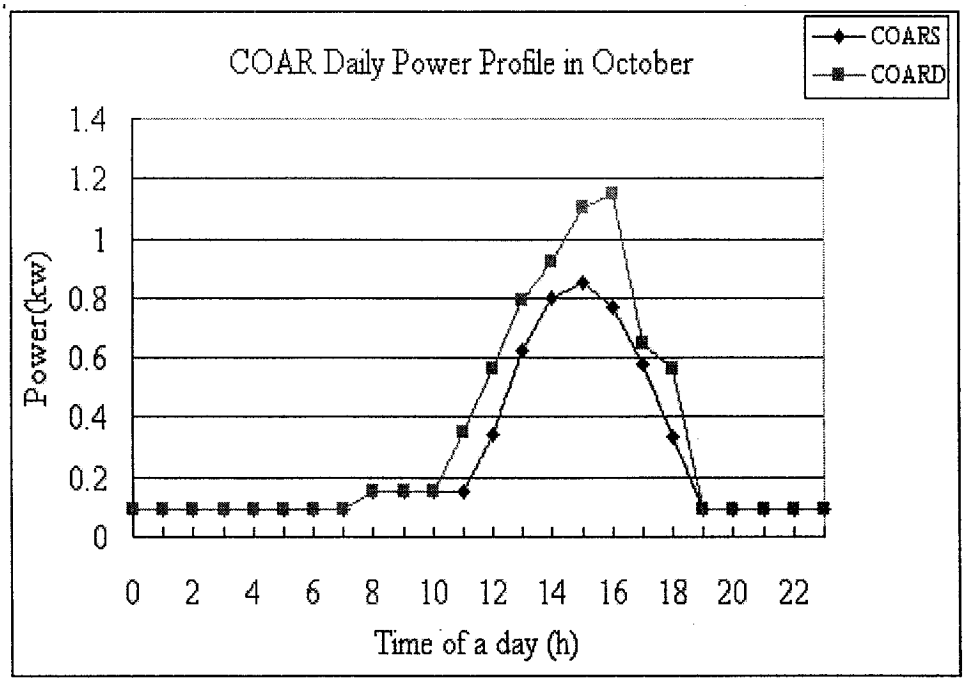


Figure 4.8 COAR daily power profile in October
(COARS=Steady state, COARD=Dynamic)

## 4.6 Dynamic analysis

The steady state economy cycle results provide little insight into such matters as system stability and short-term transient responses, which occur as a result of sudden changes in cooling loads. Steady state data neglect the influence of transient load changes, which are important in comfort, cost and control issues. For these reasons, the dynamic model developed in chapter 3 was used to carry out dynamic simulation tests.

### 4.6.1 Dynamic analysis of COAR strategy

Simulation runs were made using the dynamic model in which outdoor air ratio was kept constant. The zone temperature has no constrains during the unoccupied time, while it has a setpoint of 24℃ in the occupied time. Heat pump and coil only provide cooling in the occupied time. As well as OA ratio was kept constant (0.2) throughout 24-hour-a-day. Three typical day cases were simulated. The daily energy consumption obtained is shown in Table 4.1, and daily power profiles are depicted in Figures 4.6, 4.7, and 4.8. A comparison with steady state analysis shows that steady state analysis could over estimate the energy savings by more than 20%.

Table 4.1 COAR Strategy Daily Energy Consumption

| COAR Strategy Daily Energy Consumption (MJ) | | | |
|---|---|---|---|
| | August | May | October |
| Steady state | 95.14 | 30.87 | 21.88 |
| Dynamic | 116.44 | 38.05 | 27.72 |
| Percent difference (%) | 22.4 | 23.3 | 26.7 |

## 4.6.2. Dynamic analysis of VOAR strategy in VAV system

In this section, the simulation of a single zone VAV-HVAC system with variable outdoor air strategy (VOAR) is presented. Free cooling is delivered by fan during the unoccupied period, whereas heat pump and cooling coil offer cooling to the zone during the occupied cycle. In occupied period, zone temperature is maintained at 24℃ through a PI control strategy.

A series of VOAR schemes relying on various strategies were examined. There are: Base Case (BC), On-off Control (OC), Energy Balance (EB), and proportional band Control (PBC).

### 4.6.2.1 Base case (BC) VOAR strategy

Outdoor air (OA) ratio is based on outdoor air temperature $t_o$, which has high limit ($h_{lim}$), low limit ($l_{lim}$) and mean value ($v_m$). The OA ratio is normalized with respect to its maximum value so that it varies between a minimum $OA_{min}$ and a maximum ratio of 1. The following equations describe the variable outdoor air ratio (VOAR) strategy as a function of outdoor air temperature.

$$x_v = OA_{min} + (1 - OA_{min}) \frac{t_o - l_{lim}}{v_m - l_{lim}} \qquad (4.11.1)$$

$$x_v = OA_{min} + (1 - OA_{min}) \frac{h_{lim} - t_o}{h_{lim} - v_m} \qquad (4.11.2)$$

Equation (4.11.1) is valid when $t_o$ is between $l_{lim}$ and $v_m$, and equation (4.11.2) for $t_o$ between $v_m$ and $h_{lim}$; otherwise, $x_v$ is equal to $OA_{min}$ when $t_o$ is beyond $h_{lim}$ and $l_{lim}$ limits.

Figure 4.9 demonstrates this type of relationship. This method is the most popular in real systems, so we refer to it as the base case. Figure 4.10 shows the typical daily simulation results using the base case (case 1) strategy.

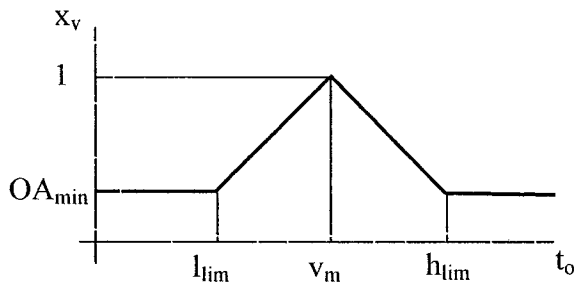


Figure 4.9 Relationship between OA ratio and OA temperature $t_o$ in BC

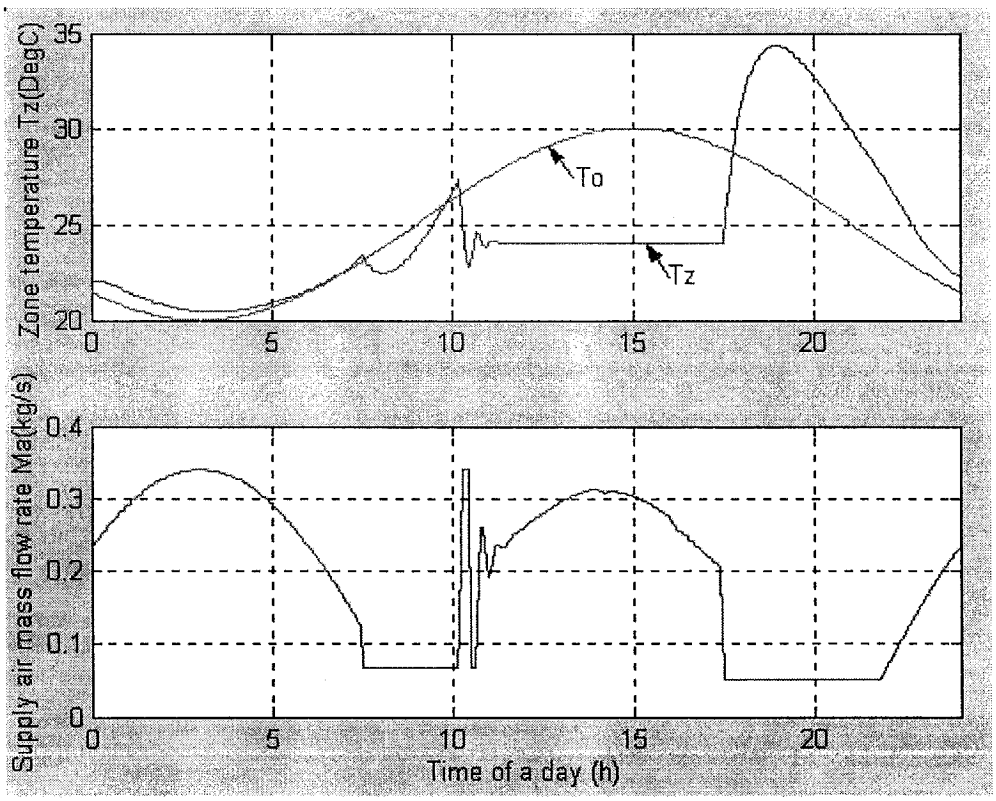


Figure 4.10 OA cycle base case performance (case1)

### 4.6.2.2 On-off control (OC) VOAR strategy

On-off control of OA is another conventional method used in the real systems. Normally, one determines $x_v$ by comparing OA temperature $t_o$ with zone temperature setpoint $t_{zset}$. Here, one more case is examined, in which $t_o$ is compared with actual zone temperature $t_z$. Therefore, the two on-off control cases in this strategy are defined as follows:

$$\text{Method-1: } x_v = \begin{cases} OA_{\min}, & if \quad t_o > t_{zset} \\ 1, & if \quad t_o \le t_{zset} \end{cases} \tag{4.12.1}$$

$$\text{Method-2: } x_v = \begin{cases} OA_{\min}, & if \quad t_o > t_z \\ 1, & if \quad t_o \le t_z \end{cases} \tag{4.12.2}$$

The results obtained with the strategy are summarized in Table 4.2 as case9 and case10 respectively.

### 4.6.2.3 Energy Balance (EB) VOAR strategy

From sensible energy balance equation on a zone, four different versions of estimating $x_v$ were studied. In these equations, $q_s$ represents either zone transient sensible cooling load $q_s$ or zone daily maximum sensible cooling load $q_{s,max}$, and $t_z$ is the actual zone temperature and $t_{zset}$ is the zone temperature setpoint.

$$x_v = \frac{q_{s,\max}}{M_a c_{p,a}(T_{zset} - T_o)} \tag{4.13.1}$$

$$x_v = \frac{q_s}{M_a c_{p,a}(T_{zset} - T_o)} \tag{4.13.2}$$

$$x_v = \frac{q_{s,\max}}{M_a c_{p,a}(T_z - T_o)} \tag{4.13.3}$$

$$x_v = \frac{q_s}{M_a c_{p,a}(T_z - T_o)} \qquad (4.13.4)$$

For clarity these four strategies are referred to as case2, case3, case4, case5 respectively.

### 4.6.2.4 Proportional Band Control (PBC) VOAR strategy

In this section, the outdoor air ratio $x_v$ is defined as a linear function of zone temperature; OA temperature and a proportional band which is proportional to the difference between $t_z$ and $t_o$ in a certain proportional band. Equation (4.14) reveals this relationship.

$$x_v = OA_{\min} + (1 - OA_{\min})\frac{t_z - t_o}{n} \qquad (4.14)$$

This equation is valid when $t_o$ is between $t_z$ and $t_z$-n; and has limiting values such as and $x_v$=$OA_{min}$ when $t_o$>= $t_z$, and $x_v$= 1 when $t_o$<$t_z$-n.

There different cases were analyzed with PB (Proportional Band) n=1,2,3.These cases are referred to as case6, case7, and case8 respectively. The result with n=2, which is the best case (case7) is displayed in Figure 4.11.

### 4.6.2.5. Energy performance of VOAR strategies

Simulation runs were made using the above VOAR strategies. As a measure of effectiveness of these strategies, daily energy consumption was computed. In the daily energy index equation (4.15), a comfort penalty factor was added in addition to the energy consumed by fan and the heat pump. The rationale for this was that large variations in zone temperature contribute to occupant discomfort and therefore it should

be included as a measure of performance.

$$E_{daily} = \int_0^{24}(P_{fan})dt + \int_0^{24}(P_{heatpump})dt + \alpha\int_0^{24}(t_z - t_{zset})^2 dt \qquad (4.15)$$

In equation (4.15), $\alpha$ is a penalty factor; $P_{fan}$ is given by equation (4.9). $P_{heatpump} = (COP)u_{hp}U_{hp\max}$, where COP is defined by equation (3.9). $u_{hp}$ is the ratio of the actual heat pump capacity to maximum capacity, and $U_{hpmax}$ is the maximum heat pump input. The daily energy consumption obtained from VOAR strategies are summarized in Table 4.2. A bar chart visualization of the result is shown in Figure 4.12.

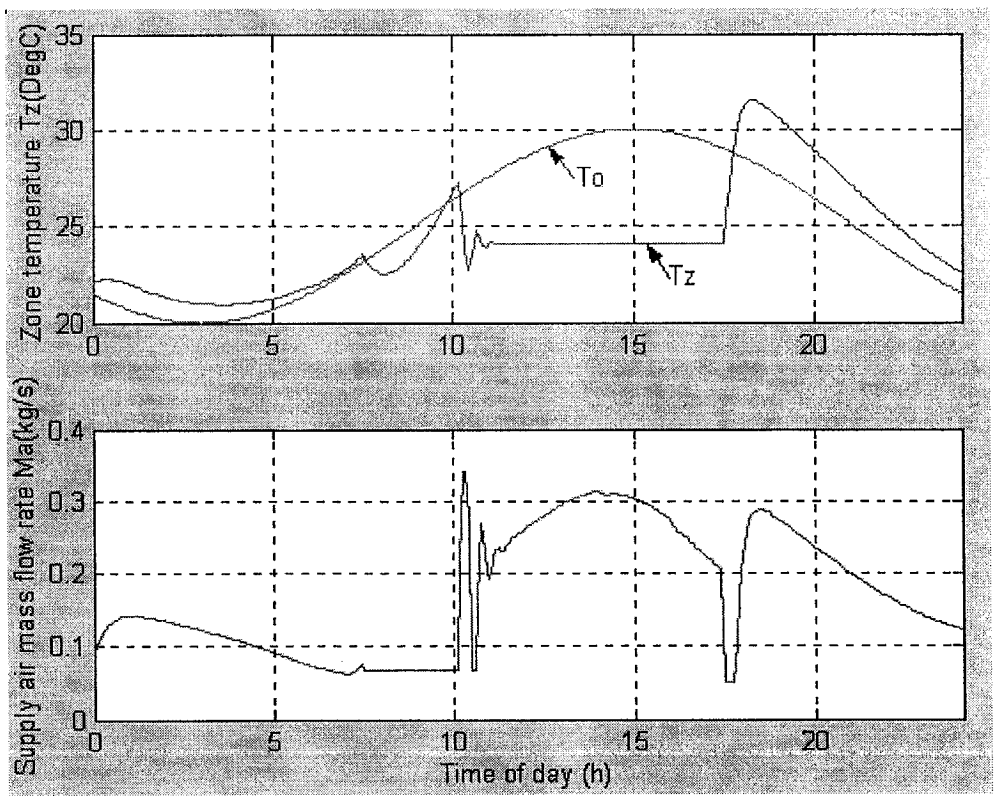


Figure 4.11 Performance of OA cycle (case 7)

Table 4.2 Daily energy consumption of VOAR strategies

(Units: MJ)

| Case 1 | Case 2 | Case 3 | Case 4 | Case 5 |
|---|---|---|---|---|
| **BC** | **EB** | | | |
| | 1 | 2 | 3 | 4 |
| 142.8566 | 143.3675 | 137.8587 | 128.9742 | 128.8704 |
| | | | | |
| Case 6 | Case7 | Case 8 | Case 9 | Case 10 |
| **PBC** | | | **OC** | |
| 1 | 2 | 3 | 1 | 2 |
| 124.9192 | 124.0159 | 124.2558 | 145.6045 | 129.0028 |

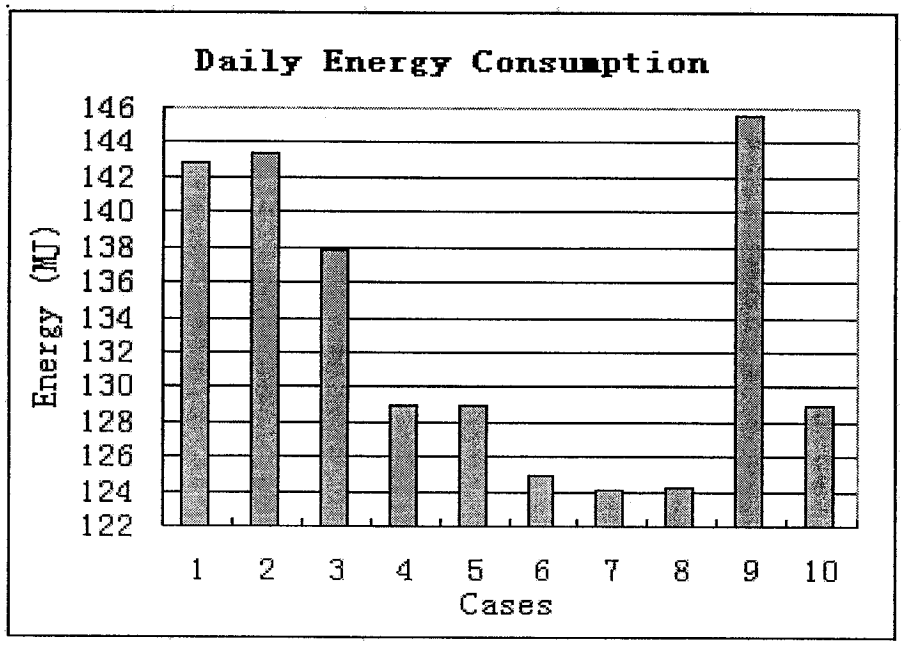


Figure 4.12 Daily energy consumption of VOAR strategies (cases 1-10)

### 4.6.2.6 Discussion and results

Figures 4.10 and 4.11 illustrate the performances of case1 and case7. From these two figures, we can see that the "free-cooling" is used more effectively in case7 than in case1. Although the effect on zone temperature caused by different OA strategy during midnight to the start time is not significant, the difference is significant after the stop time (18:00). How much energy is saved by "free-cooling" strongly depends on how large the

thermal capacity of the building and how long the "free-cooling" occurs before the start time. Therefore, maximizing OA volume when OA temperature is less than zone temperature isn't always feasible. The indoor/outdoor thermal conditions should be paid particularly attention in the application; otherwise, not only can no energy be saved, but also it may lead to more fan energy consumption as in case1.

From Table 4.2, we see that the results from cases 6, 7, and 8 are almost the same as PBC, whereas others are quite different, for example, the energy balance (EB) and on-off control (OC). The difference between the highest (case 2) and the lowest (case 5) in EB category was 10%. The difference between the two cases (case9 and case10) in OC category was 11.4%.

Figure 4.12 reveals that the energy consumption is the highest in case 9, and the lowest is case 7. Their difference is 14.8%. Also in the energy balance case4, 9.7% energy was saved compared with case1 (Base case). Based on these results, the following conclusions can be draw:

1. Savings are achieved when actual zone temperature $t_z$ is used in the VOAR strategy (cases 4, 5, 6, 7, 8, 10) compared with cases in which zone temperature setpoint $t_{zset}$ was used (cases 2, 3, 9).
2. The proportional band control PBC (cases 6, 7, 8) strategy was the best energy saving strategy, although the differences among them are not significant.
3. Practical difficulties could arise in terms of frequent switching when OAR is

modulated according to $t_o \leq t_z$ or $t_{zset}$. A 2 ℃ difference such as $t_o \leq (t_z - 2)$ is more appropriate to avoid frequent fan motor switching.

## 4.7 Conclusion

From the steady state and dynamic case studies performed in this chapter, the following conclusions about OA economy cycle strategies are made.

1. Daily energy consumption is smaller in steady state than in dynamic simulations because the auxiliary energy consumption due to zone temperature swing hasn't been included in steady state analysis. The temperature swings mainly depend on OA temperature ($t_o$), zone load ($q_s$) and OA ratio ($x_v$).
2. Daily energy consumption among the ten OA strategies investigated are significantly different. The biggest difference can reach to 14%.
3. On-off control strategy can effectively save energy, so that it may be worth considering the use of on-off control for outdoor air in existing energy management systems.
4. The best VOAR strategy is the proportional band control method, which is easy to realize in real systems. Only zone temperature ($t_z$) and OA temperature ($t_o$) have to be measured. The proportional band (n) strongly depends on zone thermal capacity.

# Chapter 5 EMC algorithms: Programmed start /stop time

Start/stop strategy is a common EMC function used in many buildings. In this chapter mathematical models to describe start/stop strategy will be developed. First a reduced order dynamic model is used to develop the start/stop model. The model is then verified using full-model developed in chapter 3. Also, the applications of start/stop model for use in buildings with different thermal mass characteristics are proposed.

## 5.1 Programmed start time

The decision as to when HVAC system should be restarted is important for energy conservation because most of buildings aren't occupied 24-hour-a-day. The start-lead-time strongly depends on the outdoor air and inside space temperatures as well as system thermal characteristics. In this section, a start-lead-time model will be developed.

### 5.1.1 Development of the start-lead-time model

To fix ideas, a reduced order dynamic model is used to develop a start-lead-time model. From the zone energy balance principle, we have

$$ETC\frac{dT_z}{dt} = M_a c_{p,a}(T_a - T_z) + q_s + \alpha_z(T_o - T_z) \qquad (5.1)$$

Where ETC represents buildings' equivalent thermal capacity, $M_a$ the supply air

mass flow rate, and $c_{p,a}$ is the air thermal capacity, $q_s$ is the zone sensible cooling load. $T_a$, $T_z$, and $T_o$ are supply air temperature SAT, zone temperature, and OA temperature, respectively. From this model, we can obtain the lead time required to reach the zone setpoint under a series of initial zone temperature $t_{zin}$ and OA temperature $t_o$ conditions.

Because our purpose is to know how long the zone temperature ($t_z$) takes to reach its setpoint. The lead time values were obtained by carrying out several open-loop tests. The data was gathered in three sets of arrays under fixed operating conditions: initial zone temperature array [$t_{zin}$], outdoor air temperature [$t_o$], and time matrix [$T_{start}$]. Figure 5.1 illustrates the relationship between start-lead-time ($T_{start}$) and OA temperature ($t_o$) under different initial zone temperatures ($t_{zin}$). Similarly, Figure 5.2 illustrates the relationship between start-lead-time and initial zone temperature ($t_{zin}$) under different OA temperature ($t_o$). A three-dimensional plot in Figure 5.3 shows the relationship among these three parameters ($T_{start}$, $t_{zin}$, $t_o$).

A simple equation with three parameters was found to fit the data very well. This equation, referred to here as start-lead-time equation, is given below.

$$T_{start} = a_1(t_{zin} - t_{zset}) + a_2(t_{zin} - t_{zset})(t_o - t_{zset}) + a_3 \qquad (5.2)$$

Where $a_1$, $a_2$, and $a_3$ are coefficients. From this equation, we can see that start-lead-time consists of three parts. The first one is a linear function of zone temperature error, which is the difference between zone temperature and its setpoint as shown in Figure5.1. The second part is a product function of the two temperature differences, the difference between outdoor air and zone temperature setpoint, and the zone temperature error. This

trend is shown in Figure 5.2. The last term is a constant, which accounts for the system's thermal inertia. Even if the zone temperature equals its setpoint, the HVAC system needs to be started ahead of occupancy time.

Figure 5.4 shows a comparison of lead time computed from the model equation (5.2) and the original start time values obtained from computer simulations. The solid lines in Figure 5.4 are from model, and the dash lines represent the data in Figure 5.1. Although there are slight differences in the extremely high ($t_{zin}$=30℃) and low ($t_{zin}$=25℃) boundaries of the initial zone temperature, the results show good agreement in the middle range(initial zone temperature $t_{zin}$=26℃~29℃).

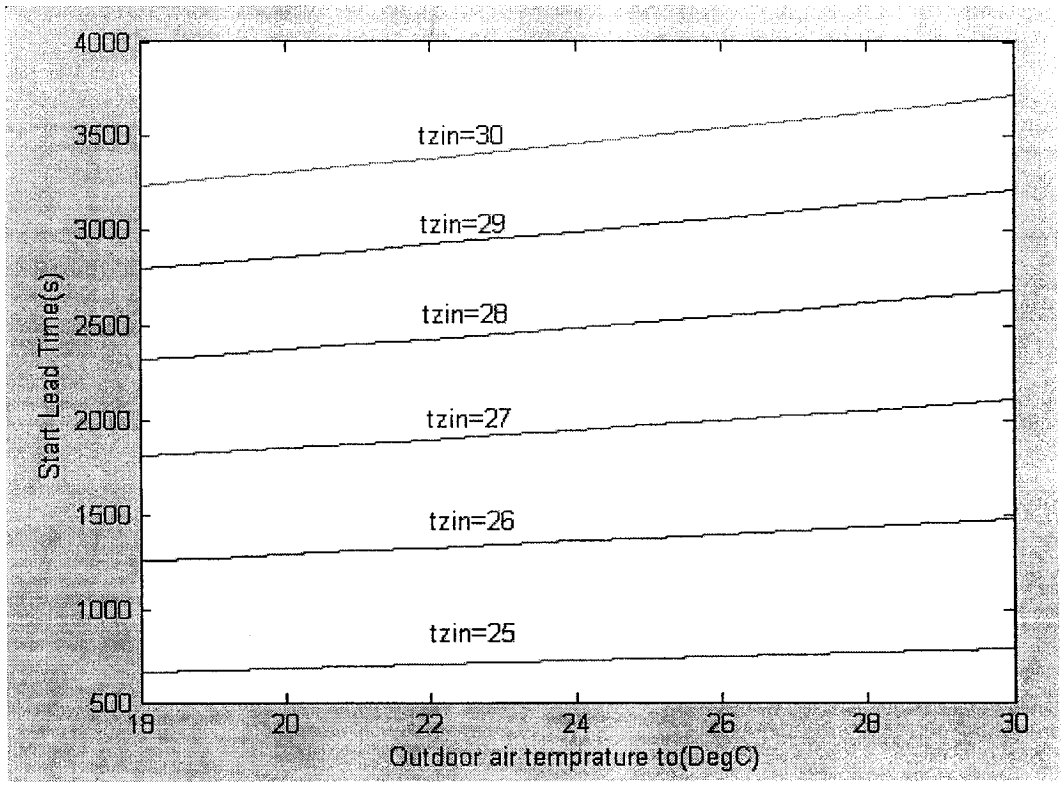


Figure 5.1 Start-lead-time sets under different initial zone temperature ($t_{zin}$)

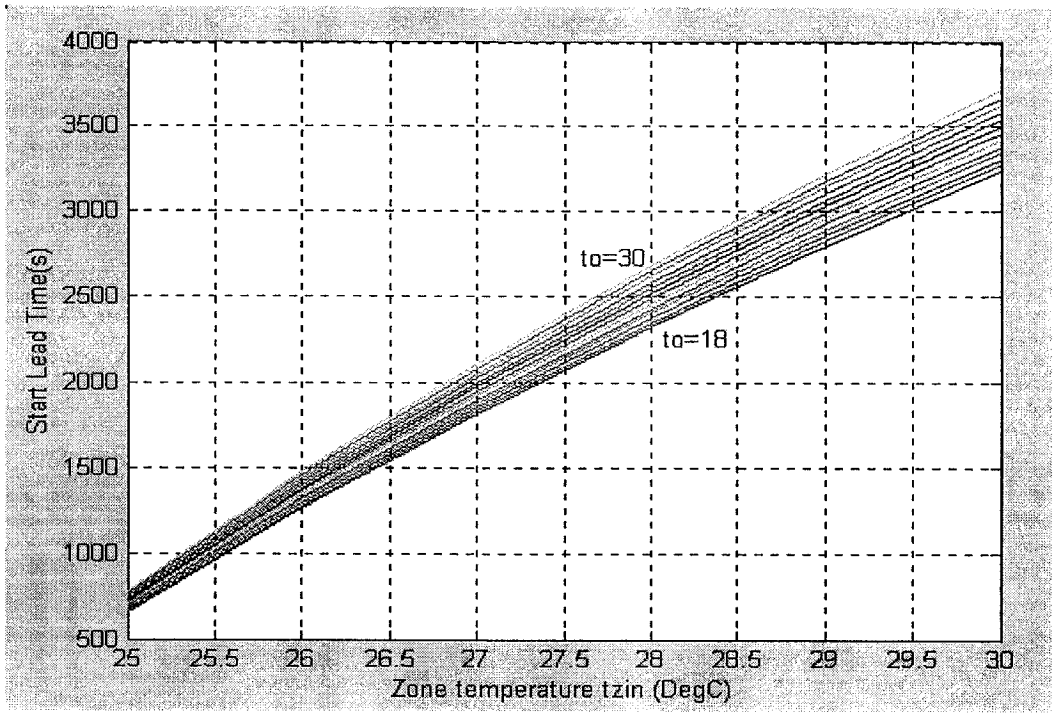


Figure 5.2 Start-lead-time sets under different OA temperature ($t_o$)

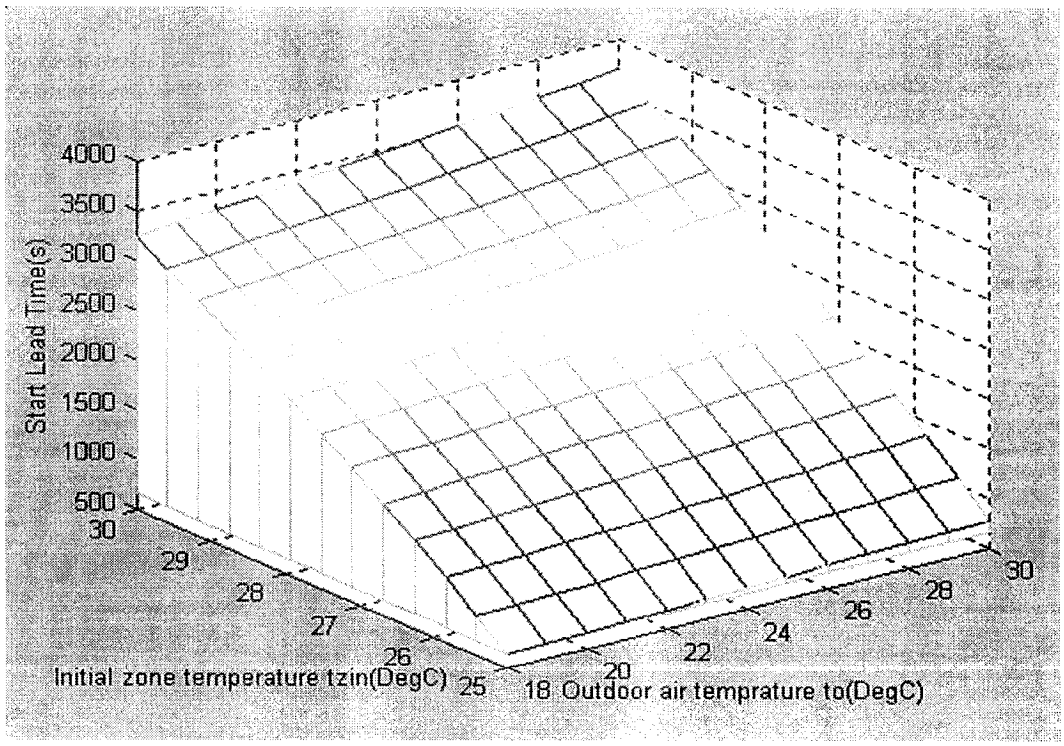


Figure 5.3 Relationship among start-lead-time, initial zone temperature ($t_{zin}$) and outdoor air temperature ($t_o$)

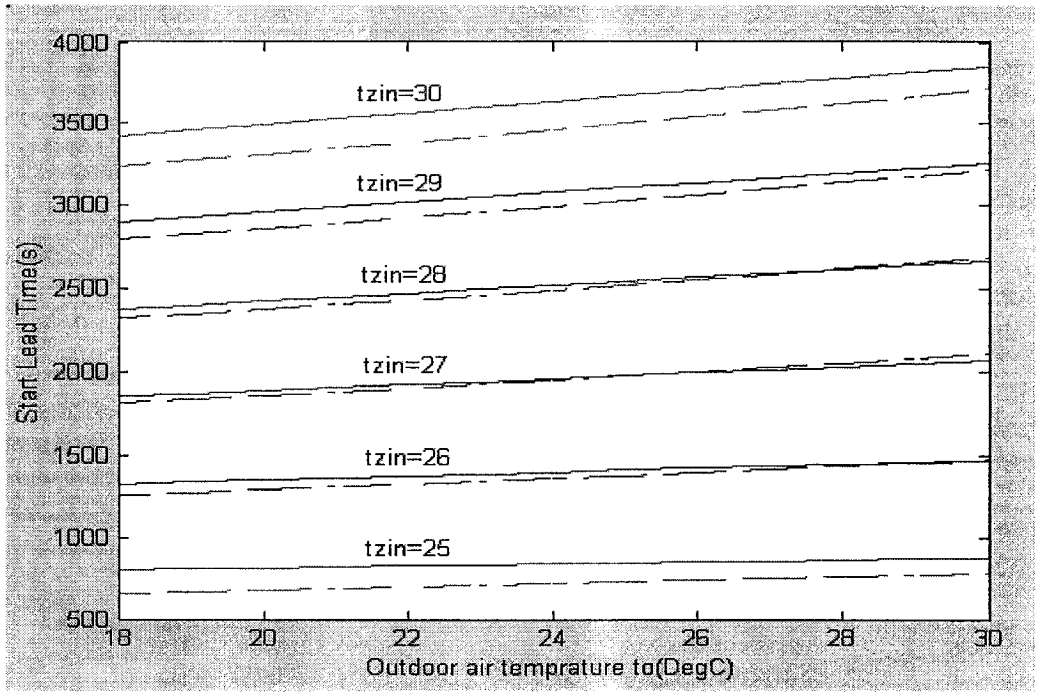


Figure 5.4 Start-lead-time profile (Model and original values) (case1)

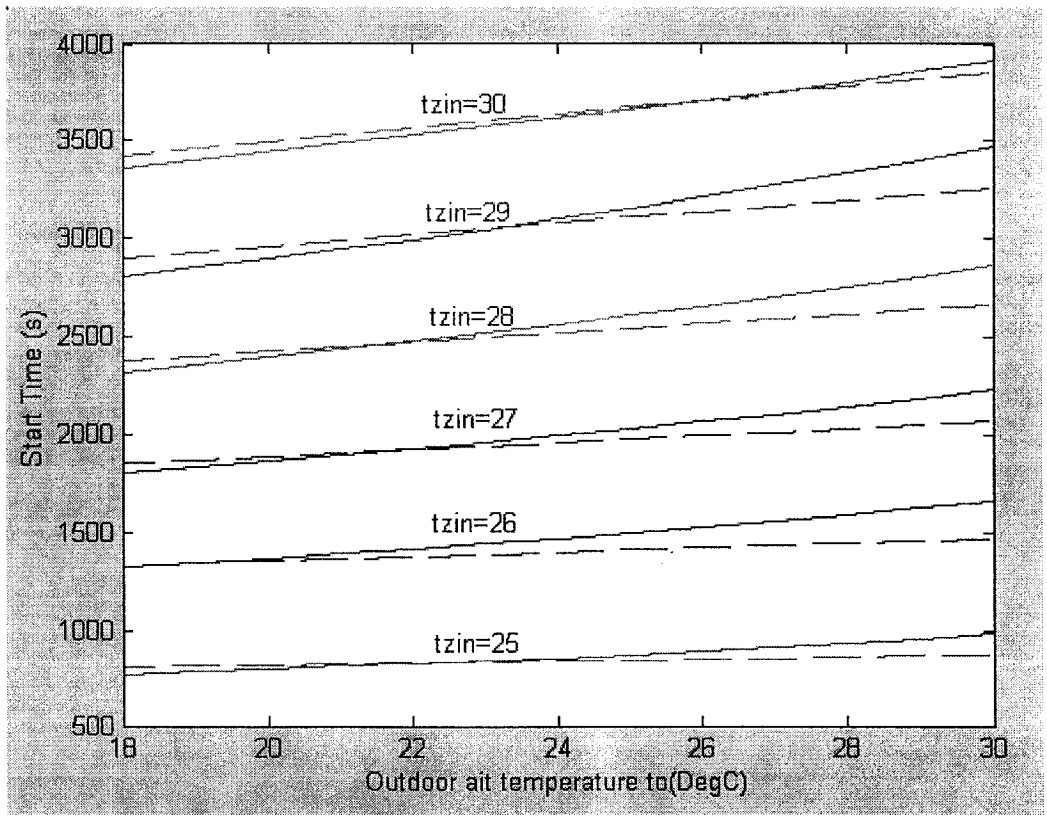


Figure 5.5 Validation of start-lead-time model (full model)

### 5.1.2 Validation of the start-lead-time model

In order to simplify the problem, we used a reduced order model to derive the start-lead-time equation (5.2) in the previous section. In this section, we verify this model using complete dynamic models, which were developed in chapter 3. This full-order model consists of zone model, cooling coil sensible models and the chiller and storage tank model.

#### 5.1.2.1. Validation using full-order models

From the open loop simulation of the full-order models, we obtain a series of zone temperature profiles under different initial value ($t_{zin}$) and different OA temperature ($t_o$) conditions. Accordingly, a time matrix [$T_{start}$], at which zone temperature ($t_z$) reaches its setpoint, was created. This relationship is shown in Figure 5.5 by solid lines. Also shown in Figure 5.5 are the dash lines, which represent the result from model equation (5.2). It can be seen that the result match very well. The biggest deviation, which occurs when OA temperature $t_o$ is up to 30℃ and initial zone temperature $t_{zin}$ is 29℃, is less than 200s. As a result, we can conclude that start-lead-time model derived by reduced model matches very well the full-order models' predictions.

#### 5.1.2.2 The effect of thermal capacity on the start-lead-time

Simulation runs were made using the reduced order model to study the effect of zone thermal capacity (ETC) on the start-lead-time. When the ETC was changed by one

half and one third, the model coefficients $a_1$, $a_2$, and $a_3$ also changed by half and one-third as well. This is shown in Figure 5.6 (thermal capacity reduced by half) and Figure 5.7 (one third thermal capacity). In these figures, the solid lines are from model equation, and dash lines are from the reduced order system model.

By comparing the result in Figure 5.4 with Figure 5.6 and 5.7, it was found that the start-lead-time is proportional the system ETC. As a result, we infer that the start-lead-time coefficients $a_1$, $a_2$, and $a_3$ are linear functions of the system equivalent thermal capacities (ETC). Figure 5.8 reveals this relationship.

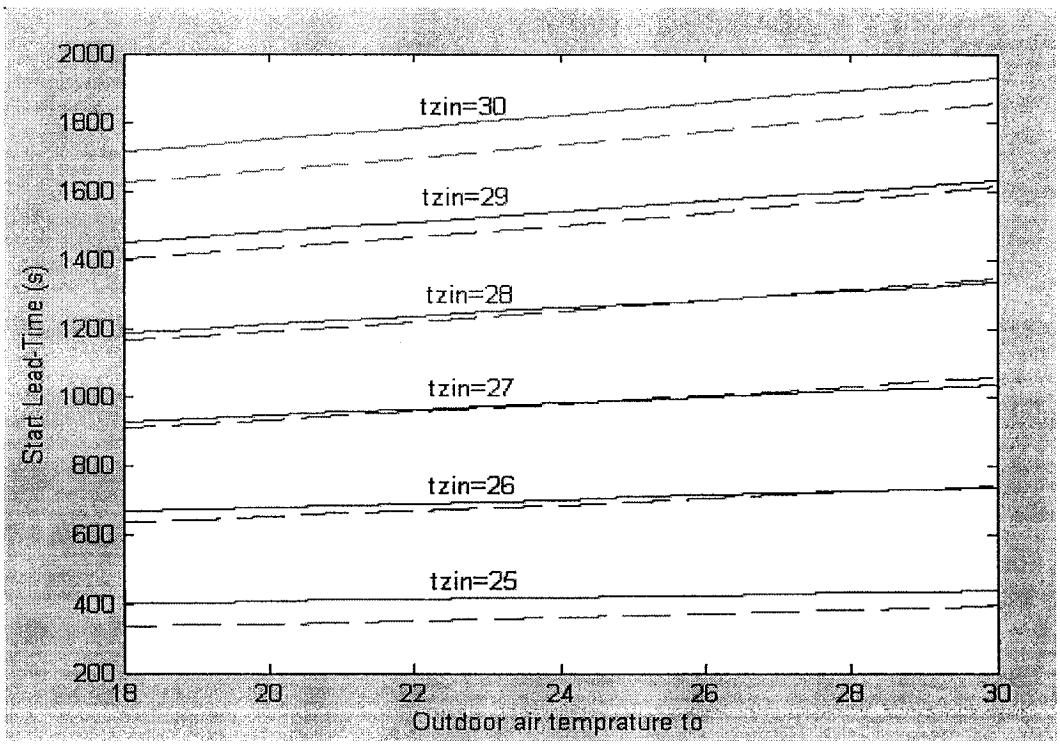


Figure 5.6 Modeling start-lead-time profile (case2)

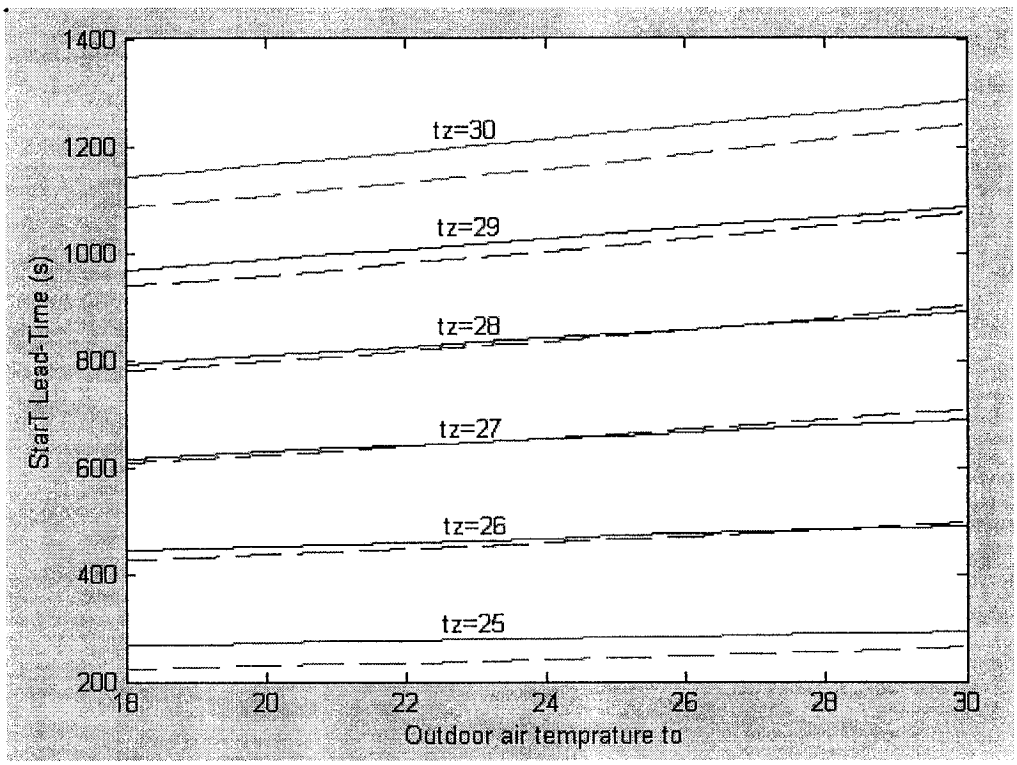


Figure 5.7 Modeling start-lead-time profile (case3)

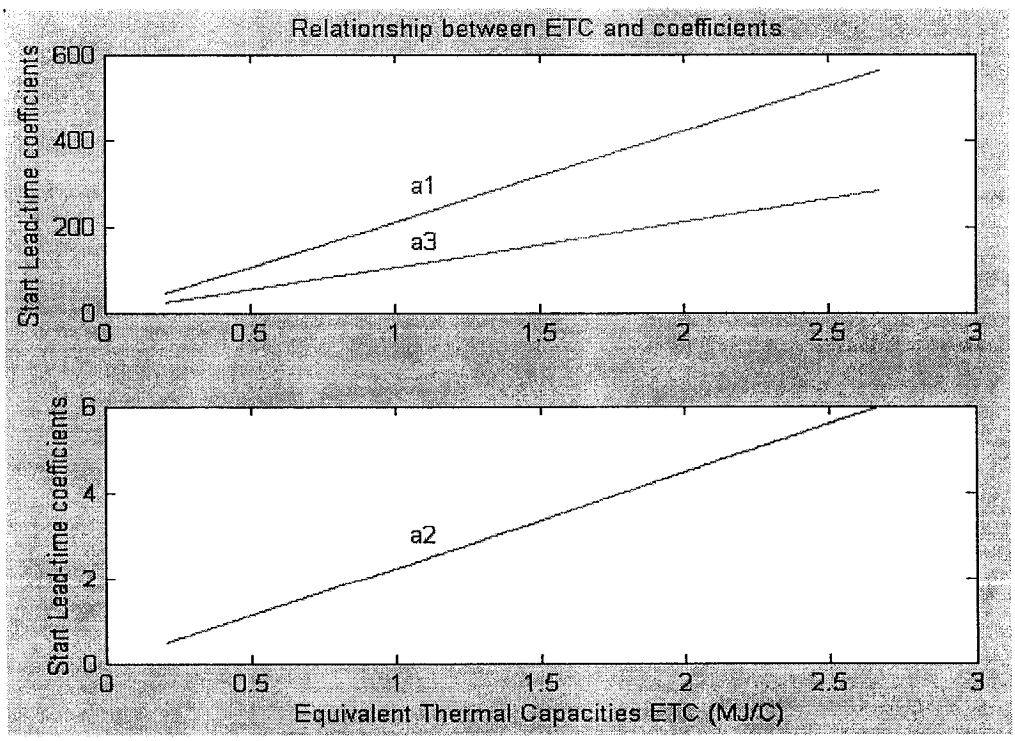


Figure 5.8 Relationship between start-lead-time coefficients and ETC

### 5.1.3 Application of the start-lead-time model

From the above discussion, it is clear that the thermal capacity of building envelope sufficiently influences the building thermal behavior and therefore the start-lead-time. Since the thermal capacity of the building varies significantly based on construction details, it was decided to investigate the effect of building thermal mass on start-lead-time using ASHRAE defined construction types such as light, medium, and heavy construction. To this end, a more detailed zone thermal model was used. The energy balance on zone air was described by

$$C_z \frac{dT_z}{dt} = M_a c_{p,a}(T_s - T_z) + \sum_{env} uA(T_{env,i} - T_z) + \sum_{window} uA(T_{out} - T_z) + \alpha(T_{out} - T_z) + q_s \quad (5.3)$$

Where $C_z$ is room air thermal capacity; right hand side has five terms: these are heat exchange between supply air and room, room surface and room air, window and room, infiltration and air changes and room sensible load consisting solar radiation and internal loads.

The surface temperature of enclosure element was modeled as

$$C_i \frac{dT_i}{dt} = \sum_j \frac{T_j - T_i}{R_{i,j}} + q_i \quad (5.4)$$

Where $C_i$ is the thermal capacity of node i, right hand side terms reflect the heat transfer between node i and all other adjacent nodes j, all heat input, respectively.

According to the ASHRAE fundamentals handbook (1997), there are three categories of buildings, which are heavy construction (634.4kg/m$^2$ or 130lb/ft$^2$), medium

construction (341.6kg/m$^2$ or 70lb/ft$^2$) and light construction (146.4kg/m$^2$ or 30lb/ft$^2$).

By simulating combined the zone model (5.3) and building envelope model equation (5.4), we obtained a series of start-lead-time curves for three different building construction types under three different loads (low, medium, and high loads). Figures 5.9, 5.10, 5.11 illustrate the start-lead-time trend (solid line) of three building types under high load conditions. The solid lines are from the detailed the zone model and dash lines represent the model (equation 5.2) values. These figures describe the thermal behavior of different types of buildings under different load condition when the system restarts.

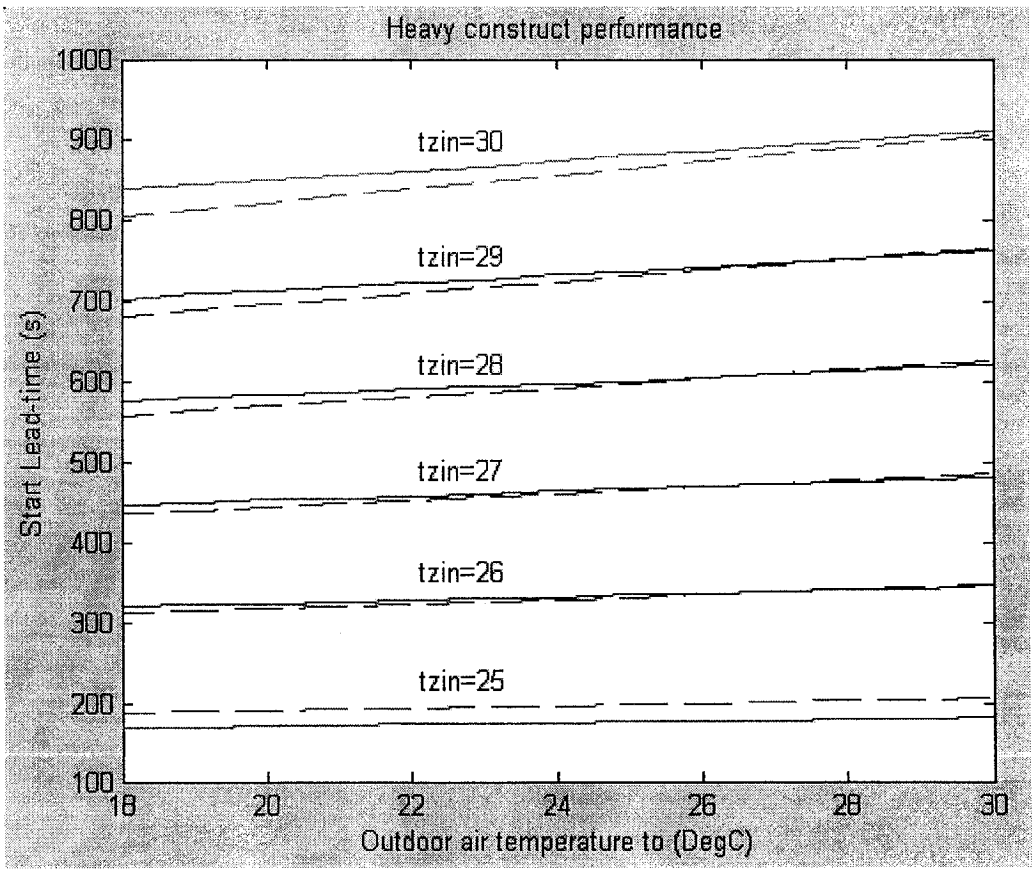


Figure 5.9 Heavy construction performance under high load

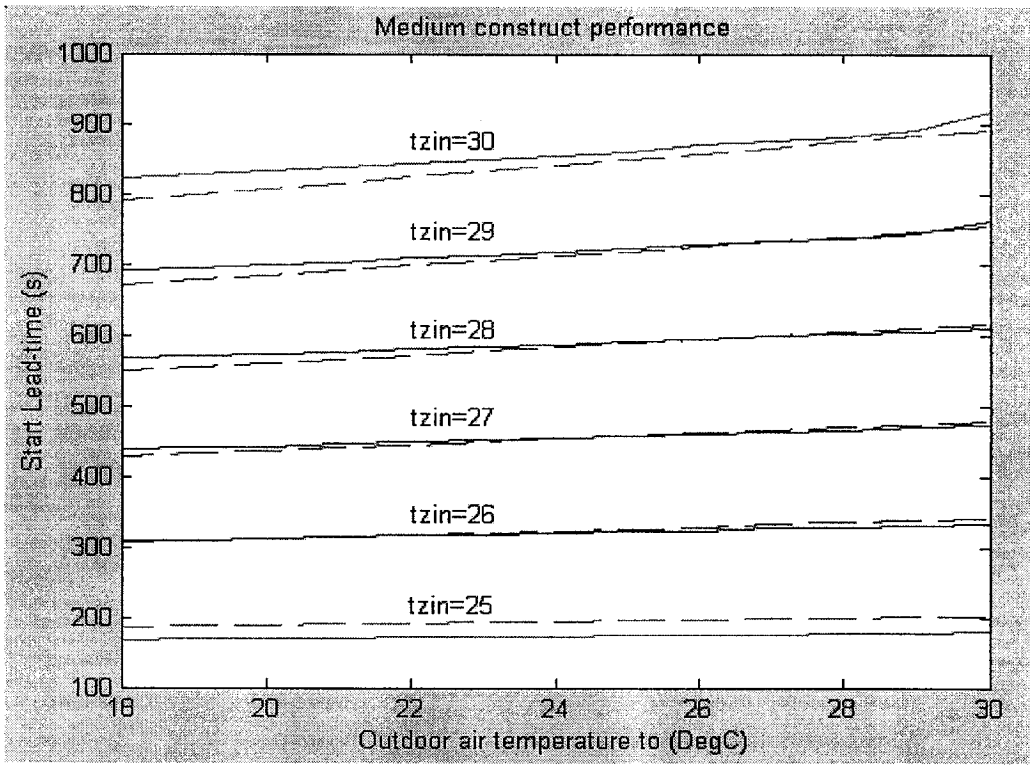


Figure 5.10 Medium construction performance under high load

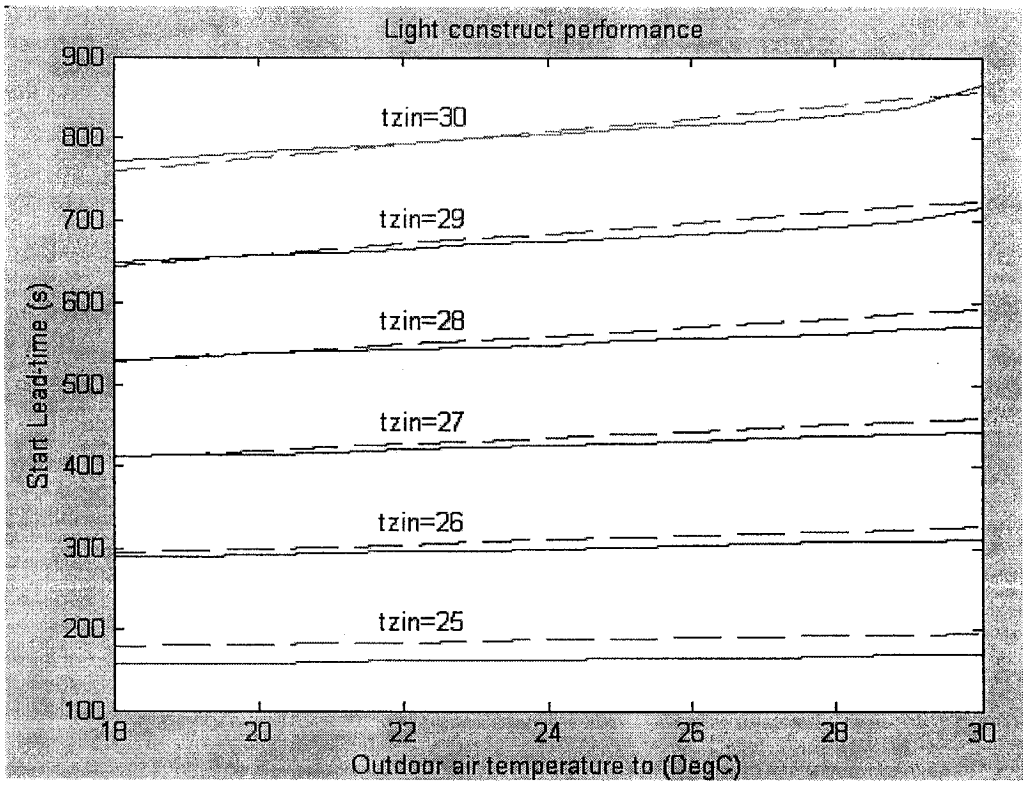


Figure 5.11 Light construction performance under high load

Also, we obtain the coefficients under different load ratio, which is defined as the load when the system restarts to the design load. Low, medium and high load respectively represent the ratio of 6.8%, quarter and one-third. Figure 5.12 reveals their relationship. Different load creates different start-lead-time in different building construction; moreover, this difference is bigger in light buildings than that in heavy ones. The reason is that ETC of light construction is lower than that of heavy building, so the light building is more sensitive to the load change than the heavy one does. Whereas, with the load gradually increasing, the light building shows decreased sensitivity to lead time. In the medium load conditions, the lead time difference between light and heavy buildings are not very significant.

In addition, the influence on the start-lead-time due to the different supply air temperature SAT was investigated. Figure 5.13 depicts the performance of start-lead-time coefficients under different SAT and three building constructions. The room temperature can rapidly decrease to its setpoint when SAT is low. However, with SAT increasing, the required period of cooling down rises significantly. Moreover, the influence of SAT on start-lead-time is bigger in heavy building than that in light construction. The reason is that ETC of heavy construction is higher than that of light building; therefore, heavy building needs longer time to cool down.

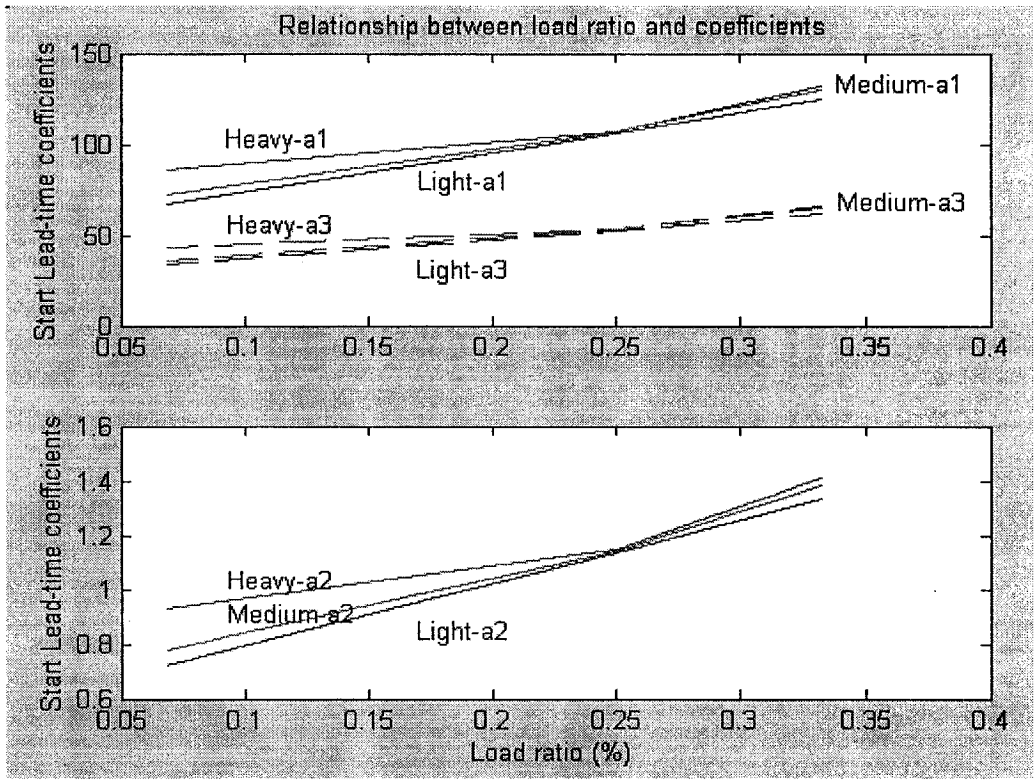


Figure 5.12 Relationship between coefficients and loads

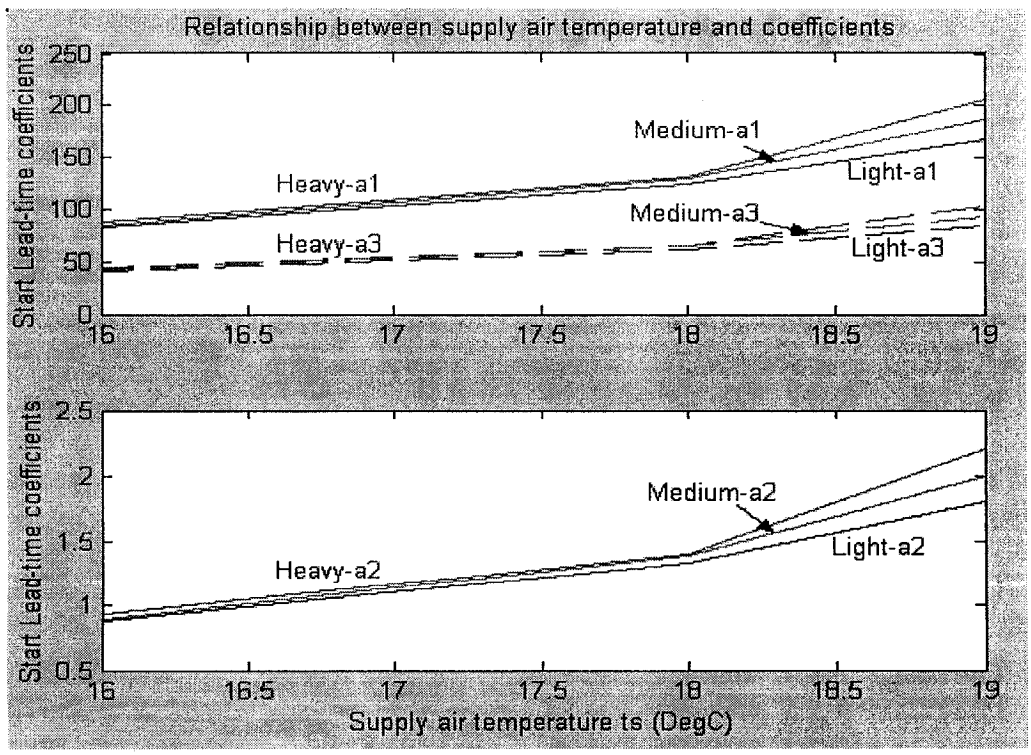


Figure 5.13 Relationship between coefficients and SAT

Finally, we summarize three sets of start time coefficients of three building types under different load conditions. Tables 5.1, 5.2, 5.3 depict the results under different supply air temperatures. In addition, we found the ETC, which gave start time result similar to these obtained from three construction types under three different loads and three supply air temperature conditions. The results summarized in Table 5.4.

Table 5.1 Start-lead-time coefficients ($t_s$=16℃)

| | Low load | | | Medium load | | | High load | | |
|---|---|---|---|---|---|---|---|---|---|
| | $a_1$ | $a_2$ | $a_3$ | $a_1$ | $a_2$ | $a_3$ | $a_1$ | $a_2$ | $a_3$ |
| Heavy construction | 57.31 | 0.61 | 28.66 | 70.97 | 0.76 | 35.48 | 87.09 | 0.93 | 43.54 |
| Medium construction | 46.98 | 0.5 | 23.49 | 68.96 | 0.73 | 34.48 | 83.95 | 0.9 | 41.97 |
| Light construction | 44.33 | 0.47 | 22.17 | 69.47 | 0.74 | 34.74 | 82.0 | 0.87 | 41.0 |

Table 5.2 Start-lead-time coefficients ($t_s$=18℃)

| | Low load | | | Medium load | | | High load | | |
|---|---|---|---|---|---|---|---|---|---|
| | $a_1$ | $a_2$ | $a_3$ | $a_1$ | $a_2$ | $a_3$ | $a_1$ | $a_2$ | $a_3$ |
| Heavy construction | 86.42 | 0.92 | 43.21 | 107.07 | 1.14 | 53.53 | 131.45 | 1.41 | 65.72 |
| Medium construction | 72.44 | 0.77 | 36.22 | 106.26 | 1.13 | 53.13 | 129.33 | 1.38 | 64.66 |
| Light construction | 67.26 | 0.72 | 33.63 | 105.66 | 1.13 | 52.83 | 124.44 | 1.33 | 62.22 |

Table 5.3 Start-lead-time coefficients ($t_s$=19℃)

| | Low load | | | Medium load | | | High load | | |
|---|---|---|---|---|---|---|---|---|---|
| | $a_1$ | $a_2$ | $a_3$ | $a_1$ | $a_2$ | $a_3$ | $a_1$ | $a_2$ | $a_3$ |
| Heavy construction | 134.94 | 1.44 | 67.47 | 167.16 | 1.79 | 83.58 | 205.12 | 2.20 | 102.56 |
| Medium construction | 104.47 | 1.12 | 52.23 | 153.42 | 1.64 | 76.71 | 186.66 | 2.00 | 93.33 |
| Light construction | 90.90 | 0.97 | 45.45 | 142.13 | 1.52 | 71.06 | 168.16 | 1.82 | 84.08 |

Table 5.4 Start ETC of three typical building types under different load conditions

| | Low load | | | Medium load | | | High load | | |
|---|---|---|---|---|---|---|---|---|---|
| Unit (℃) | $t_s$=19 | $t_s$=18 | $t_s$=16 | $t_s$=19 | $t_s$=18 | $t_s$=16 | $t_s$=19 | $t_s$=18 | $t_s$=16 |
| Heavy construction | 0.644 | 0.412 | 0.273 | 0.798 | 0.511 | 0.339 | 0.98 | 0.627 | 0.416 |
| Medium construction | 0.499 | 0.346 | 0.224 | 0.732 | 0.507 | 0.329 | 0.891 | 0.617 | 0.4 |
| Light construction | 0.434 | 0.321 | 0.211 | 0.678 | 0.504 | 0.331 | 0.803 | 0.594 | 0.391 |

(units: MJ/℃)

### 5.1.4 Conclusions

From previous analysis, we note that start-lead-time is a function of system operating parameters and thermal capacity of the building structure. Hence, we can draw the following conclusions:

1. The start-lead-time significantly varies with initial zone temperature $t_{zin}$; the difference can be around 2800s when zone temperature increases by 5℃ (from 25℃ to 30℃) (Figure 5.2). Moreover, the higher the zone temperature, the longer lead time is required.
2. OA temperature slightly affects the start-lead-time. The biggest difference is only 400s when outdoor temperature raises 12 ℃ (from 18℃ to 30℃) (Figure 5.1). Similarly, the higher the OA temperature, the longer the lead time.
3. Room sensible load influences the start-lead-time. There are significant differences between different loads even for the same building. (Figure 5.12 and Table5.1) Furthermore, the difference is bigger in light construction than it in

heavy construction.

4. Start-lead-time varies strongly as a function of SAT (Figure 5.13). Generally, the higher SAT, the longer start-lead-time is.
5. Building type is the other major aspect to influence the start-lead-time. Generally, the heavier the building, the longer the start time is.
6. Three coefficients $a_1$, $a_2$, $a_3$ proportionally vary with the building type and load.
7. The start time values, which are calculated from the proposed model, match well with the full-order model, and also have excellent agreement with the more detailed system model consisting of zone model and exterior envelope models.
8. Although the result shows similar trends for different building types, it may not be feasible to extend the result to all buildings without fine-tuning the coefficients of the model.
9. This approach can assist engineers easily realize optimum start time control in real systems. Only indoor and OA temperatures need to be measured in a specific system.

## 5.2 Programmed stop time

It is well known that the use of stop-lead-time can also achieve energy savings. This section will include the development of a stop-lead-time model, validation of the model, and application of the model.

### 5.2.1 Development of the stop-lead-time model

HVAC systems are stopped before the end of the occupancy time. To develop a model to predict the stop-lead-time, we use the same approach as earlier. We begin the analysis with a reduced order model. However, there are some differences that should be paid attention to compared with the start time model. First of all, from the zone model, the heat transfer between zone and supply air should be removed because we are interested in the time, in which the cooling system is shut down. Another important thing is that we have to choose an acceptable final zone temperature value $t_{zf}$, at which the occupants still feel comfortable even if the system is shut down. In addition, the air-delivery system still works while stopping the heat pump in order to satisfy the requirement of the fresh air. Hence, the energy balance equation of the zone becomes

$$ETC\frac{dT_z}{dt} = q_s + x_v m_a c_{pa}(T_o - T_z) + \alpha_z(T_o - T_z) \qquad (5.5)$$

Using this equation, we follow the same procedure to obtain sets of data for the stop-lead-time, at different initial zone temperature (zone current temperature), final zone temperature, and OA temperature. Figure 5.14 illustrates the functional relationship.

The stop-lead-time function was obtained by using curve fitting. The following equation was found to model the stop-lead-time result well.

$$T_{stop} = b_1(t_{zf} - t_{zin}) + b_2(t_{zf} - t_{zin})(t_o - t_{zset}) \qquad (5.6)$$

Where $b_1$, $b_2$ are the coefficients; $t_{zf}$ is the desired final temperature at the end of occupied time, and $t_{zin}$ is initial temperature at the point the heat pump is stopped. The first term in equation (5.6) is a linear function of the difference between actual zone temperature and desired final zone temperature, that is the acceptable increment of zone temperature. The second term is the product function of difference between expected zone temperature and initial zone temperature and outdoor air temperature and zone temperature setpoint and the expected zone temperature increment. Obviously, the stop time equals to zero when zone final temperature is same as the initial value. Furthermore, the time the system can shut down depends on another difference even if there is no difference between outdoor air temperature and zone temperature setpoint.

In Figure 5.15, the dash lines represent the results obtained from equation (5.6); solid lines are from the simulation data. These two sets of curves match each other well.

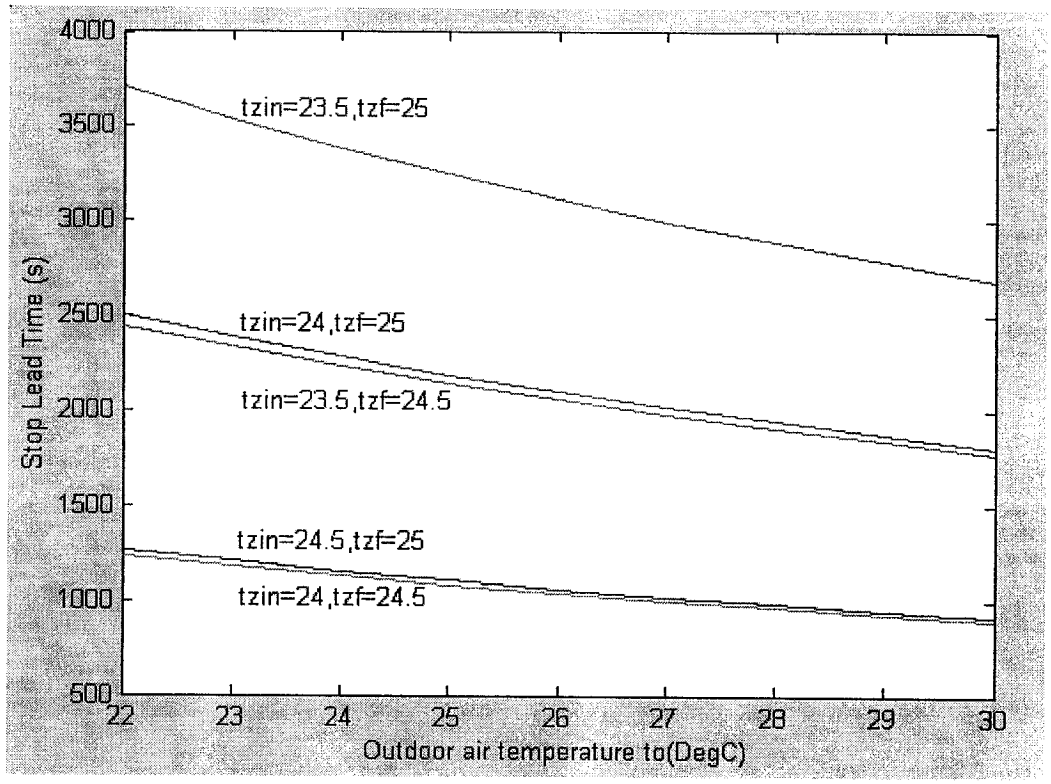


Figure 5.14 Stop-lead-time profile

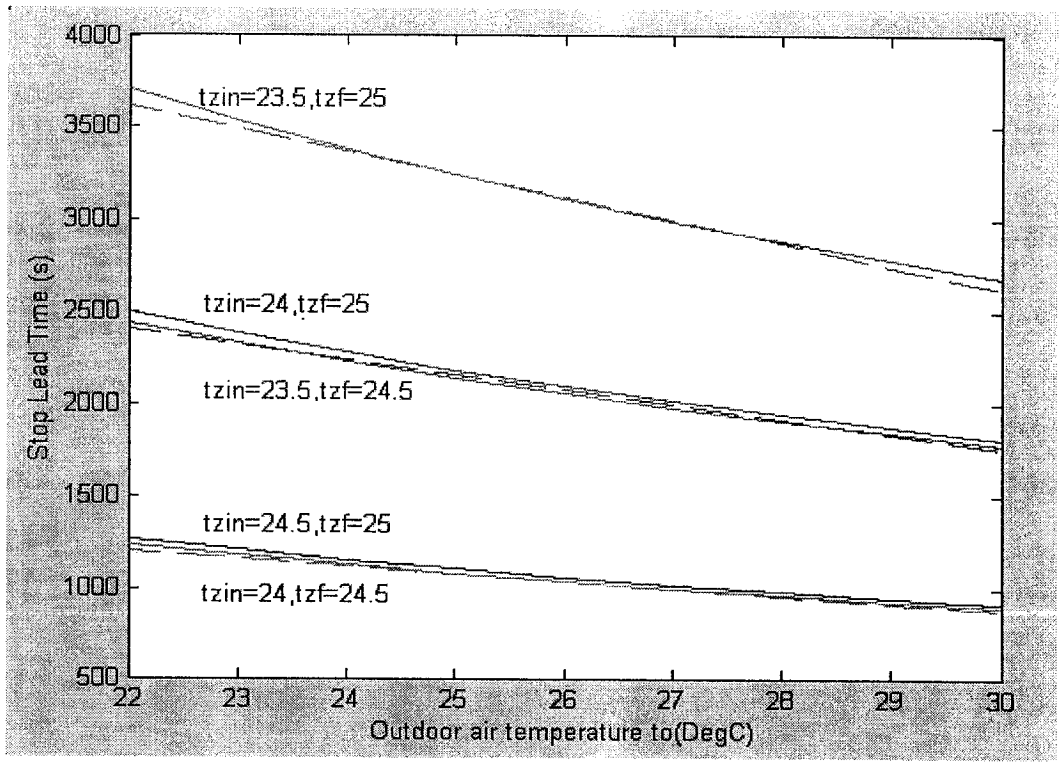


Figure 5.15 Modeling stop-lead-time profile (case1)

## 5.2.2 The effect of thermal capacity on the stop-lead-time model

The effect of thermal capacity of the structure was investigated by changing the zone thermal capacity by half (case 2) and one third (case 3). The results are depicted in Figure 5.16 and 5.17 respectively. It was noted that the stop time model coefficients decreased linearly as a function of thermal capacity. Shown in Figure 5.18 are the stop-lead-time coefficients as a function of equivalent thermal capacity. It is worth noting that the coefficients $b_1$ and $b_2$ change in opposite directions as the ETC is increased.

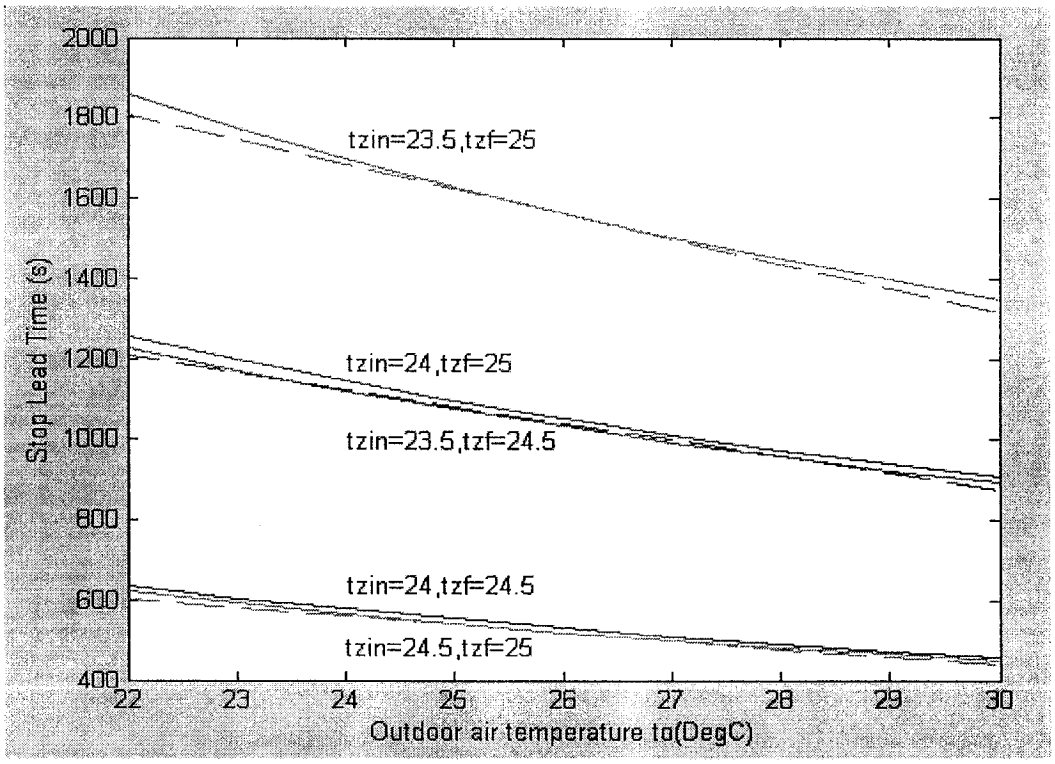


Figure 5.16 Modeling stop-lead-time profile (case2)

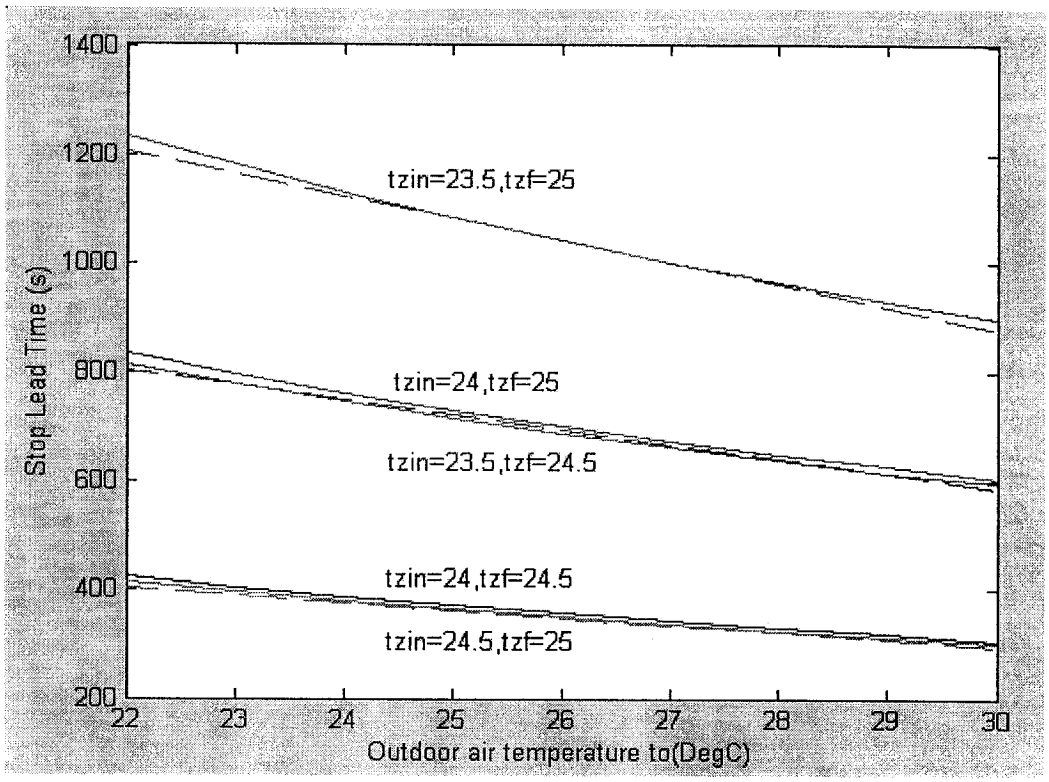


Figure 5.17 Modeling stop-lead-time profile (case3)

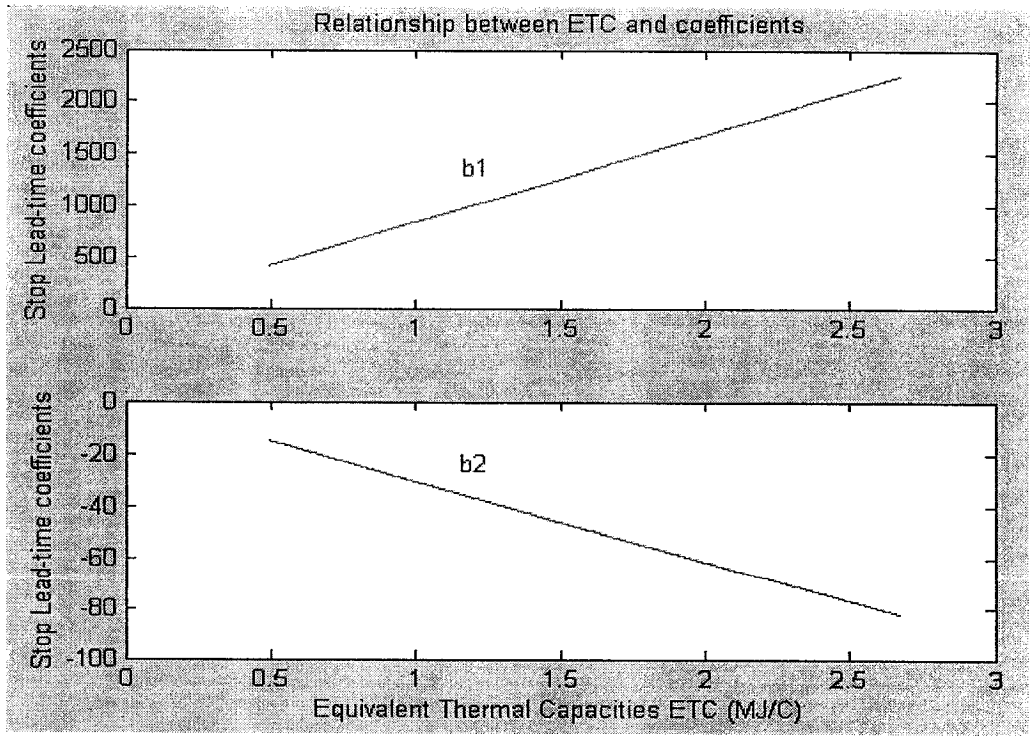


Figure 5.18 Relationship between stop-lead-time coefficients and ETC

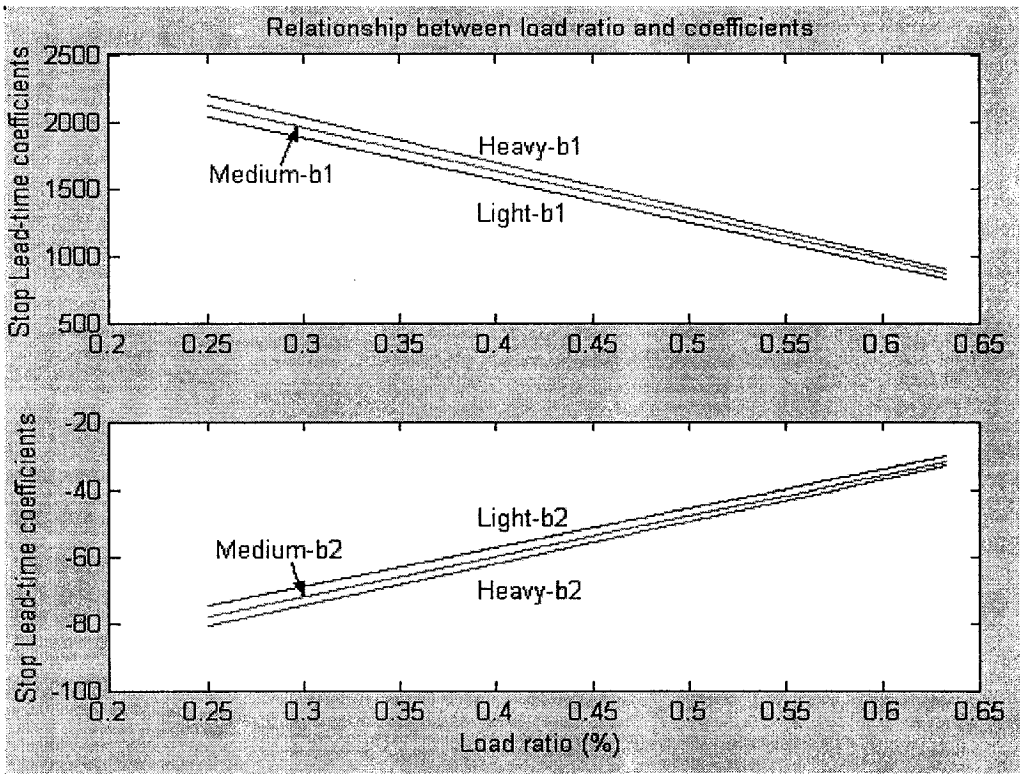


Figure 5.19 Relationship between stop-lead-time coefficients and load ratio

Table 5.5 Stop-lead-time coefficients of three typical building types under different load conditions

| | Low load | | Medium load | | High load | |
|---|---|---|---|---|---|---|
| | $b_1$ | $b_2$ | $b_1$ | $b_2$ | $b_1$ | $b_2$ |
| Heavy construction | 2196.78 | -80.51 | 1465.85 | -53.67 | 898.24 | -32.92 |
| Medium construction | 2112.24 | -77.40 | 1408.16 | -51.6, | 863.69 | -31.65 |
| Light construction | 2034.0 | -74.54 | 1356.0 | -49.69 | 831.70 | -30.48 |

Table 5.6 Stop ETC of three typical building types under different load conditions (unit: MJ/℃)

| | Low load | Medium load | High load |
|---|---|---|---|
| Heavy construction | 2.615 | 1.604 | 1.069 |
| Medium construction | 2.515 | 1.543 | 1.028 |
| Light construction | 2.421 | 1.485 | 0.990 |

### 5.2.3 Application of the stop-lead-time model

Analyses of the stop-lead-time for the same three types of building construction (ASHRAE fundamentals handbook (1997)) were made. Neglecting the cooling load from the supply air because the coil is shut down, zone model equation 5.4 becomes

$$C_z \frac{dT_z}{dt} = \sum_{env} uA(T_{env,i} - T_z) + \sum_{window} uA(T_{out} - T_z) + (\alpha + x_v M_a c_{p,a})(T_{out} - T_z) + q_s \qquad (5.7)$$

And the zone envelope model remains the same as in equation 5.4. Simulation runs were made to determine the stop-lead-time coefficients for three types of buildings under different load conditions. Figure 5.19 shows the results. From this figure, we can see that the coefficients vary linearly as a function of load. Moreover, the period that the system with lower load stops before the end of the occupied time is longer than that of the system with higher load. This is because low-load-system requires long time period to raise unit degree in temperature. It may be noted from Figure 5.18 and 5.19 that the stop-lead-time coefficient change in opposite directions as a function of ETC and load ratio.

In addition, Tables 5.5 and 5.6 summarize the stop time coefficients and ETC of three building types under different load conditions.

### 5.2.4 Conclusions

The following conclusions are made based on the simulation results:

1. One of the key factors that affect the stop time is the difference between initial

and expected zone final temperature, that is, the expected increment of zone temperature; moreover, the bigger this difference, and the longer the stop time is. Particularly, the biggest time difference can be up to 2500s when the temperature increment raises from 0.5℃ to 1.5℃;

2. Another main aspect is the system's ETC, which is proportionally influences the stop time model coefficients. They have different stop time in the three different construction types of buildings (heavy, medium and light). The heavier the building, the longer the system stop-lead-time is.
3. The system's current load is important factor to determine the stop time. Furthermore, the higher the system output, the shorter is the stop-lead-time.
4. The stop-lead-times are almost the same when the expected zone temperature increments are the same though lower initial temperature gets a little bit lower time value (comparison line $t_{zin}$=24.5℃, $t_{zf}$=25℃ and $t_{zin}$=24℃, $t_{zf}$=24.5℃, or line $t_{zin}$=23.5℃, $t_{zf}$=24.5℃ and $t_{zin}$=24℃, $t_{zf}$=25℃ in figures 5.14, 5.15, 5.16, 5.17.).
5. This strategy can be easily implemented in real systems because only two parameters are required which can be measured easily.

# Chapter 6 EMC algorithms: Reset and occupied time control strategies

This chapter demonstrates two important EMC functions, which are commonly used in HVAC systems. Section 6.1 emphasizes on supply air temperature SAT reset, and section 6.2 illustrates the occupied time control strategies.

## 6.1 SAT reset algorithm

One important way to minimize the use of mechanical cooling energy in HVAC systems is to raise the SAT during occupied periods when cooling loads are not at their peak value. Historically, HVAC systems were designed with constant SAT that was able to meet peak condition. However, the peak condition rarely occurs. By adjusting this temperature to meet real-time load condition, sufficient amounts of energy can be saved. In this chapter, three reset algorithms are analyzed and compared with constant SAT method.

### 6.1.1 Development of cooling load model

Performing reset strategies requires an estimate or prediction of building load. This section focuses on developing predictive sensible cooling load model $q_s$. Generally, room sensible cooling load constitutes four components of load, which are building envelop load, solar radiation load, internal load, and air change and infiltration loads.

Firstly, we use the predictive strategy to forecast OA temperature. The OA temperature model used by Cho and Zaheer-uddin (2002), which was adapted from the model described in DOE-2 program, is very useful to predict the hour-by-hour values of outdoor temperatures. Some inputs are needed in order to use the model; these are expected maximum ($T_h$) and minimum ($T_l$) OA temperatures and their time-of-day occurrences ($t_h$, $t_l$). Accordingly, the temperature model consists three equations:

$$T = T_v - T_d \cos[(\frac{\pi}{24-(t_h - t_l)})(t - t_l)] \quad \text{when } t \leqslant t_l \qquad (6.1\text{-}1)$$

$$T = T_v - T_d \cos[(\frac{\pi}{(t_h - t_l)})(t - t_l)] \quad \text{when } t_l < t \leqslant t_h, \qquad (6.1\text{-}2)$$

$$T = T_v - T_d \cos[(\frac{\pi}{24-(t_h - t_l)})(t - t_h) - \pi] \quad \text{when } t \geqslant t_h, \qquad (6.1\text{-}3)$$

Where $T_v = \frac{T_h - T_l}{2}$, $T_d = \frac{T_h + T_l}{2}$

Then, we calculate hourly cooling load based on this forecasted outdoor temperature (equation 6.1-2) during the occupied time. Finally, the model of predictive cooling load was derived as a function of the room peak load $q_{s,peak}$, OA temperature $t_o$, and the difference between outdoor temperature average value $t_{o,mean}$ and room temperature setpoint $t_{z,set}$. The equation is

$$q_s = q_{s,peak}(a_1 t_o^{\,2} + a_2 t_o + a_3 + a_4(t_{z,set} - t_{o,mean})) \qquad (6.2)$$

Where $a_1$, $a_2$, $a_3$, $a_4$ are coefficients. This equation reveals that the predicted load ratio is a second-order polynomial; it also includes the deviation of outdoor and indoor temperature. This study focuses on the heavy building construction. Figure 6.1 illustrates

coefficient $a_1$ of load prediction with different amplitude when OA temperature peak changes from 24℃ to 34℃. Similarly, Figure 6.2 displays the coefficients $a_2$, $a_3$ vary with both peak and amplitude of OA temperature. In addition, in Figure 6.2, the numbers such as $a_2$-8, $a_3$-12 represent the difference between the maximum and minimum values of OA temperature, respectively, such as 12℃, 10℃, and 8℃. The magnitudes of the coefficients for different OA conditions are depicted in Table 6.1.

### 6.1.2 The SAT model

From the zone sensible heat balance equation $q_s = M_a c_{p,a}(t_{z,set} - t_s)$, we can let the supply air temperature (SAT) $t_s$ equal to:

$$t_s = t_{z,set} - \frac{q_s}{M_a c_{p,a}}$$

By substituting for $q_s$ from equation 6.2, the $t_s$ equation becomes:

$$t_s = t_{z,set} - \frac{q_{s,peak}}{M_a c_{p,a}}(a_1 t_o^{\,2} + a_2 t_o + a_3 + a_4(t_{z,set} - t_{o,mean})) \tag{6.3}$$

Alternatively, we may replace the transient supply air mass flow rate by the maximum value. As a result, another SAT setpoint equation is given by

$$t_s = t_{z,set} - \frac{q_{s,peak}}{M_{a,\max} c_{p,a}}(a_1 t_o^{\,2} + a_2 t_o + a_3 + a_4(t_{z,set} - t_{o,mean})) \tag{6.4}$$

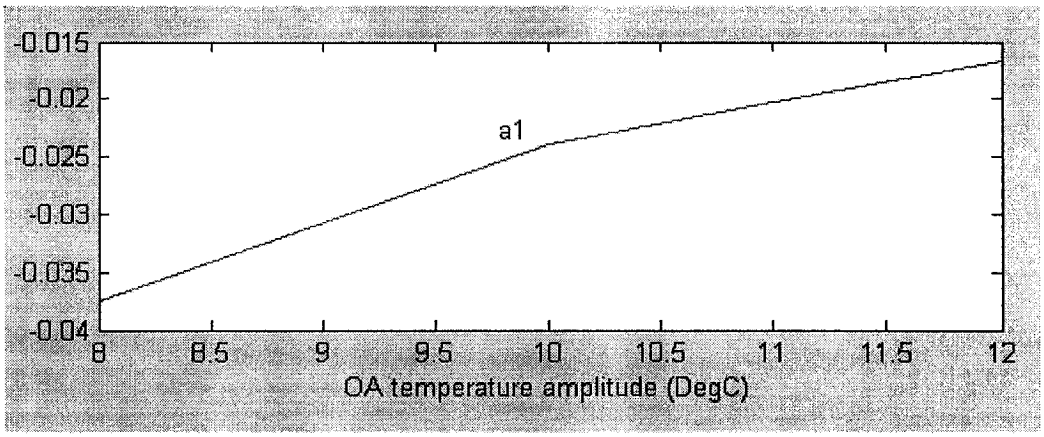


Figure 6.1 Coefficient $a_1$ varies with OA temperature amplitude

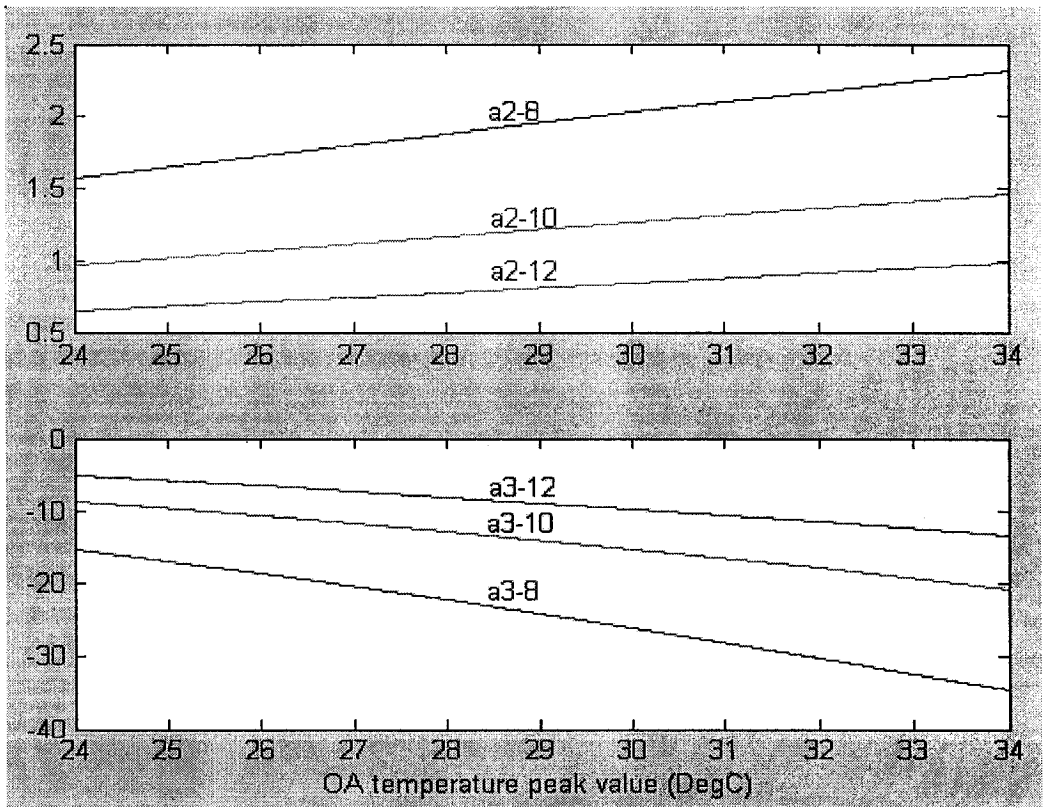


Figure 6.2 Coefficient $a_2$, $a_3$ vary with peak and amplitude of OA temperature

### 6.1.3 Dynamic performance of reset algorithms

The most commonly used strategy is the constant supply air temperature setpoint (CSATS). Three different algorithms are also described in this section. In order to simulate the room temperature and compute system energy consumption during occupied period of the day, a PI controller is used to implement the reset strategies.

#### 6.1.3.1. Constant SAT setpoint algorithm

Constant SAT setpoint (CSATS) is the most common technique in HVAC systems. We simulate its performance with following assumptions. First, the room temperature is supposed to maintain its setpoint 24℃ and SAT is held constant at 13℃. Then, OA temperature $t_o$ is predicted using equations 6.1-1, 2, 3 with average value of 25℃ and 10 ℃ daily range. The room sensible load $q_s$ is forecasted using equation 6.2. The room temperature and SAT profiles are depicted in Figure 6.3. The responses show that zone temperature reach its setpoint after two and half hours. The supply air temperature likewise reaches setpoint after about 3 hours. The maximum deviation from setpoint is somewhat large. This could be minimized by choosing better PI gain constants.

#### 6.1.3.2. Linear supply air temperature setpoint algorithm

In the linear SAT setpoint (LSATS) approach, the SAT setpoint is assumed to be a linear function of room temperature over a certain range. SAT setpoint has high and low boundaries, which are high limit ($t_{s,h}$) and low limit($t_{s,l}$). Likewise, space temperature has its high ($t_{z,h}$) and low ($t_{z,l}$) limits. Then $t_s$ setpoint can be computed from

$t_s = t_{s,h}$ when $t_z \leq t_{z,l}$ (6.5-1)

$$t_s = t_{s,h} - \frac{t_{s,h} - t_{s,l}}{t_{z,h} - t_{z,l}}(t_z - t_{z,l}) \quad \text{when } t_{z,l} < t_z < t_{z,h} \qquad (6.5\text{-}2)$$

$t_s = t_{s,l}$ when $t_z \geq t_{z,h}$ (6.5-3)

Figure 6.4 illustrates room and SAT setpoint profile. These results were obtained with $t_{s,h}$ equal to 18℃ and $t_{s,l}$ equal to 13℃. Accordingly, $t_{z,h}$ is equal to 26℃ and $t_{z,l}$ is 22℃, and $t_{z,set}$ is 24℃. The room temperature reaches its setpiont faster (about two hours) with smaller oscillations (maximum 2℃) compared with the CSATS (Figure 6.3). Furthermore, $t_{a,set}$ has appropriate trend that is a higher $t_z$ produces lower $t_{a,set}$, and lower $t_z$ causes higher $t_{a,set}$, and $t_{a,set}$ stays constant as $t_z$ reaches constant setpoint.

### 6.1.3.3. Improved SAT setpoint algorithm

The improved supply air setpoint strategy was defined as follows:

$t_s = t_{s,h}$ when $t_z \leq t_{z,l}$

$$t_s = t_{zset} - \frac{q_{s,peak}}{m_a c_{pa}}(a_1 t_o^{\,2} + a_2 t_o + a_3 + a_4 (t_{zset} - t_{o\_mean})) \quad \text{when } t_{z,l} < t_z < t_{z,h}$$

$t_s = t_{s,l}$ when $t_z \geq t_{z,h}$

The results obtained by implementing this strategy are depicted in Figure 6.5.

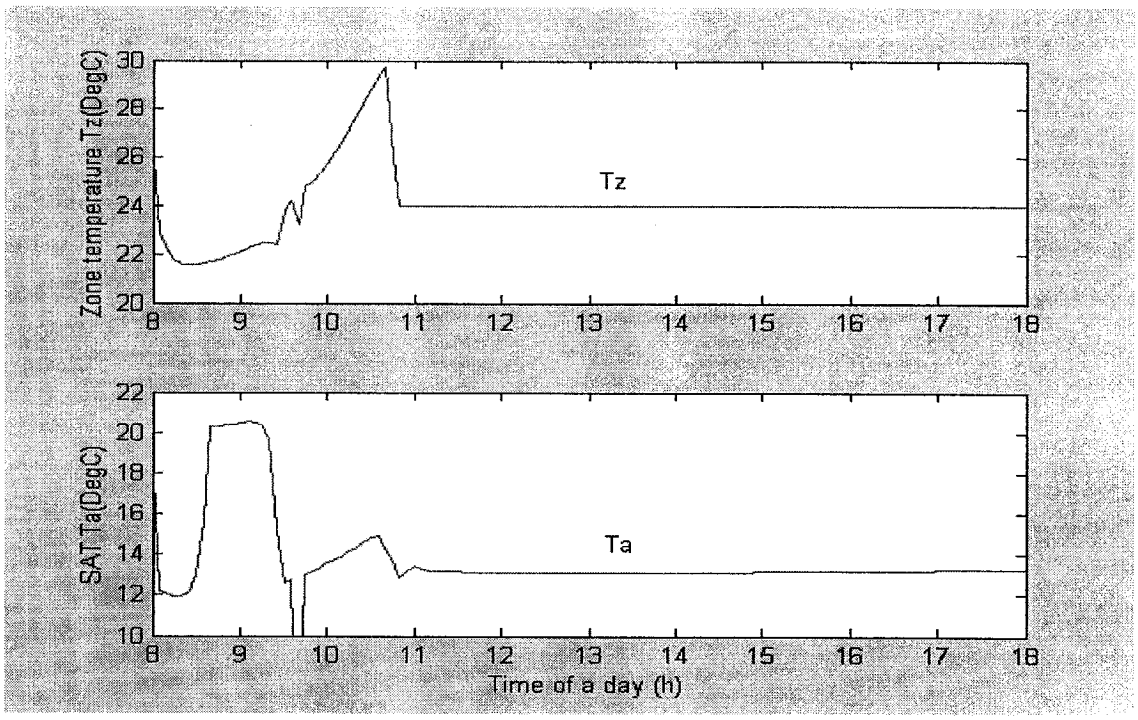


Figure 6.3 Constant supply air temperature setpoint responses

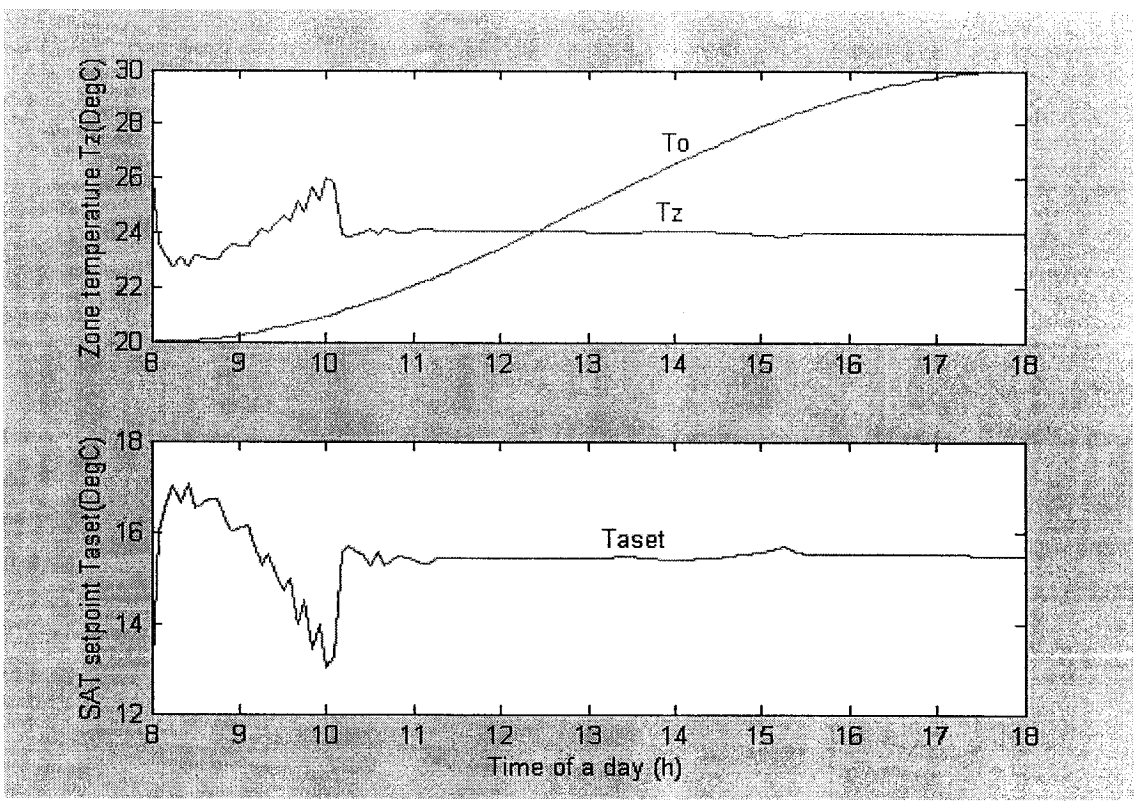


Figure 6.4 Linear supply air temperature setpoint responses

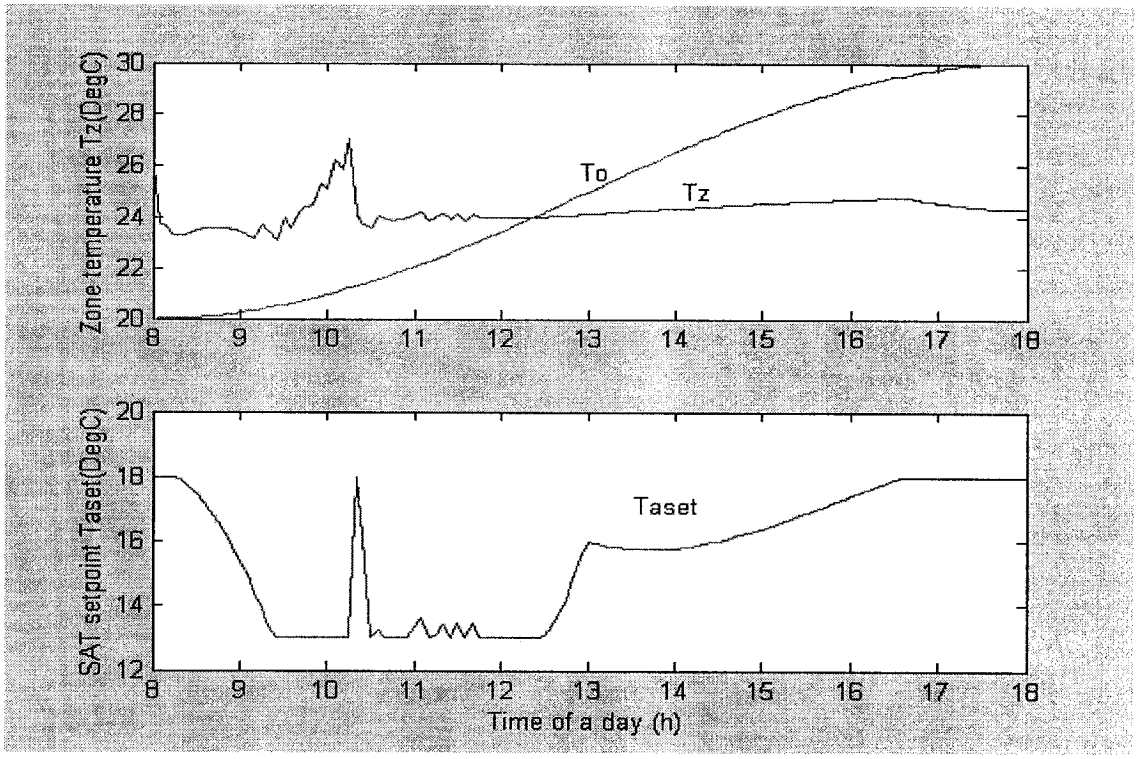


Figure 6.5 Improved supply air temperature setpoint responses

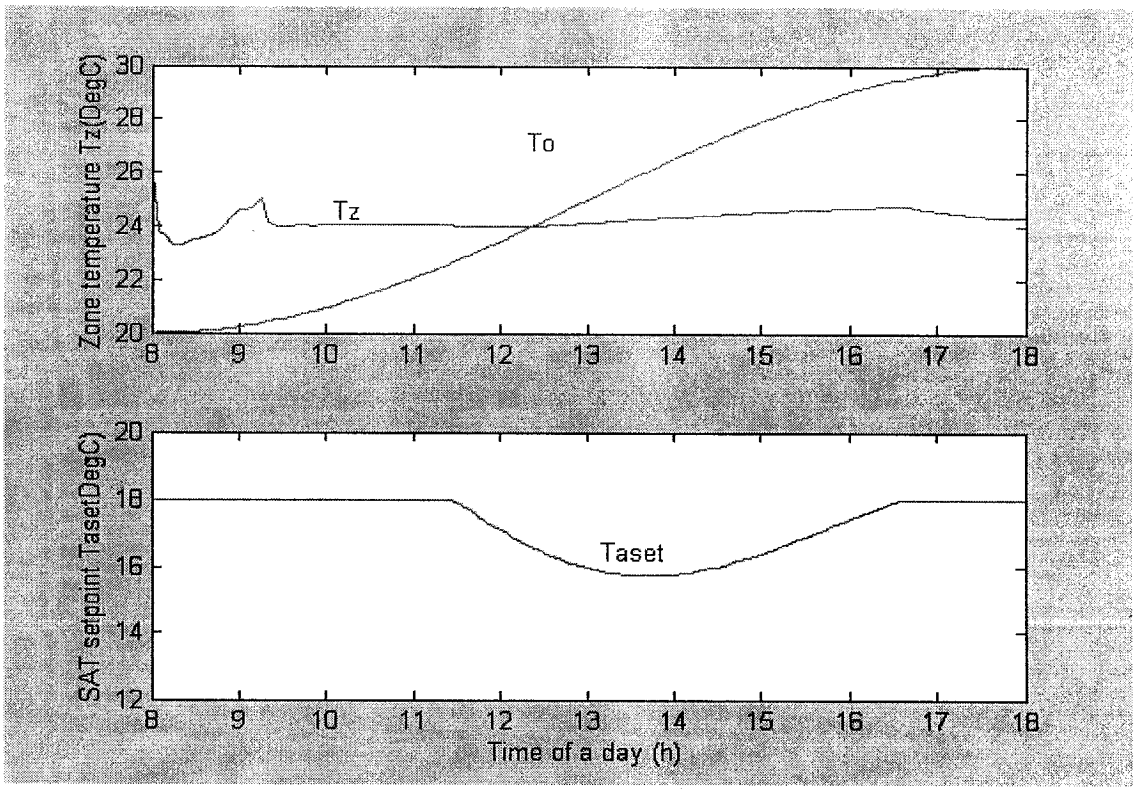


Figure 6.6 Alternate supply air temperature setpoint responses

### 6.1.3.4. Alternate SAT setpoint algorithm

The alternate SAT setpoint strategy is similar to the improved SAT scheme except for the use of $M_{a,max}$ in predicting the supply air temperature. The simulation results obtained from this scheme are shown in Figure 6.6.

## 6.1.4 Three typical day energy consumption

By using four SAT reset schemes described before three typical days' energy consumption simulations were made. Table 6.2 and Figure 6.7 show three daily simulation results. The three days selected were typical days in the months of May, August, and October.

A comparison of energy consumption (Table 6.2 and Figure 6.7) obtained from these four strategies shows that ASATR strategy result in lowest energy consumption all days and the savings can be up to 7% (in August) while savings in May and October range between 3 to 6% because the need for cooling exists only during part of the occupied time.

## 6.1.5 Conclusions

From the results obtained we can conclude that

1. Constant setpoint scheme consumes more energy and takes longer time to reach steady state with significant oscillations.
2. All of linear, improved, and alternate strategies have the limitations about the setpoint (high and low limit), and all can save energy and obtain good

performances, which take shorter time to reach steady state with smaller oscillations. The differences among these three techniques are not significant.

3. The ASATS strategy resulted in 7% of energy savings compared with constant supply air temperature setpoint strategy.

Table 6.1 Coefficient of predicted cooling load

| | OA amplitude | OA Peak Temperature (℃) | | | | | |
|---|---|---|---|---|---|---|---|
| | | 34 | 32 | 30 | 28 | 26 | 24 |
| $a_1$ | 12 | -0.0168 | -0.0167 | | | | |
| | 10 | -0.024 | | | | | |
| | 8 | -0.0375 | | | | | |
| $a_2$ | 12 | 0.9812 | 0.9104 | 0.8437 | 0.777 | 0.7103 | 0.6436 |
| | 10 | 1.4447 | 1.3486 | 1.2526 | 1.1565 | 1.0604 | 0.9644 |
| | 8 | 2.3161 | 2.1660 | 2.0159 | 1.8659 | 1.7158 | 1.5657 |
| $a_3$ | 12 | -13.3528 | -11.4116 | -9.6575 | -8.0369 | -6.5496 | -5.1958 |
| | 10 | -20.7144 | -17.9211 | -15.32 | -12.9109 | -10.694 | -8.6691 |
| | 8 | -34.7289 | -30.2468 | -26.0649 | -22.1831 | -18.6014 | -15.32 |
| $a_4$ | 12 | -0.015 | | | | | |
| | 10 | | | | | | |
| | 8 | | | | | | |

Table 6.2 Three days energy consumption

| SATR algorithm | | CSATS | LSATS | ISATS | ASATS | (1-4)/1 (%) |
|---|---|---|---|---|---|---|
| Number in Figure 6.5 | | 1 | 2 | 3 | 4 | |
| Typical days | May | 36.54 | 34.78 | 34.58 | 34.33 | 6.05 |
| | August | 110.5 | 106.8 | 104.42 | 102.56 | 7.18 |
| | October | 26.13 | 25.32 | 25.51 | 25.18 | 3.63 |

(Unit: MJ)

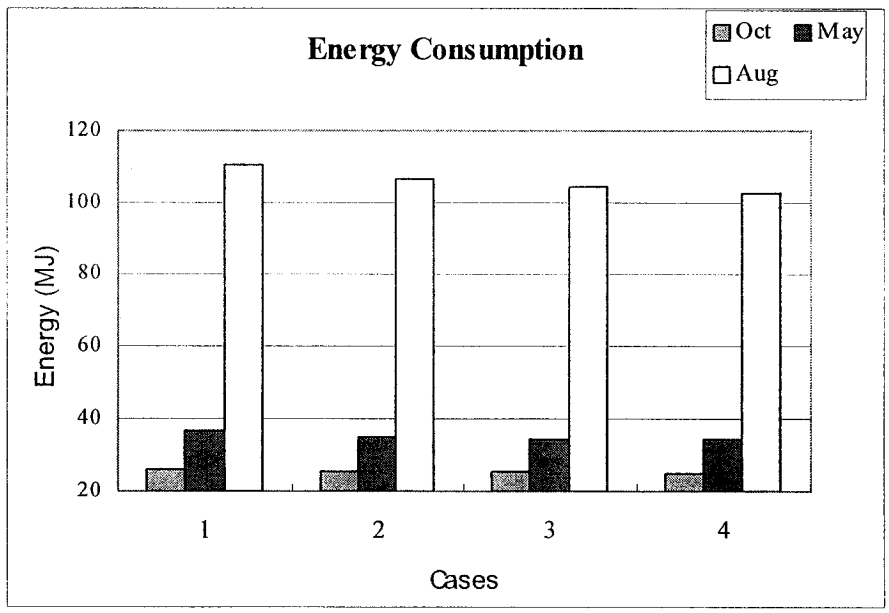


Figure 6.7 Three typical days' energy consumption

## 6.2. Occupied time control strategies

Occupied period control schemes are the most important and complex EMC functions because they could affect the system response, stability, energy consumption and thermal comfort level. Several control strategies can be used to control HVAC system such as those reviewed in the literature survey. Although researchers have been orientating to optimal control recently, PI control is the most common and widely used control scheme in practical HVAC systems. This is the reason that PI control strategy is employed as one control method to study the system characteristics in this thesis. Alternatively, an adaptive control strategy is also proposed for regulating the HVAC thermal processes during occupied period.

### 6.2.1. PI control strategy

PI controller is a typical modulating controller used in HVAC systems. In a closed-loop system with PI controller, a sensor provides feedback signal (Figure 6.8) of a controlled variable. This variable is compared with its setpoint and their difference (error) is multiplied by a constant (proportional gain), and summed with the results of the integral of the error multiplied by another constant (integral gain) to obtain an output. The output signal is sent to the actuator thus initiating the regulation of the process.

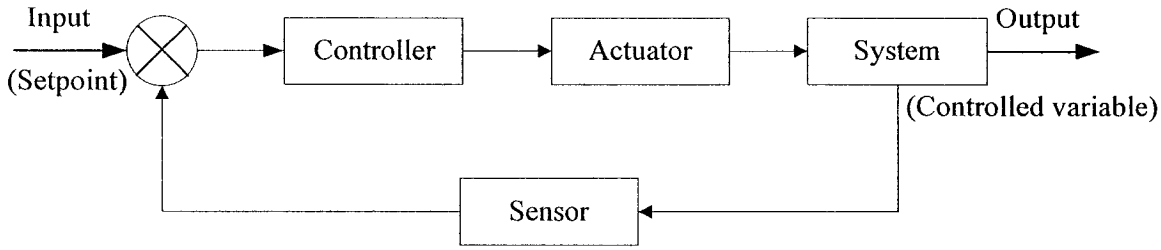


Figure 6.8 Diagram of a closed-loop control procedure

Typically, the single zone VAV system under consideration involves three closed control loops. The state variables are zone temperature $t_z$, SAT $t_a$, RWT $t_{wr}$. The control variables are supply air mass flow rate $M_a$, supply water mass flow rate $M_w$, and heat pump actual input $U_{hp}$. Consequently, loop 1 is supply air mass flow rate ($M_a$) control loop. Room temperature ($t_z$) error signals the controller to tailor the air mass flow rate by modulating terminal damper position. Transient $t_z$ above setpoint produces an increment of $M_a$ by increasing the damper opening. Otherwise, reducing the mass flow rate increases the lower $t_z$ to reach its setpoint. Secondly, loop 2 is water mass flow rate ($M_w$) loop. Varying $M_w$ is achieved by adjusting the valve position. When $t_a$ is higher than its setpoint, actuator accordingly opens the valve until temperature reaches its setpoint. Finally, heat pump input ($U_{hp}$) is control loop 3. Likewise, RWT $t_{wr}$ error determines the heat pump input. Increasing the input when $t_{wr}$ is greater than its setpoint, while decreasing the input when $t_{wr}$ is lower than its setpoint.

### 6.2.1.1 PI control model

PI controller is used to generate the control input from the error signal. Its output (u)

is made up of two components: one proportional to the error, and another proportional to the integral of the error. Equation 6.6, 6.7, 6.8 describe the three controllers used in the simulations.

Zone temperature control

$$u_{sa} = k_{pa}(t_z - t_{zset}) + k_{ia}\int_0^t (t_z - t_{zset})dt \tag{6.6}$$

Discharge air temperature control

$$u_{sw} = k_{pw}(t_a - t_{aset}) + k_{iw}\int_0^t (t_a - t_{aset})dt \tag{6.7}$$

Heat pump control

$$u_{hp} = k_{php}(t_{wr} - t_{wrset}) + k_{ihp}\int_0^t (t_{wr} - t_{wrset})dt \tag{6.8}$$

Where $u_{sa}$, $u_{sw}$, $u_{hp}$ separately represent damper, valve and heat pump controllers' outputs. $k_{pa}$, $k_{pw}$, $k_{php}$ are the proportional gains and $k_{ia}$, $k_{iw}$, $k_{ihp}$ are the integral gains. The terms of $(t_z-t_{zset})$, $(t_a-t_{aset})$, $(t_{wr}-t_{wrset})$ are the respective errors from the setpoints. Therefore, the corresponding controlled variables can be calculated by the following equations:

$$M_a = u_{sa} M_{a\max} \tag{6.9}$$

$$M_w = u_{sw} M_{w\max} \tag{6.10}$$

$$U_{hp} = u_{hp} U_{hp\max} \tag{6.11}$$

Where $M_a$, $M_w$, $M_{amax}$, $M_{wmax}$ respectively represent supply air mass flow rate, water mass flow rate, and their maximum values, given in kg/s; $U_{hp}$, $U_{hpmax}$ are heat pump input power and maximum value, given in kw.

### 6.2.1.2 Method of tuning proportional and integral gains

There are several methods for tuning PID controllers, but they are applicable only

for experimental process, not for the computer simulation unless transfer function of the processes can be found (Kamimura. et al.1994). Although determining appropriate proportional and integral gains is difficult, there are still some basic rules that we could follow to shorten the tuning time and reduce the number of trails.

The controller gains were selected using trial and error. It was found $k_{pa}$, $k_{ia}$ are the vital factors impacting the system stability because zone model has the biggest time constant. After some iterations, a set of gains were extrapolated that gave good temperature control. The magnitudes of the gains used in the simulation are:

$k_{pa}$=0.225, $k_{ia}$=0.00225; $k_{pw}$=1, $k_{iw}$=0.05; $k_{php}$=20, $k_{ihp}$=0.01.

### 6.2.1.3 Simulation results

The simulations were made using single zone model with coil and a terminal VAV box and heat pump supplying the cooling. The system is supposed to turn on during occupied time from 08:00 to 18:00 and turn off during unoccupied period. Meanwhile, system keeps constant OA ratio 15% of the total supply air mass flow rate at that time. The room temperature setpoint is 24℃ and SAT constant setpoint is 13℃, the return water temperature was set to 12℃.

In addition, OA temperature and zone sensible load profiles were assumed. We simulated OA temperature using a cosine function, such as

$$T = T_d + T_v \cos(\frac{2\pi}{24}t + \frac{3}{4}\pi).$$

Figure 6.9 shows OA temperature and load distributions profiles. Figure 6.10 depicts the zone, supply air, return water and supply water temperature responses with

fine-tuned PI controllers. Figure 6.11 shows three controllers' outputs $u_{sa}$, $u_{sw}$, and $u_{hp}$. Figure 6.10 shows that the time constant to reach setpoint is highest for zone temperature control loop (80 minutes), while other two loops responses are much faster. Further, three temperatures reach their setpoints; the maximum overshoot 8.3% was found in $t_z$ and $t_a$ and $t_{wr}$ showed no oscillations. Moreover, the steady state errors of $t_z$ and $t_{wr}$ are exactly equal to zero, while $t_a$ has a slight error from its setpoint.

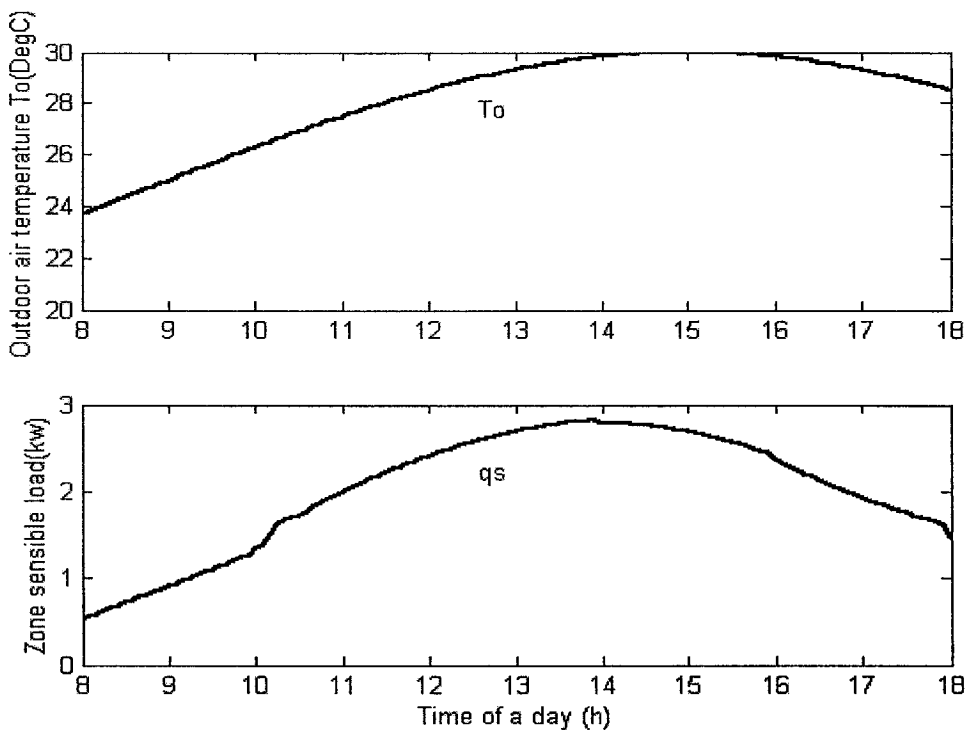


Figure 6.9 OA temperature and zone load profiles used in simulations

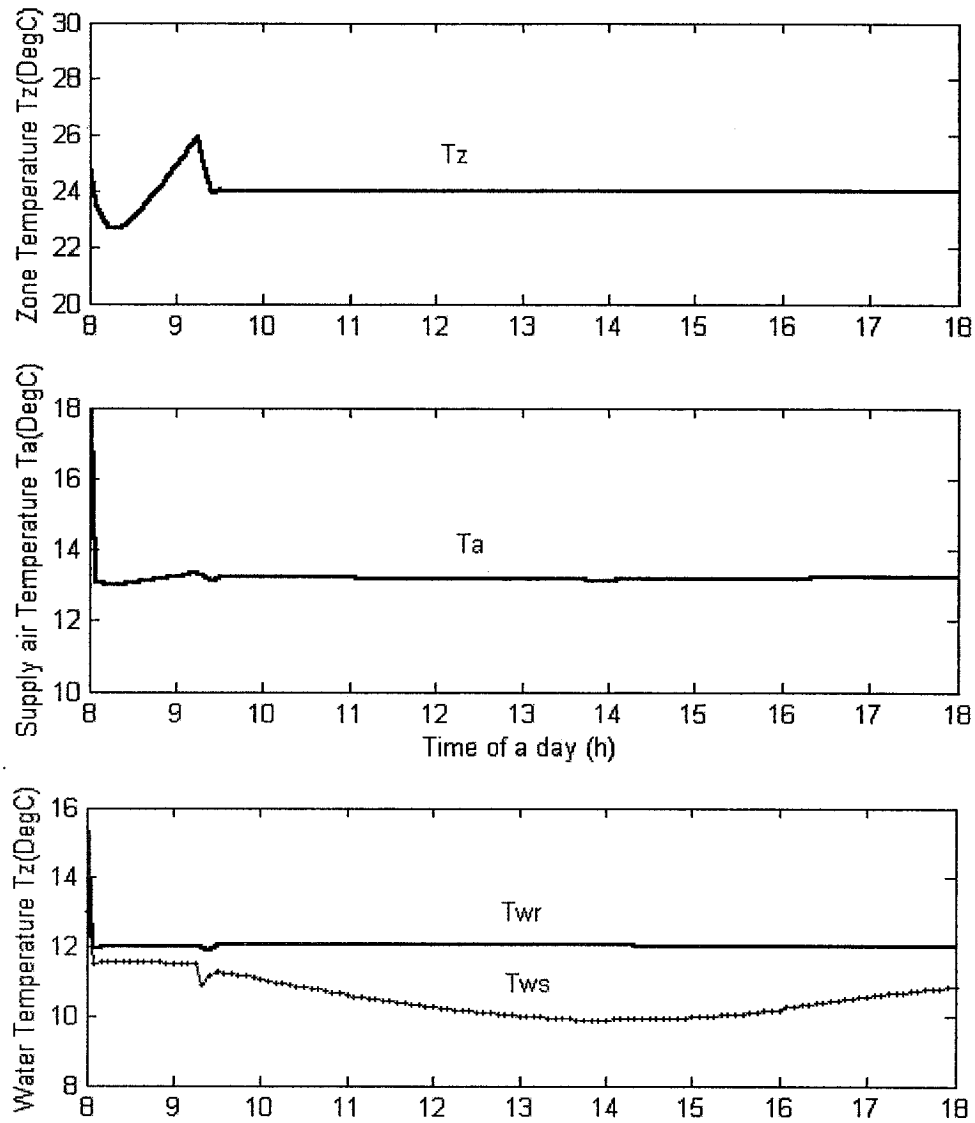


Figure 6.10 Temperature performances using PI control algorithm

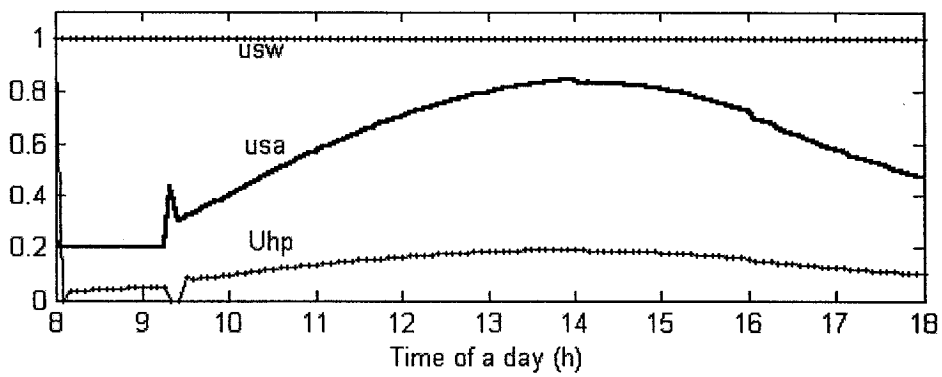


Figure 6.11 Controllers' output profiles using PI control algorithm

### 6.2.2. Adaptive control strategy

Although PI control can give good performance, it is difficult to select appropriate proportional and integral gains for multiple control loops. Furthermore, a fine-tuned PI control system may require constant updating against uncertain changes in the system. This is because strong interactions among various loops. Given this trend, it is important to develop simple control algorithm, which can be easily implemented. With this as the motivation, in this section, an adaptive control algorithm is explored, which is relatively simple, has rapid response, can be easily tuned, as well as has closed-loop stability and acceptable performance in the process disturbances and dynamics. In other words, this version of adaptive control not only conserves the merits of PI control, but also overcomes the deficiency of PI controllers.

In practice, proportional–only controller can result fast response with an offset. The higher the gain the faster will be the response of the control system, but the higher gain also cause overshoot or even the system could cycle indefinitely. To this end, we preserve quick response by means of keeping the proportional control part in our model. Also, we introduce a new variable to modulate the constant gain in order to minimize the steady state error.

#### 6.2.2.1. Adaptive control algorithm

From the previous explanation, the controllers' outputs using adaptive control strategy for the same three closed-loops described before are described by the following

equations.

$$u_{sa}(i+1) = A_a u_{sa}(i) + B_a k_a (t_z(i) - t_{zset}) \quad (6.12)$$

$$u_{sw}(i+1) = A_w u_{sw}(i) + B_w k_w (t_a(i) - t_{aset}) \quad (6.13)$$

$$u_{hp}(i+1) = A_{hp} u_{hp}(i) + B_{hp} k_{hp} (t_{wr}(i) - t_{wrset}) \quad (6.14)$$

Where i is the sampling interval; $u_{sa}(i+1)$, $u_{sw}(i+1)$, $u_{hp}(i+1)$ are current values; $A_a$, $A_w$, $A_{hp}$, $B_a$, $B_w$, $B_{hp}$, are the constant weighted coefficients. Normally, A has higher weighting than B. The sum of A and B was equal to 1, but sometimes they may be greater or less than 1. In addition, $k_a$, $k_w$, $k_{hp}$ are the adaptive gains.

### 6.2.2.2 Simulation results

The simulation conditions were kept the same as that in the previous section. By carefully choosing the values of A and B, better responses could be achieved. In the situation under consideration, we selected $A_a$=0.45, $B_a$=0.4; $A_w$=0.9, $B_w$=0.25; $A_{hp}$=0.3, $B_{hp}$=0.24.

The adaptive gain k is another important parameter for the control action. Basically, the value of k varies with the variation of the system characteristics. The adaptive gain k was defined as

$$k = \frac{q_s}{M_{a\max} c_{pa} (t_z - t_a)} \quad (6.15)$$

The fine-tuned adaptive control responses are displayed in Figures 6.12 and 6.13. Figure 6.12 shows that the steady state time of $t_z$ loop is about 60 minutes and much bigger times for both $t_a$ and $t_{wr}$ loops. Moreover, $t_z$ loop has near 8.33% undershoot

without overshoot, $t_a$ with slight undershoot and $t_{wr}$ with no overshoot. All control loops reach their setpoints with no steady-state errors.

Comparing the responses in Figures 6.12, 6.13 with the Figures 6.10, 6.11, the fact is apparent that $t_z$ reaches steady state in adaptive control quite faster than in PI control. Another finding is that the controllers are modulated more smoothly using adaptive algorithm than in PI control scheme (For example, $u_{sa}$, $u_{hp}$ show no sudden changes).

### 6.2.3. Conclusions

From the control loop responses, the following conclusions were arrived at.

1. Improved EMC functions with PI and adaptive control can give better performance and reach steady state faster than base case which uses on-off control strategy; zone temperature has smaller overshoot and undershoot in PI controller, while only undershoot in adaptive controller.
2. Both PI and adaptive control can save energy comparing with base case. The savings can be up to 12%. The computed daily energy consumption was 124.28 MJ (PI control), 123.78 MJ (Adaptive control) and 139.2 MJ (Base case).
3. From the point of view of tuning, adaptive control is much easier than PI control while giving the same good performance.

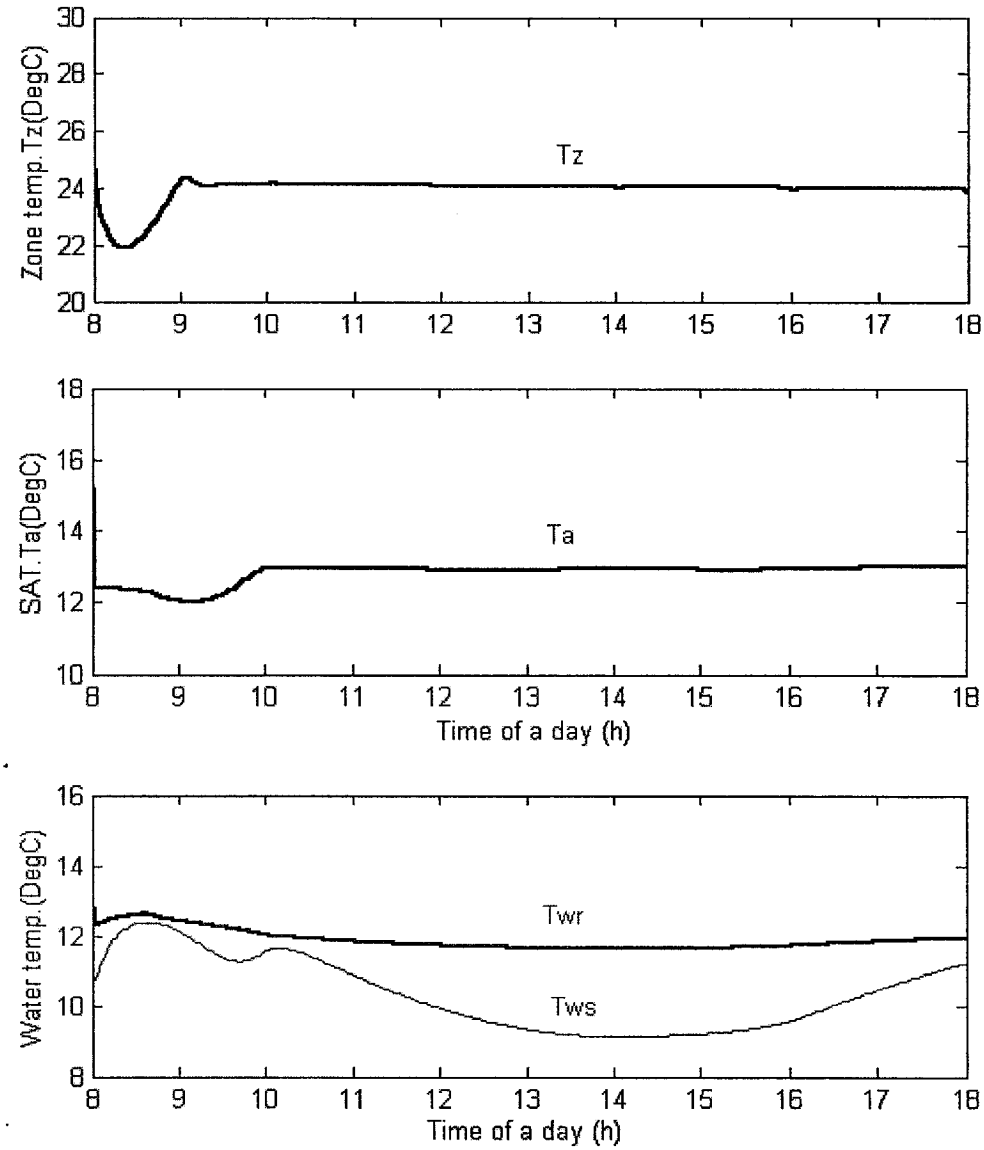


Figure 6.12 Temperature profiles using adaptive control strategy

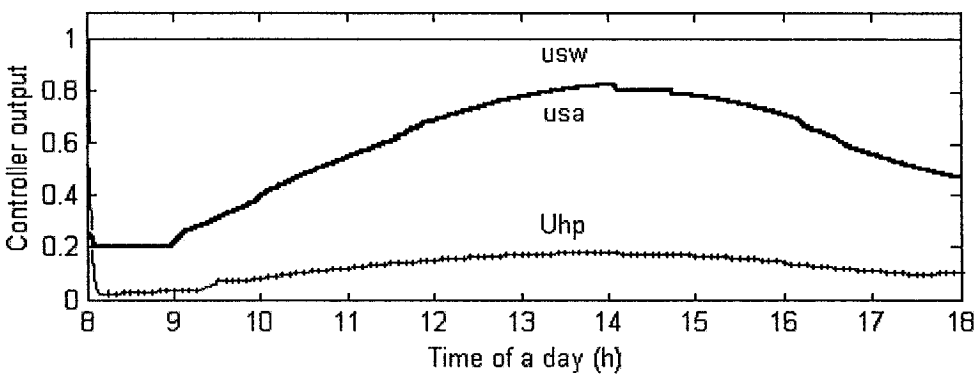


Figure 6.13 Controllers' output profiles using adaptive control strategy

# Chapter 7 Real time implementation of improved EMC functions

## 7.1 Introduction

After developing individual EMC functions, it is of interest to develop an integrated energy management system in which all the developed EMC functions can be activated according to time of year, month, and daily operation of building systems. In this chapter, the implementation aspects of the developed algorithms are discussed. As well examples showing the typical daily operation of EMC system in real time are given.

## 7.2 EMC system configuration

Generally, the EMC system should track a certain sequence relying on the time of a day, the day of a year. According to the time and indoor and outdoor conditions, one or several EMC functions may be executed each time. Typically, for one-day operation, the system experiences night cycle, start-time period, occupied time period, stop-time period, and night cycle again. Figure 7.1 depicts the structure of the system implementing EMC functions. Meanwhile, the system is supposed to obey the internal logical relationship.

### 7.2.1. Year-month-day function

In the preliminary step, the system can automatically discriminate which season it is currently depending on the month in a pre-designed calendar. For example, March to

May belong to spring; June to August are summer; September to November are fall; December, January and February belong to winter months. The outdoor condition in both spring and fall are mild, so they may follow three operating modes: heating, cooling or no heating/cooling only ventilation depending on the actual circumstances. Three seasonal operational models are thus incorporated in the system. These are summer, winter, and spring/fall models. Figure 7.2 depicts the flowchart of this scheme.

Next, the system estimates if it is a normal cycle (workday cycle) or holiday/weekend cycle according to the day of the year. If it is a holiday (i.e. Christmas) or weekend (Saturday and Sunday), the system goes through holiday algorithm. On the other hand, if it is a normal day, the system goes into the typical daily operational phase. During this period, just like the previous chapter, we divide a day into four time periods. These are nighttime, startup period, occupied time, and shut down period. Eventually, a certain number of routines can be tracked during a workday. The following describes the relationship between time period and the corresponding operating cycle in a one-day process.

## 7.2.2. Time – of – day EMC functions

### 7.2.2.1. Night cycle operation

At first, night cycle (NC-Figure 7.3) is enabled when it is in the nighttime (0:00-7:00). For example, if it is summer season, the system turns to summer night cycle (SNC-Figure 7.4), in which the cooling is shut down, but how the fan and the dampers

work depends on the comparison between OA temperature and room space temperature. There are three choices: maximizing OA damper and fan when OA temperature $t_o$ is less than certain value (for example, in this thesis, 2℃ is suggested) than zone temperature $t_z$; closing OA damper and fan when $t_o$ is greater than $t_z$; otherwise, enable OA cycle. Likewise, winter night cycle (WNC-Figure 7.5) will work when it is in winter season. The control strategy is quite different from the one in summer. One difference is that the heating system still turns on when $t_z$ is less than the minimum value (For example 15℃). The heating can turn off only when $t_z$ is greater than the minimum value. Another difference is that the OA damper completely closes during the whole nighttime whether the fan turns on or not. In addition, PI or adaptive control and reset cycle (include $t_z$, $t_a$, and $t_{wr}$, their setpoints ($t_{zset}$=15℃, $t_{aset}$=28℃, $t_{wrset}$=40℃) are different from the daytime) will be involved in to modify the damper, valve and heat pump input when the heating is on.

### 7.2.2.2. Start-up operation

Next, the time clock turns to 07:00-08:00; the system goes into start time cycle (STC-Figure 7.6). The system calculates the time needed to pre-cool/heat the system in order that the zone temperature can reach its setpoint at the time occupants arrive using the developed model (Equation 5.2). If the real time is earlier than the start-lead-time, the system keeps the previous cycle; otherwise, the system turns to STC. In STC, EMCS offers the HVAC system full supply airflow rate, half of water mass flow rate and heat pump output.

### 7.2.2.3. Occupied period operation

The primary and the most complex strategy is enabled during occupied period (08:00-17:00). The first step is that the system enables occupied cycle (OPC-Figure 7.9). For the summer season, the priority checks the enthalpy of OA and inside air. As a result, the system goes through enthalpy cycle (ENC-Figure 7.8) when the outdoor enthalpy is less than that of indoor air. In ENC, on-off control method is employed. In other words, when OA is appropriate, EMCS shuts down cooling and signals for maximum OA and fan capacity. Besides, if the outdoor enthalpy is greater than that of indoor air, the system works based on OPC. The system between these two circumstances works relying on the comparison of the outdoor and indoor air temperature and enthalpy. If $t_o$ is greater than $t_z$, EMCS turns on the cooling and maintains minimum OA. If $t_o$ is less than $t_z$, EMCS turns off the cooling and modulates the OA damper, which is described in equation 7.1. Note that there is no ENC employed in winter season.

$$OA = OA_{\min} + (1 - OA_{\min}) \frac{H_{in} - H_{out}}{\varepsilon} \qquad (7.1)$$

In OPC, three possible cycles could be enabled. The first one is either PI or adaptive control. Figure 7.9 shows their implementation flowcharts. In addition, OA cycle (Figure 7.10), and reset cycle (Figure 7.11) are enabled during occupied period. In PI control, $t_z$, $t_a$, and $t_{wr}$ are continuously measured and simultaneously compared with their setpoints (in summer, $t_{zset}$=24℃, $t_{aset}$=13℃(low limit), $t_{wrset}$=12℃; in winter, $t_{zset}$=21℃, $t_{aset}$=33℃, $t_{wrset}$=45℃). The controller outputs can be calculated based on variable error signals using

equations 6.6, 6.7, and 6.8 at each sampling interval. The controller modulates the appropriate actuator to regulate the process variables close to their respective setpoints. Figure 6.8 illustrates this process.

In the adaptive control scheme, error signals are feedback to adaptive control algorithms, which compute the actuator input for the next time intervals. Modulation of dampers is achieved in the same way as PI controllers to regulate the process outputs. Typical responses of adaptive control loops were shown in Figure 6.13.

### 7.2.2.4. Outdoor air economy cycle

OA economic cycle is a temperature based economy cycle (Figure 7.10). In this cycle, one modulates the OA damper relying on the comparison of $t_o$ and $t_z$. In summer, when $t_o$ is greater than $t_z$, OA damper is set to minimum, and when $t_o$ is less than a certain value (n, typically, 2℃ is suggested in this thesis) than $t_z$, OA damper is set to maximum position. Equation 7.2 is employed when $t_o$ is between $t_z$ and $t_z$-n. Figure 7.10 describes the flowchart.

$$OA = OA_{\min} + (1 - OA_{\min})\frac{t_z - t_o}{n} \qquad (7.2)$$

### 7.2.2.5. Reset cycle (Figure 7.11)

Reset cycle is based on the zone load and the difference between the indoor and outdoor temperature. In summer, only during occupied time the supply air temperature is reset, which can be computed using the model (equation 6.4) developed in the previous chapter. By using the algorithm a new setpoint is computed. The PI/adaptive control

algorithm will track the reset setpoint. In winter, reset SAT setpoint is enabled during occupied time and nighttime as well.

### 7.2.2.6. Stop cycle

The stop time cycle (SPC-Figure 7.7) is enabled during stop-time (17:00-18:00). The stop-lead–time is computed using Equation (5.6). In SPC, though the cooling /heating turns off, the fan still runs at full capacity, with minimally open OA damper and fully closed valve.

During 18:00-24:00 the night cycle is enabled thus completing a one-day operation.

### 7.2.2.7. Overall EMCS configuration

A $C^{++}$ computer program, which integrates all these EMC functions, was developed. Several tests were made to check if proper functions were enabled according to the year/month/time-of-day operation. The $C^{++}$ program consistently enabled the desired EMC functions. Figure 7.12 illustrates the overall configuration of typical EMC systems. The developed EMC functions reside in the block core EMC algorithms.

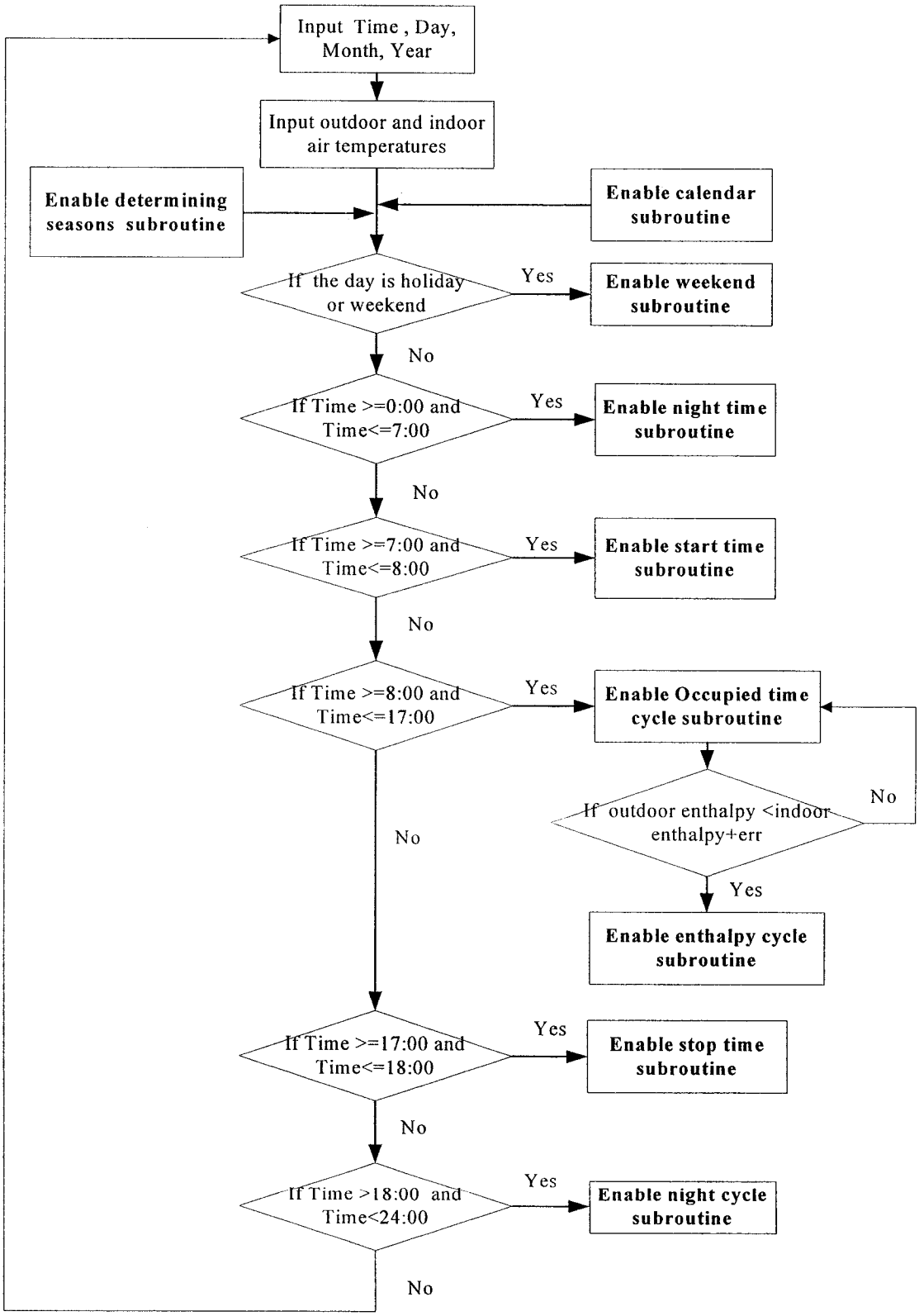


Figure 7.1 Flowchart of real-time EMC system implementation

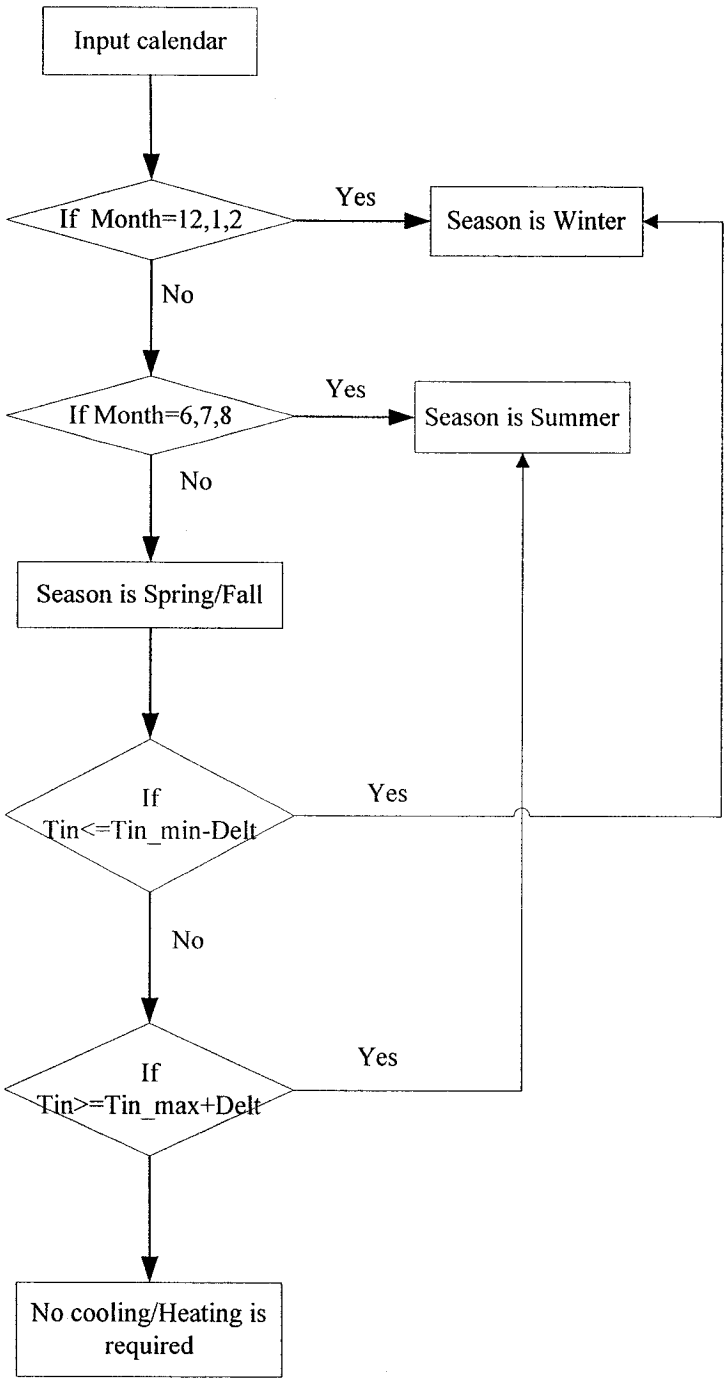


Figure 7.2 Subroutine for determining seasons

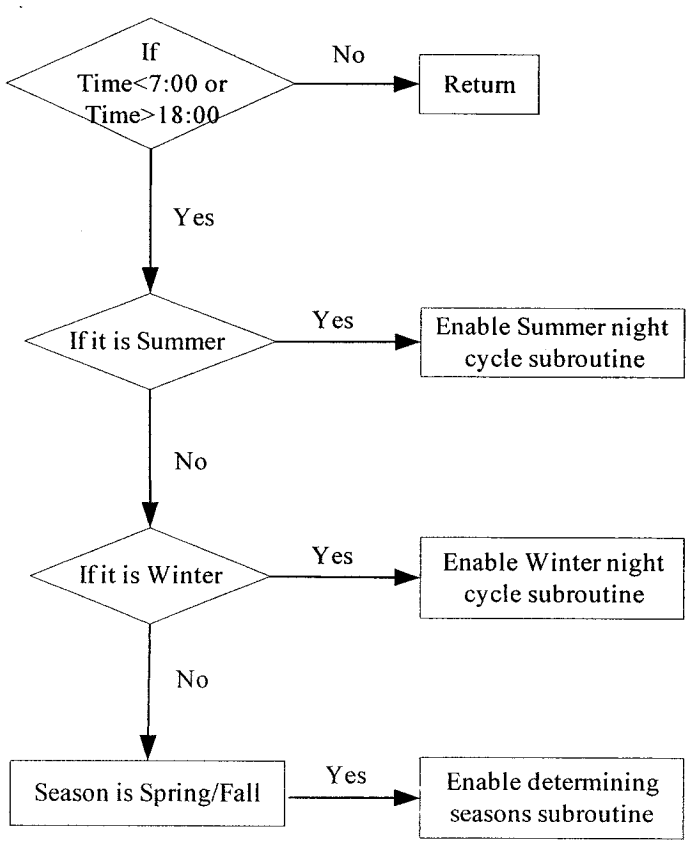


Figure 7.3 Night cycle (NC) subroutine

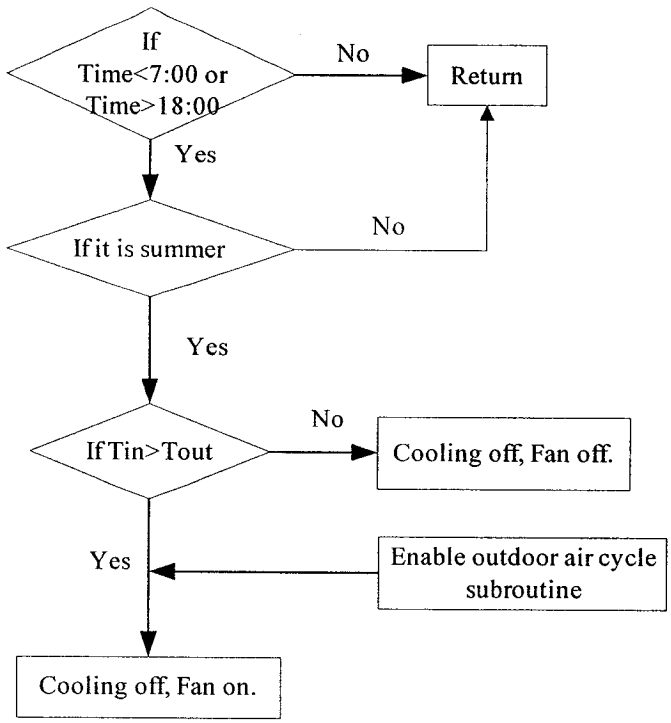


Figure 7.4 Summer night cycle (SNC) subroutine

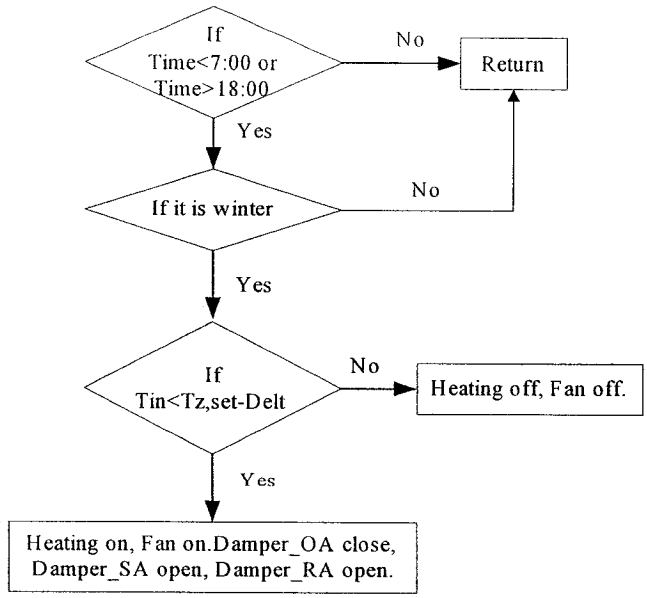


Figure 7.5 Winter night cycle (WNC) subroutine

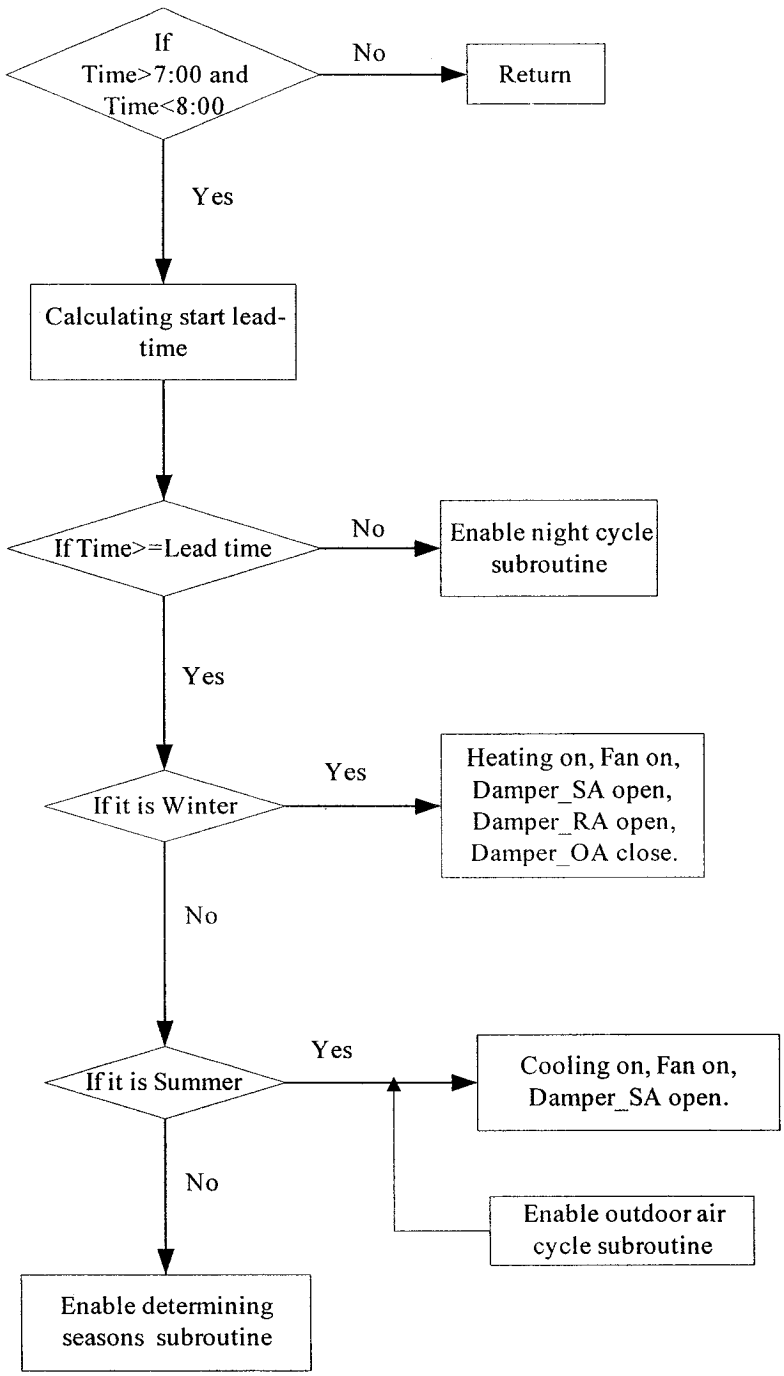


Figure 7.6 Start-time cycle (STC) subroutine

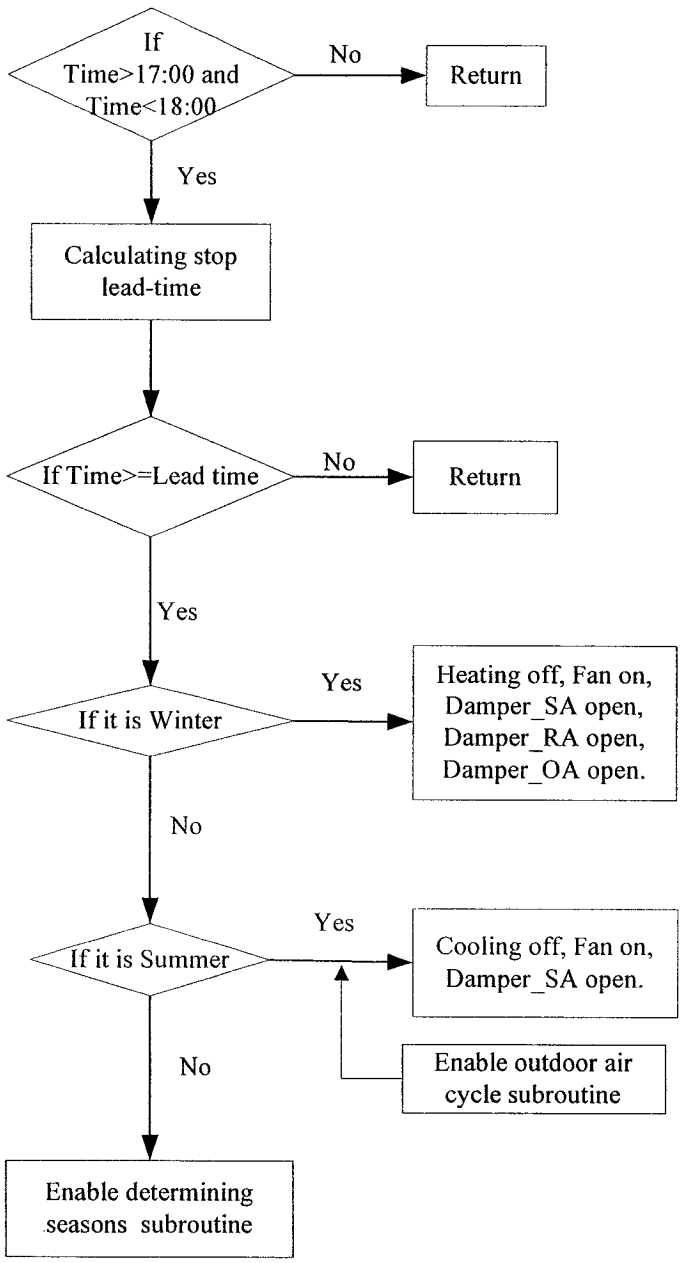


Figure 7.7 Stop-time cycle (SPC) subroutine

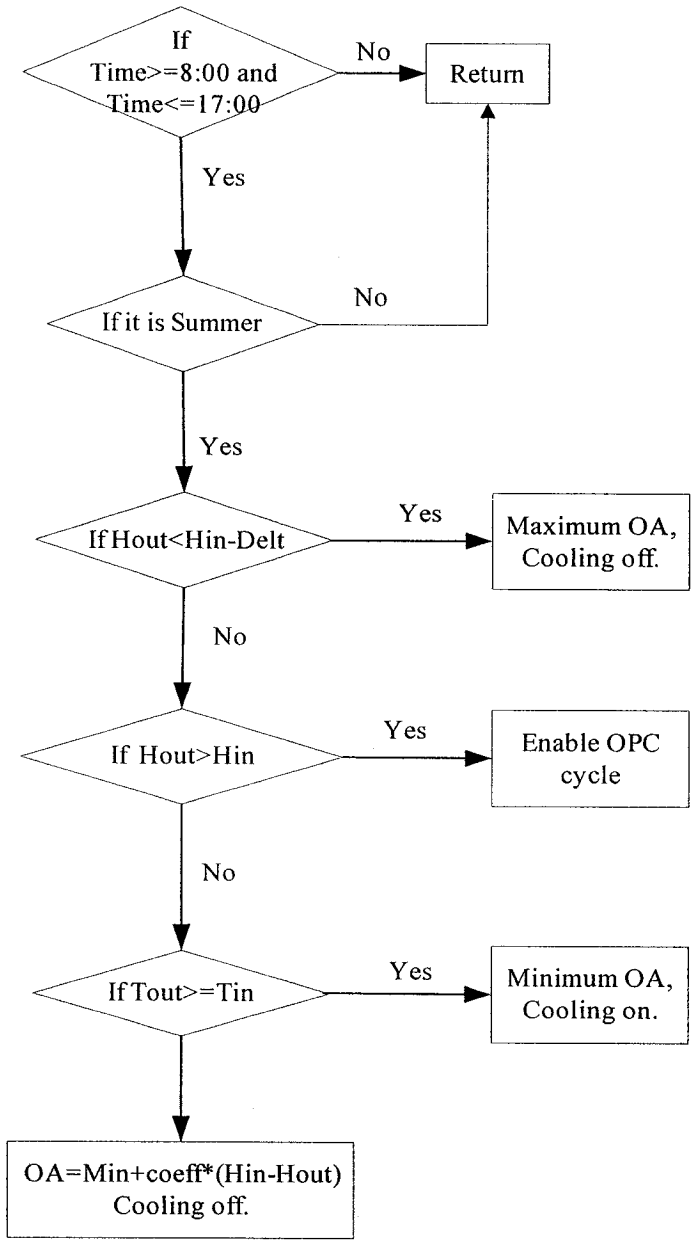


Figure 7.8 Enthalpy cycle (ENC) subroutine

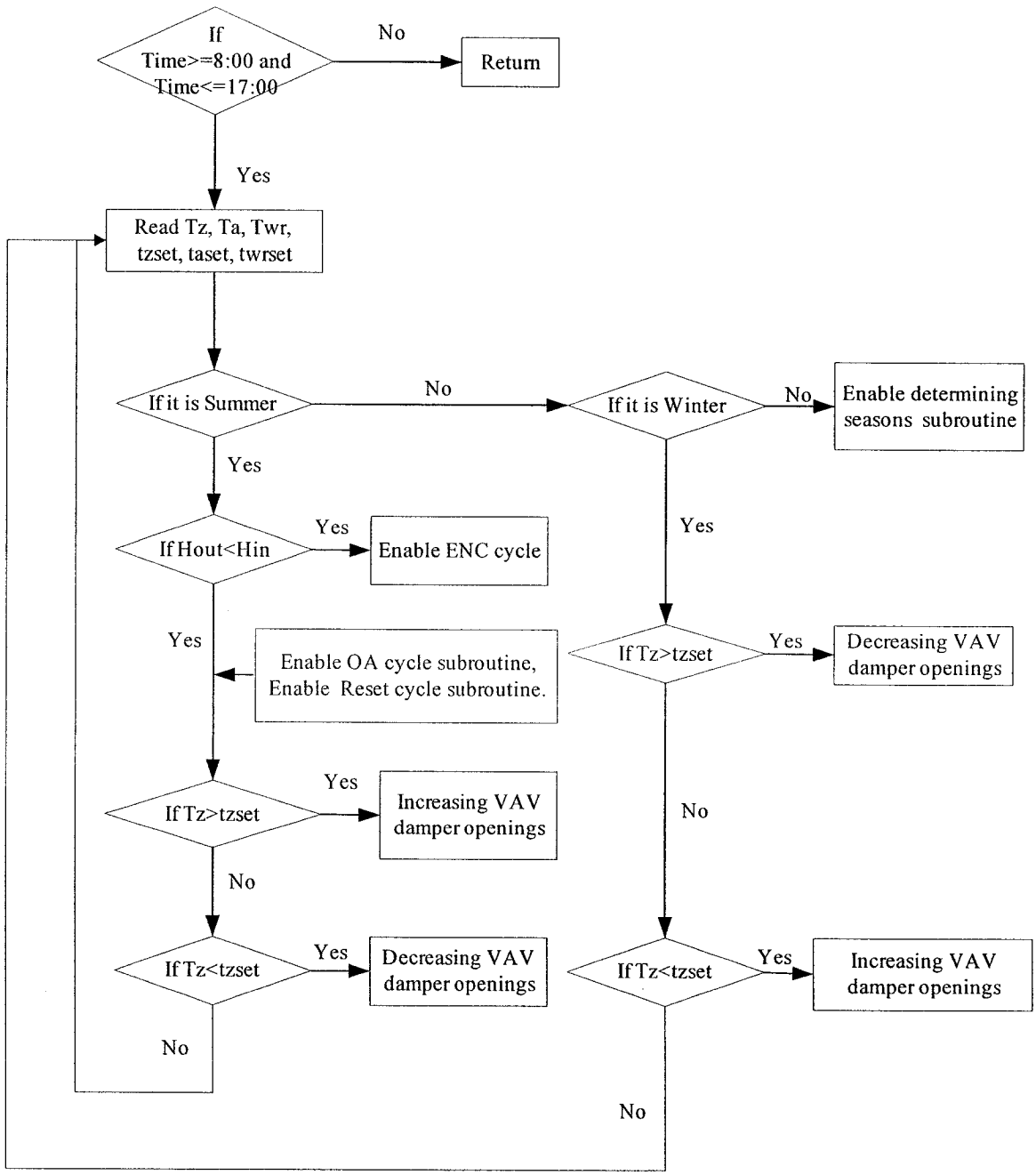


Figure 7.9 Occupied time cycle (OPC) subroutine

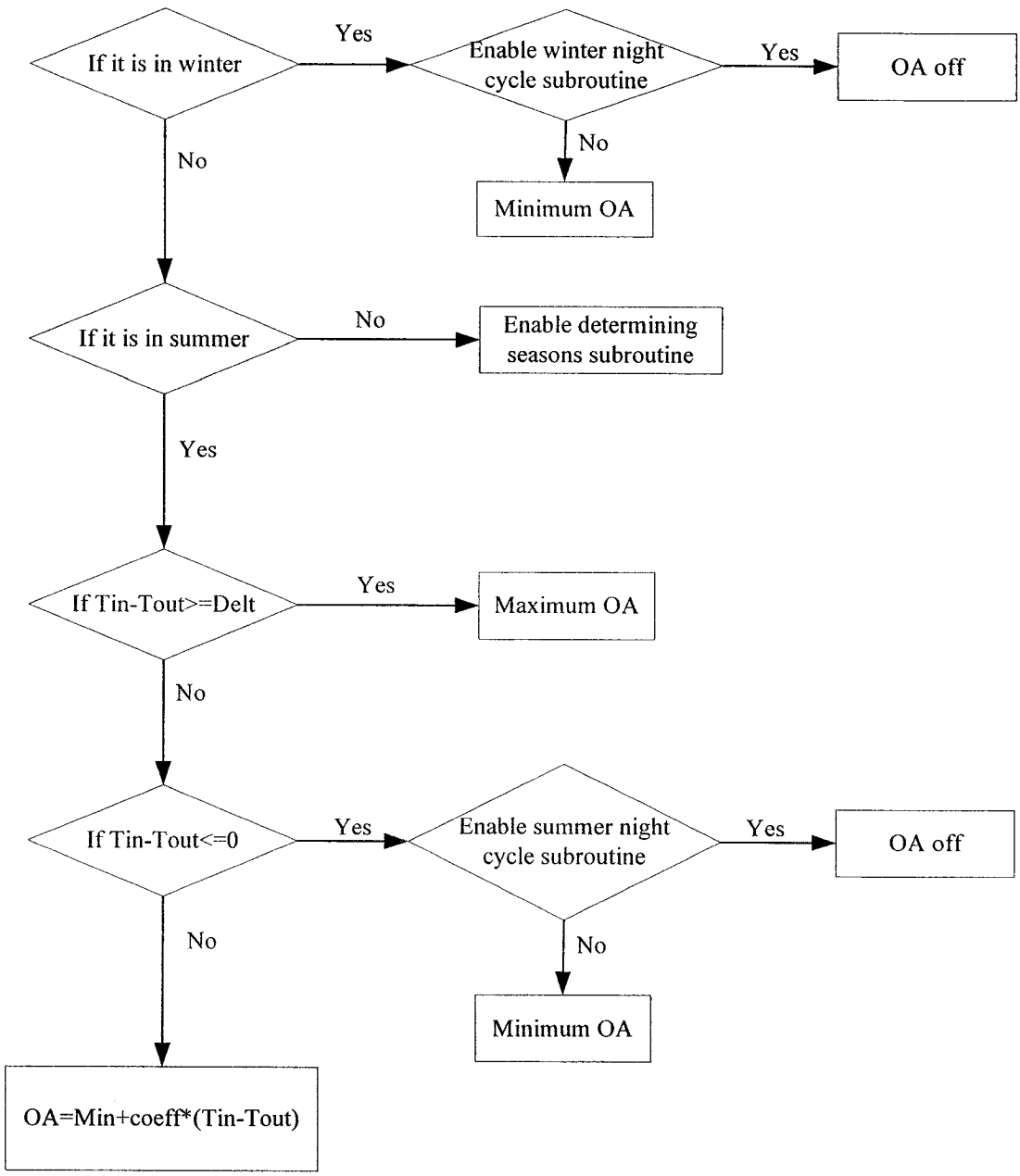


Figure 7.10 Outdoor air (OA) economy cycle subroutine

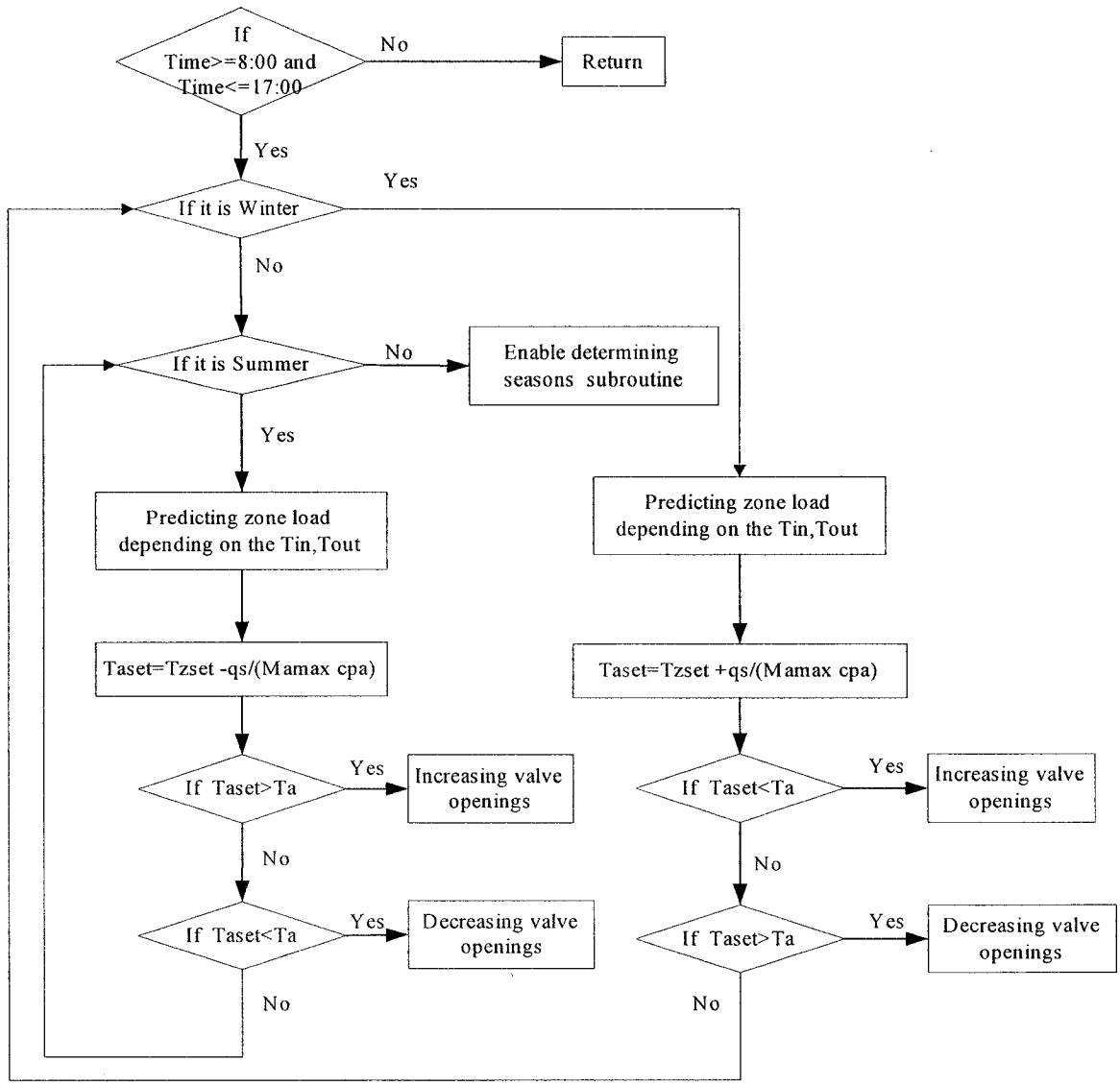


Figure 7.11 Supply air temperature (SAT) reset cycle subroutine

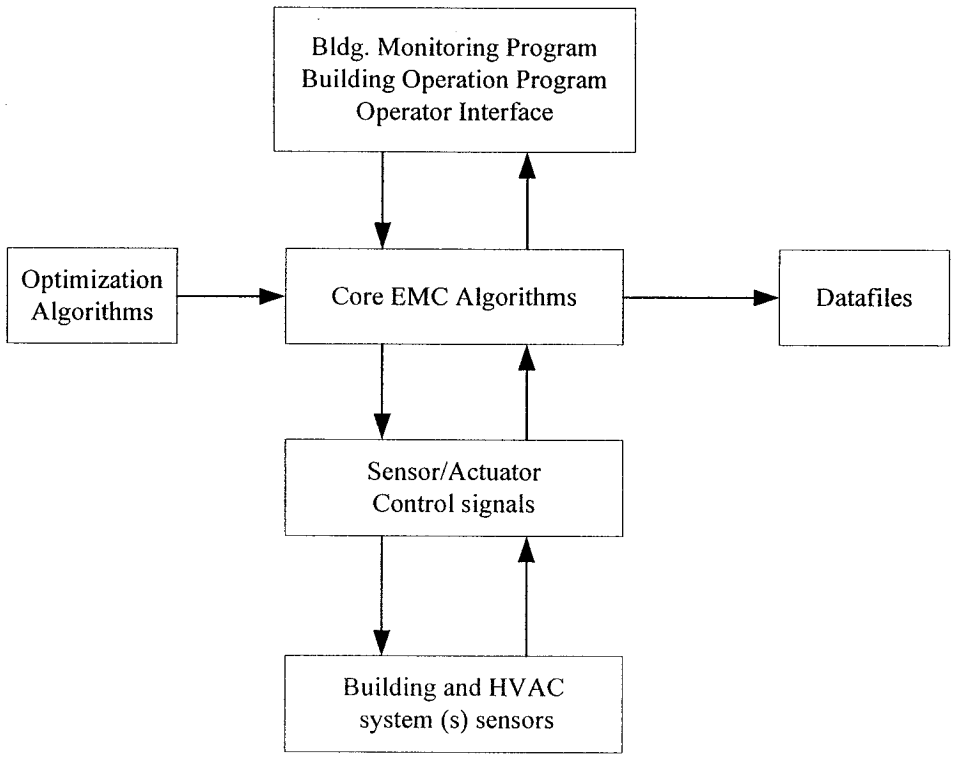


Figure 7.12 Overall configuration of Building Automation System

## 7.3 Typical daily operation

The performance of EMC functions could be evaluated by examining the output regulation properties of control algorithms as well as their energy savings potential. To this end, in this section, two different typical daily simulations were conducted, one corresponding to summer weather conditions and another for the winter weather operations. Note that in each case four different time-scheduled functions such as night cycle during unoccupied hours, start-up, occupied period and shut-down cycles are enabled. The summer time simulations responses obtained are depicted in Figure 7.13 with PI control, and Figure 7.14 using adaptive control strategy. Likewise, the winter time typical daily responses were simulated using load profiles shown in Figure 7.15. The EMC output responses are depicted in Figure 7.16.

### 7.3.1. Summer day operation

According to the time period of the day, the testing consists of four scheduled operations as described above. For summer day simulation, we chose August 22 with OA and load profiles as described in the previous chapter. The same single zone prototypical building was considered. The EMC functions' performances are shown in Figure 7.13 (PI-control) and Figure 7.14 (Adaptive control).

### 7.3.2 Winter day operation

We also performed a winter day simulation. In winter, the setpoints varied with

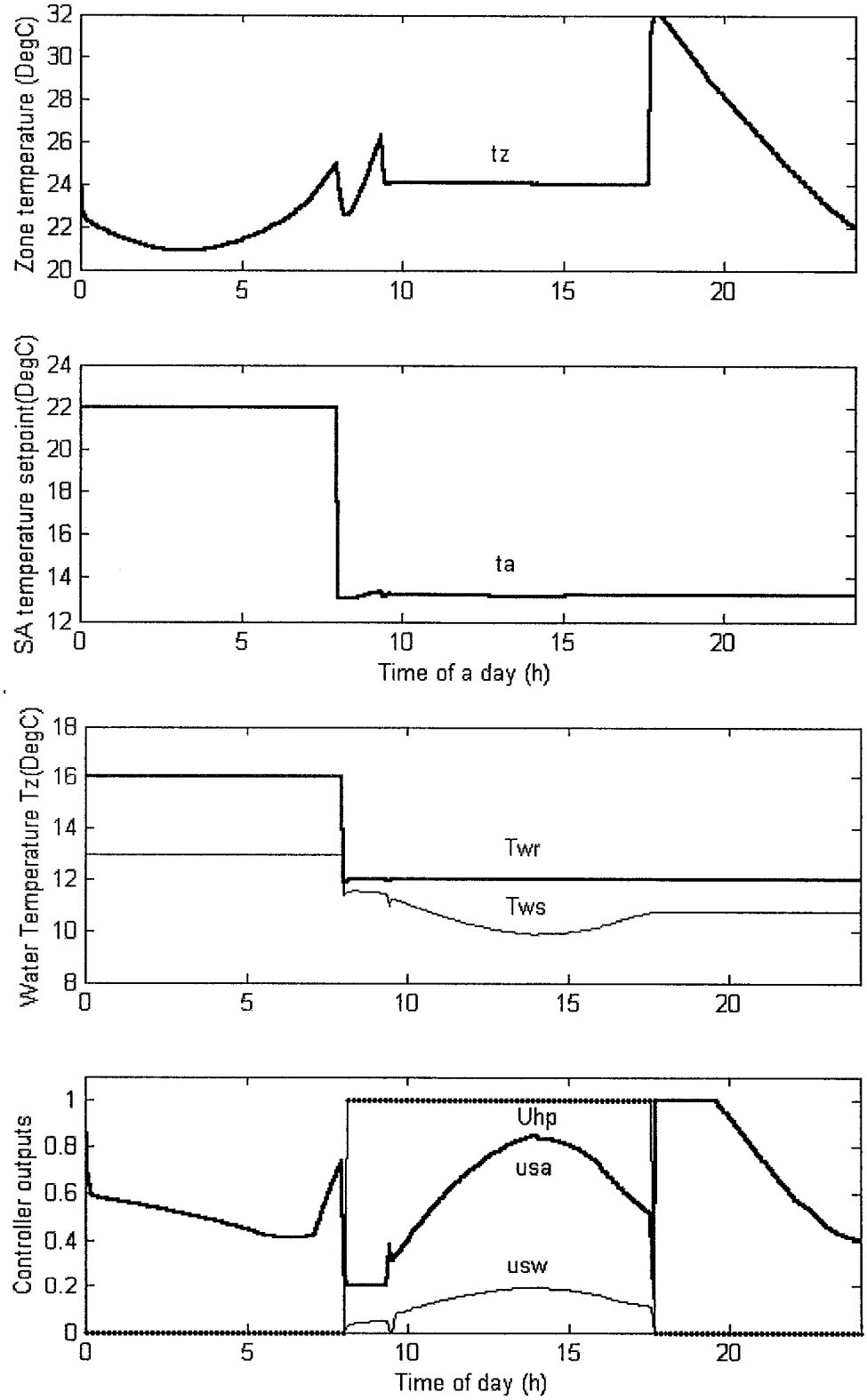


Figure 7.13 Performance of implementing EMC functions in summer

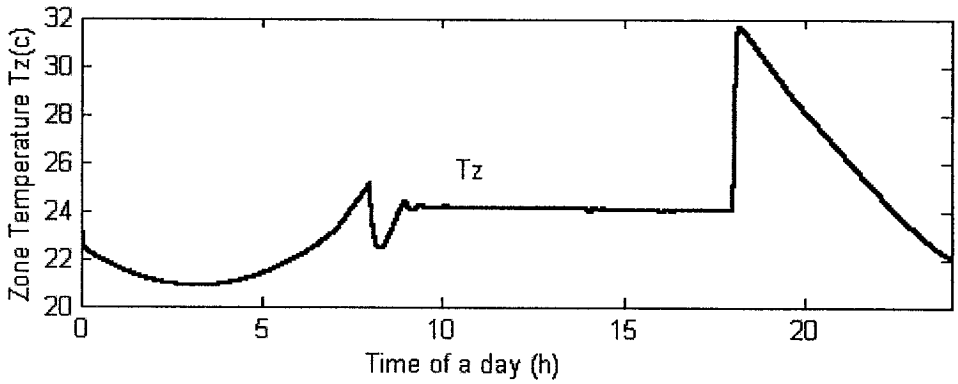


Figure 7.14 Performance of implementing EMC functions (Adaptive) in summer

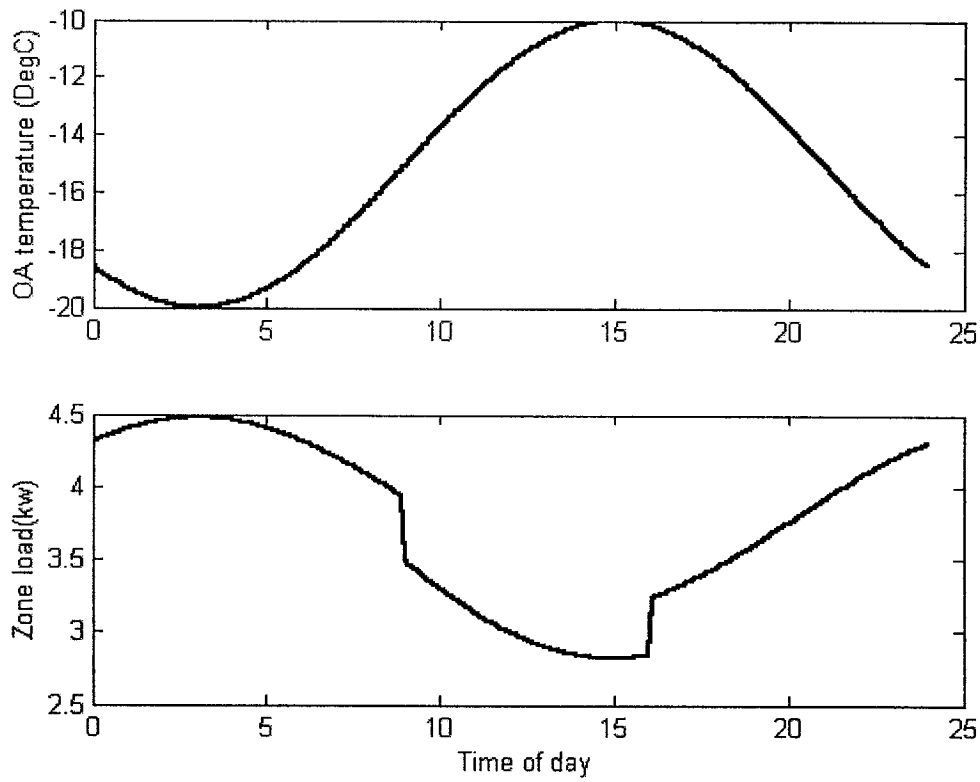


Figure 7.15 OA temperature and zone heating load profiles used in simulation in winter

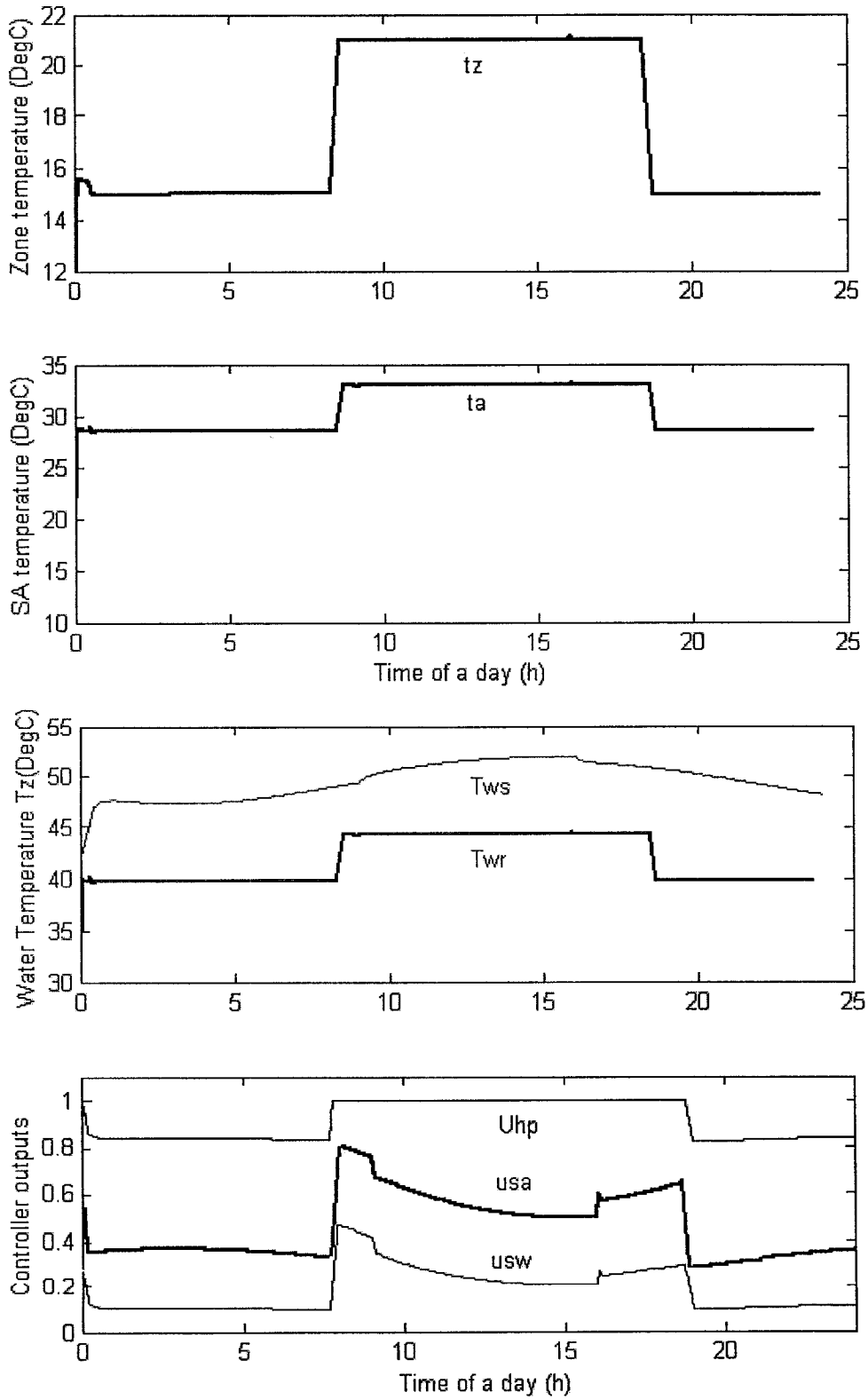


Figure 7.16 Performances of implementing EMC functions in winter

daytime and nighttime. During the occupied time, $t_{zset}$=21℃, $t_{aset}$=33℃, $t_{wrset}$=45℃; whereas during night period, $t_{zset}$=15℃, $t_{aset}$=28℃, $t_{wrset}$=40℃. Figure 7.15 shows the temperature and load profiles, and Figure 7.16 displays the performance of EMC system in winter.

Compared with the system without EMC functions, the system with EMC functions saved 14% energy in summer, and 15% energy in winter.

## 7.4. Optimal setpoints for energy efficient operation

The implementation of EMC functions with PI control or Adaptive control requires setpoints for discharge air temperature, supply or return water temperature, and zone temperature. In the most EMC systems, these setpoints are chosen arbitrarily based on past experience. However, it is important to choose setpoints, which can save more energy. To this end, a steady state optimization methodology is proposed to compute these setpoints. In the following, the optimization methodology and the results obtained are discussed.

### 7.4.1. Optimization methodology

In this section, "Medium-Scale Optimization" algorithm is utilized, which uses a Sequential Quadratic Programming (SQP) method. In this method, a Quadratic Programming (QP) subproblem is solved using an active set strategy, and an estimate of the Hessian of the Lagrangian is updated using the BFGS formula at each iteration. Also,

a line search is performed using a merit function. In other words, this method is used to solve multi-variable constraint optimization problems. First of all, an objective function needs to be built that include all of the energy consumption elements as well as the relationship between it and the variables. Next, linear and/or nonlinear constraints with equality and inequality relationships should be involved. Then, upper bounds, lower bounds, and initial values of these variables should be chosen. A computer program was developed to find the optimal solution.

The objective function is the system power, which consists of three parts, heat pump input, fan power, and pump power. The heat pump input is equal to $P_{heatpump} = u_{hp} U_{hp\max}$. The fan power $P_{fan}$ computed by equation 4.9. The pump power $P_{pump}$ is defined by $P_{pump} = u_{sw}{}^3 P_{p\max}$. $P_{pmax}$ is the maximum pump power. Therefore, the objective function becomes

$$P_{sys} = P_{heatpump} + P_{fan} + P_{pump} \qquad (7.3)$$

On the other hand, nine variables such as $u_{sa}$, $u_{sw}$, $u_{hp}$, $x_v$, $t_z$, $t_a$, $t_{wr}$, $t_{ta}$, $t_{ws}$ with upper (ub) and lower (lb) bands as well as initial values are defined in this thesis. The upper and lower bands are summarized in Table 7.1.

The steady state linear and nonlinear equality constraints are described as follow.

$$A_{eq}X = b_{eq} \quad \text{or} \quad A_{eq}X - b_{eq} = 0$$

$$X = [u_{sa}, u_{sw}, u_{hp}, x_v, t_z, t_a, t_{wr}, t_{ta}, t_{ws}]'$$

They are defined by equation7.4 thru 7.8, which are steady state energy balance equations describing the heat exchange occurred in zone, cooling coil, and heat pump.

Zone model: $M_a c_{p,a}(T_{a,s} - T_z) + q_s + \alpha_z(T_o - T_z) = 0$. (7.4)

Air side: $-\frac{h_t \eta_{s,ov} A_o}{\rho c_v A}(\bar{T}_a - \bar{T}_t) - \frac{\gamma M_a}{\rho A L_c}(T_a - T_{a,in}) = 0$. (7.5)

Water side: $\frac{h_{it} A_{it}}{m_w c_w}(\bar{T}_t - \bar{T}_w) + \frac{M_w}{m_w L_c}(T_{ws} - T_{wr}) = 0$. (7.6)

Tube:
$$\frac{1-\eta_s}{\eta_s + \frac{m_t c_t}{m_{fin} c_{fin}}}\{\frac{\gamma M_a}{\rho A L_c}(T_a - T_{a,in}) - \frac{h_{it} A_{it}}{m_{fin} c_{fin}(1-\eta_s)}(\bar{T}_t - \bar{T}_w) + (\frac{\eta_{s,ov} h_c A_o}{\rho c_v A} + \frac{\eta_{s,ov} h_c A_o}{m_{fin} c_{fin}(1-\eta_s)})(\bar{T}_a - \bar{T}_t)\} = 0 \quad (7.7)$$

Heat pump: $-M_w c_w(T_{ws} - T_{wr}) + U_{hp} U_{hp\max} COP + \alpha_h(T_{\infty,t} - T_{ws}) = 0$. (7.8)

In addition, COP model given in equation 3.9 was used.

The optimization problem was defined as the minimization of $P_{sys}$ (Equation (7.3)) subject to steady state constraints for the model Equations (7.4) through (7.8).

Table 7.1 Lower bands and upper bands of variables for optimization

| | Variable | Occupied period | | Unoccupied period | |
|---|---|---|---|---|---|
| | | Lower band (lb) | Upper band (ub) | Lower band (lb) | Upper band (ub) |
| 1 | $u_{sa}$ | 0.2 | 1 | 0 | 1 |
| 2 | $u_{sw}$ | 0 | 1 | 0 | 0 |
| 3 | $u_{hp}$ | 0 | 1 | 0 | 0 |
| 4 | $x_v$ | 0.15 | 1 | 0 | 1 |
| 5 | $t_z$(℃) | 23.5 | 24.5 | 20 | 30 |
| 6 | $t_a$(℃) | 13 | 15 | 13 | 15 |
| 7 | $t_{wr}$(℃) | 10.5 | 12 | 10.5 | 12 |
| 8 | $t_{ta}$(℃) | 11 | 13.2 | 11 | 13.2 |
| 9 | $t_{ws}$(℃) | 7 | 11.5 | 7 | 11.5 |

## 7.4.2. Simulation results and analysis

The program can automatically find an optimistic $P_{sys}$ value to match constrains during the predetermined ranges at each sampling time (that is half of hour in this case). Table 7.2 manifests the record of optimal process at one sample at noon 12:30. At this point, the program obtains the optimal value 1.1716kw after doing 18 iterations. This table is the output of computer program on screen. The first column in it "Iter" means the number of iterations; the second "F-count" is the number of function evaluations; the next one illustrates the value of objective function. From this record, with the increasing the number of iterations and evaluations, the maximum constraint and derivative trend to decrease until a small value. After 10 iterations, the objective function achieves stabilization and optimization. Figure 7.17 reveals the optimal track at this time.

Table 7.2 Optimization process record at one sample (12:30)

| Iter | F-count | f(x) | max constraint | Step-size | Directional derivative |
|---|---|---|---|---|---|
| 1 | 10 | 0.113628 | 75.02 | 1 | 0.136 |
| 2 | 21 | 0.249541 | 46.22 | 1 | 0.412 |
| 3 | 32 | 0.66192 | 24.24 | 1 | -0.104 |
| 4 | 43 | 0.567867 | 9.02 | 1 | -0.224 |
| 5 | 54 | 0.457285 | 6.106 | 1 | 0.697 |
| 6 | 65 | 1.15412 | 0.4995 | 1 | 0.105 |
| 7 | 76 | 1.25893 | 0.002225 | 1 | -0.0015 |
| 8 | 87 | 1.25743 | 4.006e-005 | 1 | -0.0497 |
| 9 | 99 | 1.2329 | 0.008101 | 0.5 | -0.0296 |
| 10 | 110 | 1.20372 | 0.01107 | 1 | -0.00411 |
| 11 | 121 | 1.19964 | 0.001504 | 1 | -0.0078 |
| 12 | 132 | 1.19196 | 0.006046 | 1 | -0.000718 |
| 13 | 143 | 1.19124 | 8.874e-005 | 1 | -0.00687 |
| 14 | 154 | 1.1845 | 0.007977 | 1 | -0.00391 |
| 15 | 165 | 1.18064 | 0.002883 | 1 | -5.21e-005 |
| 16 | 176 | 1.18059 | 2.389e-007 | 1 | -0.00912 |
| 17 | 187 | 1.17148 | 0.001127 | 1 | 0.000109 |
| 18 | 198 | 1.17159 | 2.424e-007 | 1 | -3.81e-006 |

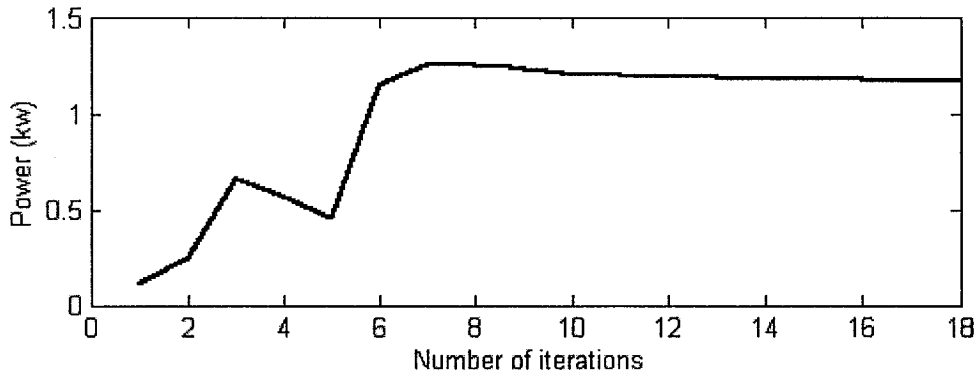


Figure 7.17 The track of optimization at noon 12:30

Figure 7.18 implies the case, which shows that the acceptable solution is to keep $t_z$ at its highest value. Simultaneously, $t_a$ is kept as low as possible, $t_{wr}$ as high as possible during occupied time, and OA has peak value at two time periods (8:00 to 8:30 and 19:00 to 19:30). This is because the zone temperature $t_z$ has big jump (from 30℃ to 24.5℃ or from 24.5℃ to 30℃) and OA temperature ($t_o$) is less than zone temperature ($t_z$) at that time. Figure 7.19 demonstrates the system power profile. From the simulation, the system total daily energy consumption $E_{daily} = \int_0^{24} (P_{sys}) dt$ was found to be 38.5 MJ.

In addition, during optimal process, we also verify if the constraints are satisfied. In other words, we put optimized parameters into the left hand of equations 7.4, 7.5, 7.6, 7.7, 7.8 and compute the values. Table 7.3 shows two typical samples' results, in which there are different numbers of iterations. The table depicts that the nonlinear equalities are exactly satisfied.

We have also investigated the case in which heat pump performance was varied to study its impact on energy consumption. When COP is decreased by 20%, the system

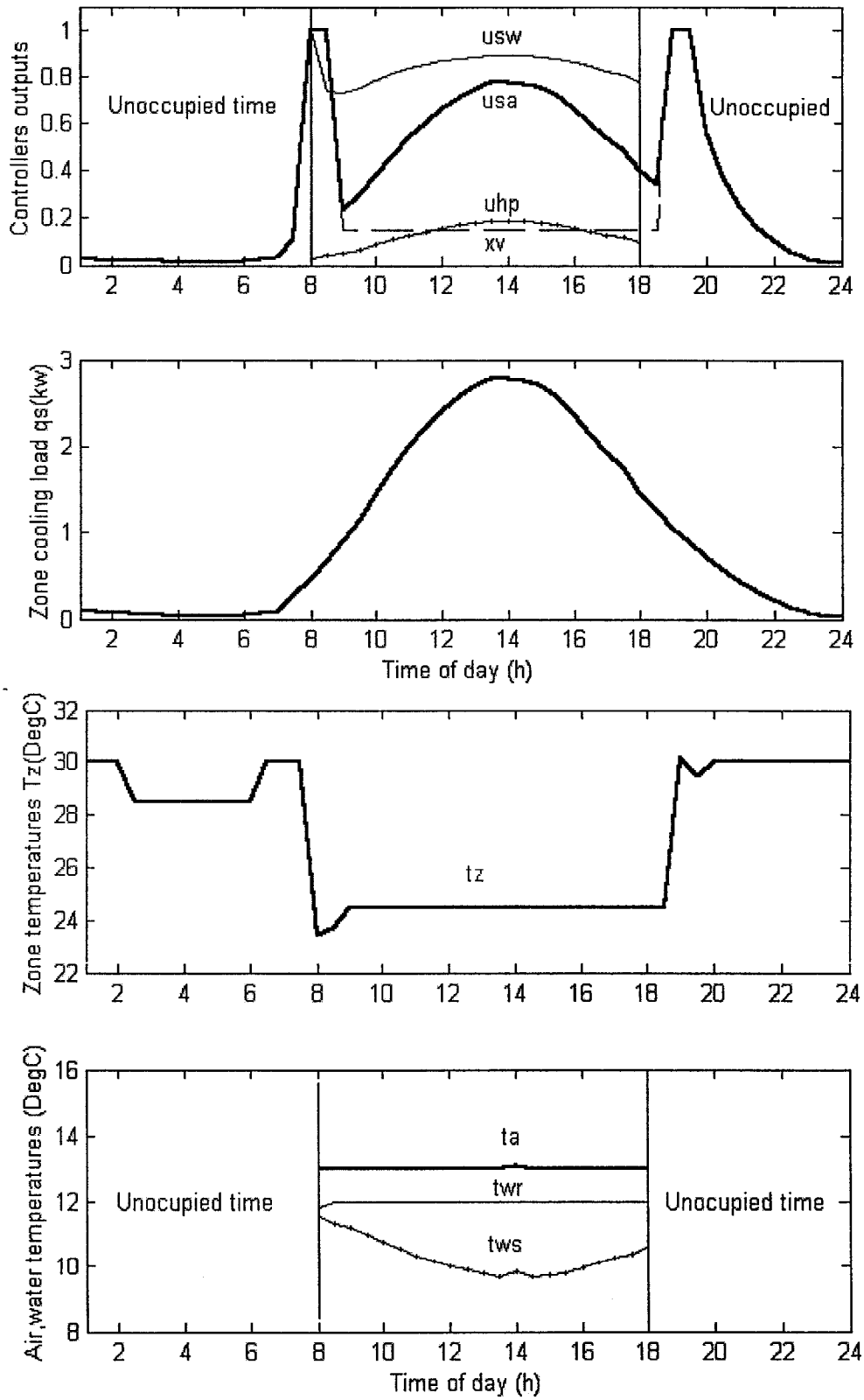


Figure 7.18 System optimization performance in summer

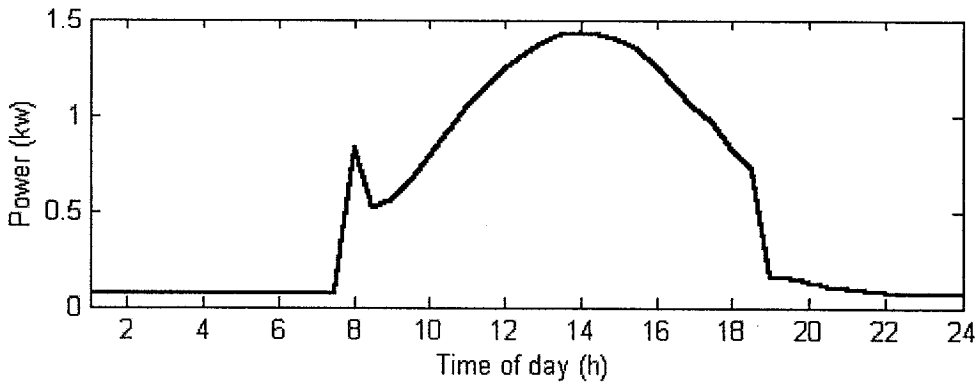


Figure 7.19 Optimized performance of system power

Table 7.3 Constraints validation of two typical samples for optimization

| Equation | Sample A ($*10^{-8}$) | | | | | Sample B ($*10^{-15}$) | | | | |
|---|---|---|---|---|---|---|---|---|---|---|
| 7.4 | $-9.5271*10^{-7}$ | | | | | $-6.9389*10^{-3}$ | | | | |
| 7.5 | -0.0 | | | 85.4 | | 0.0 | | | $-1.35*10^{2}$ | |
| 7.6 | -0.0 | | 85.4 | | 1.58 | 0.0 | | $-1.35*10^{2}$ | | 6.2 |
| 7.7 | -0.0 | 85.4 | | 1.58 | -6.1 | 0.0 | | $-1.35*10^{2}$ | 6.2 | 9.9 |
| 7.8 | -0.0 | 85.4 | 1.58 | -6.1 | 0.0 | 0.0 | | $-1.35*10^{2}$ | 6.2 | 9.9 | 0.0 |

power becomes 43.5249kw. When COP is reduced by 30%, the heat pump power is 49.5687kw. That means the system power increased by 13% and 28.7%, respectively.

## 7.4.3. Discussion

The objective of determining the optimal setpoints is to help operate the HVAC system in an optimal manner. To demonstrate this, the optimal setpoints determined above were used as tracking signals for adaptive controllers. Figure 7.20 depicts the performance using adaptive control algorithm tracking optimal setpoints. The daily energy consumption obtained from simulation is summarized in Table 7.4. Also shown in the Table 7.4 are energy consumption using other strategies.

In the table, "Base case" indicates that the system operated with duty cycle during occupied time and on/off control of OA damper during unoccupied period. The strategy "With EMC" refers to the case that operated with all EMC functions developed in this thesis.

It was found that optimization strategy predicted about 19.6% potential energy savings. The implementation of optimal setpoints resulted in 17.3% energy savings. When the optimal setpoints were not used, the implementation of EMC algorithms above produced a saving of 14%. The results do point out to the usefulness of optimal setpoint strategy in achieving energy efficient operation of HVAC systems.

Table 7.4 Summary of daily energy consumption under different strategies

| Item | Base case | With EMC | Optimization | With EMC and optimization |
|---|---|---|---|---|
| Daily energy consumption (MJ) | 47.9 | 41.2 | 38.5 | 39.6 |
| Energy savings (%) | 0 | 14 | 19.6 | 17.3 |

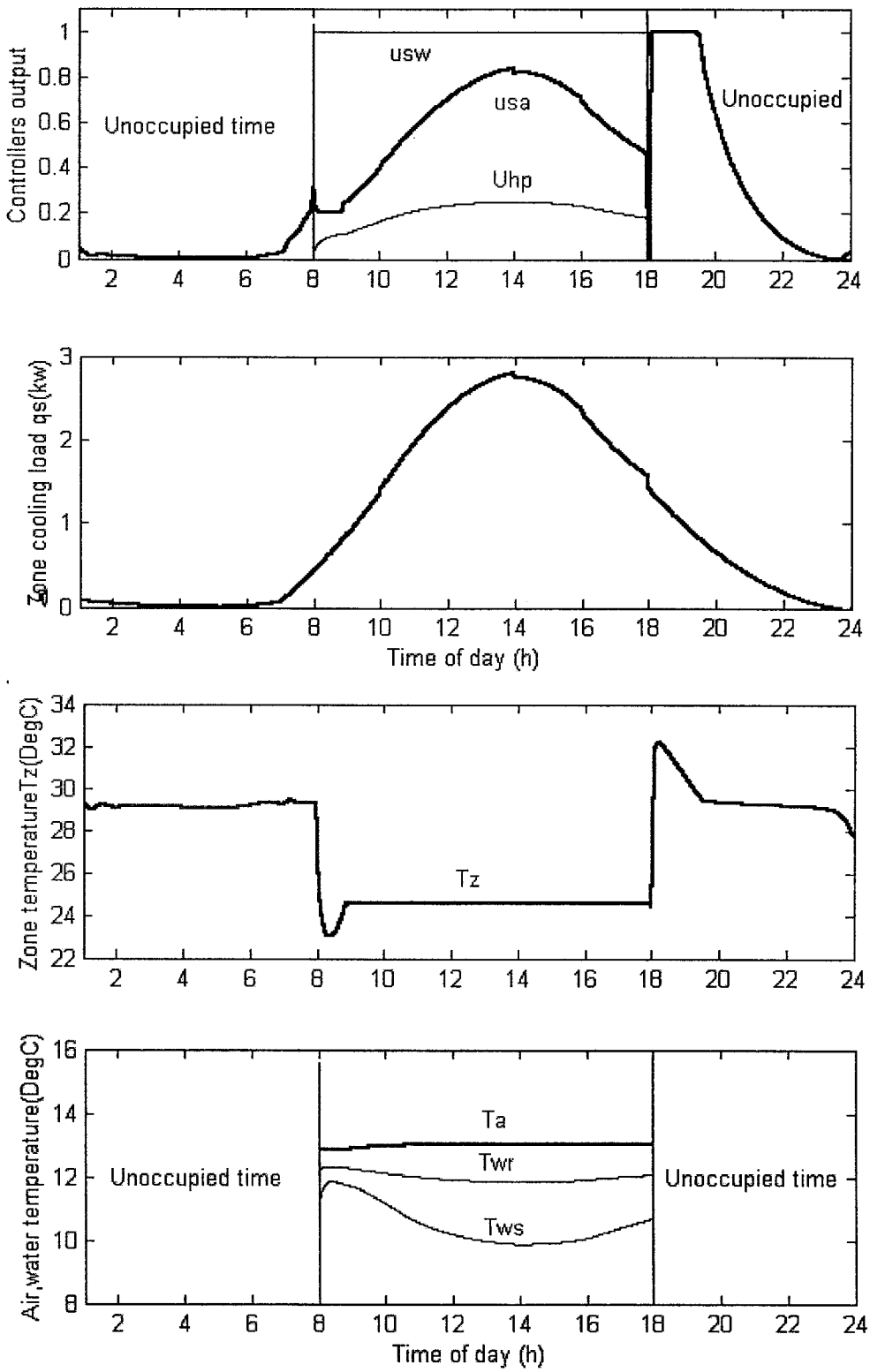


Figure 7.20 Implementation of optimal results using adaptive control strategy

# Chapter 8 Conclusions and recommendations

In this thesis, several improved EMC algorithms have been developed. Detailed simulation runs were made to compare the operating performance of the EMC strategies. A number of specific conclusions are presented at the end of each chapter. Here, most important conclusions are summarized.

1. Several OA control strategies were compared. Among them the proportional band control strategy resulted in 12% energy savings compared to the conventional OA strategy.
2. A start-time strategy is proposed. The results show that the start-lead-time is a function of indoor/outdoor temperature difference, initial building temperature, supply air temperature and thermal mass of the building.
3. A model for stop-lead-time is proposed. It was found that the stop-lead-time is very sensitive to difference between current and zone final temperature.
4. A predictive reset strategy for supply air temperature control is proposed. Results show that up to 7% energy savings can be achieved by implementing the supply air temperature reset strategy compared constant supply air temperature strategy.
5. A PI-control and an adaptive control strategies for regulating the VAV system operation during occupied hours are proposed. The adaptive control strategy is simple to implement and gives good temperature regulation.
6. An optimization methodology to compute optimal setpoints for VAV system

operation is proposed. Results show that the use of optimal setpoints resulted in 17% energy savings compared to the case when no EMC functions were used.

7. A supervisory EMC system embedded with the EMC algorithms is developed. Simulation results show that the supervisory EMC system is accurately executing each EMC algorithm according to time of year, month and daily operating schedule. Results also show that the developed EMC algorithms can save up to 14% energy compared to the case with no EMC functions.

## Recommendation for future work:

1. Humidity control is an important issue in HVAC systems and should be studied.
2. Combination of PI and adaptive control may give better results. This is because adaptive control responses are faster but accompany with small steady state error; on the other hand, PI control can achieve zero steady state error. Therefore a combined strategy is expected to do better.

# References


1. AboulNaga, M. M., Abdrabboh, S. N., 2000. "Improving night ventilation into low-rise buildings in hot-arid climates exploring a combined wall-roof solar chimney." Renewable Energy 2000,Vol.19, pp.47-54.
2. ASHRAE, 1997. Fundamentals Handbook. Atlanta: American Society of Heating, Refrigerating and Air-Conditioning Engineers.
3. Athienitis, A. K., 1994. *Building Thermal Analysis*, Electronic Mathcad Book, MathsoftInc., Boston, MA.
4. Avery, G., 1986. "Designing and controlling an outside air economizer cycle." *ASHRAE Journal*, December, 1986, pp.26-30.
5. Birtles, A B, Kolokotroni, M., Perera, M D A E S, 1996. "Night Cooling and Ventilation Design for Office-Type Buildings." Renewable Energy1996, Vol.8, n1, pp 259-263.
6. BLAST, 1979. Blast 3.0: Building Loads Analysis and System Thermodynamics Program, User Manual" Support Office, Dept. of Mechanical and Industrial Engineering, University of Illinois, Urbara-Champaign.
7. Brandemuedl, M. J., Braun, J. E., 1999. "The Impact of Demand-Controlled and Economizer Ventilation Strategies on Energy Use in Buildings." *ASHRAE Transactions*, Vol.105, Part2, pp.39-50.
8. Brandt, S. G., 1986. "Adaptive control implementation issues." *ASHRAE Transactions*, Vol.92, Part2B, pp.211-219.
9. Chen, Y. H. and Lee, K. M. 1990. "Adaptive robust control scheme applied to a single-zone HVAC system." *ASHRAE Transactions*, Vol.96, Part2, pp.896-903.
10. Clark D. R., Hurley, C. W. and Hill, C. R. 1985. "Dynamic Models for HVAC System Components." *ASHRAE Transactions*, Vol.91, Part1B, pp.737-751.
11. DOE-2, 1981. "DOE-2: Building energy user analysis program, engineering manual, Version 2.1A", Laurence Berkeley Laboratory.

12. Elmahdy, A. H., 1975. "Analytical and experimental multi-row, finned-tube heat exchanger performance during cooling and dehumidification process." Ph.D thesis, Dept.of Mechanical and Aeronautical Eng., Carleton University, Ottawa, Canada.
13. Elovitz, D. M., 1995, "Minimum Outside Air Control Method for VAV Systems." *ASHRAE Transactions*, Vol.101, Part1, pp.613-618.
14. Geros, V., Santamouris, M., Tsangrasoulis, A., Guarracino, G., 1999. "Experimental evaluation of night ventilation phenomena." *Energy and Buildings* 19999, Vol.29, pp. 141-154.
15. Goh, P. A., 1990. "Modelling and control of a variable air volume (VAV) system." Master Thesis, The Center for Building Studies, Concordia University, Montreal, Canada.
16. Grot, R. A., Harrje, D. T., 1981. "The transient performance of a forced warm air duct system." *ASHRAE Transactions*, Vol.87 part 1.pp795-804.
17. Holman, J. P., 1986. *Heat Transfer*, McGraw-Hill Inc.[QUERY9.14] USA.
18. Janu, G. J., Wenger, J. D., Nesler, C. G., 1995a. "Strategies for Outdoor Airflow Control from a Systems Perspective." *ASHRAE Transactions*, Vol.101, Part2, pp.631-643.
19. Janu, G. J., Wenger, J. D., Nesler, C. G., 1995b. "Outdoor Air Flow Control for VAV Systems." *ASHRAE Journal*, 1995,April, pp.62-68.
20. Jin, X. Q., Xia, J., Zhou, X. X., Wang, S. W., 2001. "On-Line Optimization of Energy Management and Control System for Central Air-Conditioning in Building System." *Journal of Shanghai Jiaotong University*, May 2001, Vol.35 No.2.
21. John, I. L. and Donald, H. S., 1993. "HVAC Controls and Systems". McGraw-Hill,Inc.
22. Kamimura, K., Yamada, A., Matsuba, T., Kimbara, A., Kurosu, S., Kasahara, M., 1994. "CAT (Computer-Aided Tuning) Software for PID Controllers." *ASHRAE Transactions*, Vol.100, Part1, pp.180-190.

23. Ke, Y. P., Mumma, S. A., 1997b. "Optimized Supply Air Temperature (SAT) in Variable-Air-Volume (VAV) Systems." *Energy-The International Journal* 1997, vol. 22, n. 6, pp. 601-614.

24. Ke, Y. P., Mumma, S. A., Stanke, D., 1997a, "Simulation Results and Analysis of Eight Ventilation Control Strategies in VAV Systems." *ASHRAE Transactions*, Vol.103, Part2, pp.381-392.

25. Khan, A. Y., 1994. "Heat and mass transfer performance analysis of cooling coils at part-load operating conditions." *ASHRAE Transactions*, Vol.93, Part1, pp.52-62.

26. Klein, S. A. *et al.* 1983. *TRANSYS, A Transient Simulation Program, Report 38-12, Version 12.1,* Engineering Experimentation Station, University of Wisconsin-Madison.

27. Kolokotroni, M, Aronis, A., 1999. " Cooling-energy reduction in air-conditioned offices by using night ventilation." Applied Energy 1999, Vol.63, pp.241-253.

28. Kolokotroni. M., 2001. "Night Ventilation Cooling of Office Buildings: Parametric Analyses of Conceptual Energy Impacts." *ASHRAE Transactions*, Vol.107, Part1, pp.479-489.

29. Krakow, K. I., Zhao, F., Muhsin, A. E., 2000. "Economizer Control." *ASHRAE Transactions*, Vol.106, Part2, pp.13-25.

30. Liu, Z., Xie, W., Huang, Y., 2002. "The Energy Control of Air Condition System in Intelligent Building." Proceedings of 4th World Congress on Intelligent Control and Automation June 10-14,2002,Shanghai, P.R.China.

31. Mehta, D. P., Wood, J. E., 1980. "An experimental validation of a rational model for dynamic responses of buildings." *ASHRAE Transactions*, Vol.86,

32. Mehta, D. P., 1984. "Modeling of environmental control components." *Workshop on HVAC Control: Modeling, and Simulation,* Georigia Institute of Technology, Atlanta.

33. Mumma, S.A., Bolin, R. J., 1994. "Real-time, on-line optimization of VAV system control to minimize the energy consumption rate and satisfy ASHRAE standard

62-1989 for all occupied zones." *ASHRAE Transactions*, Vol.100, Part1, pp.160-168.

34. Mutammara, A. W., Hittle, D. C., 1990. "Energy Effects of Various Control Strategies for Variable –Air-Volume System." *ASHRAE Transactions*, Vol.96, Part1, pp.98-102.
35. Payne, F. William .1984." Energy Management Control System Handbook."
36. Piao, Y. G., Zhang, H. G., Bien, Z., 1998. "A Simple Fuzzy Adaptive Control Method and Application in HVAC." IEEE1998.
37. Pinnella, M. J., 1986. "Modeling, tuning and experimental verification of a fan static pressure control system." M. S. thesis, Department of Illinois, Urbana-Champaign.
38. Rabie. N., Delport, G. J., 2002. "Energy management in a telecommunications environment with specific reference to HVAC." *Building and Environment*, Vol.37, Iss.4, Apr.2002, pp.333-338.
39. Rock, B. A., Wu, C. T., 1998. "Performance of Fixed, Air-Side Economizer, and Neural Network Demand-Controlled Ventilation in CAV Systems." *ASHRAE Transactions*, Vol.104, Part2, pp.234-245.
40. Seem, J. E., House, J. M., Klaassen, C. J., 1998. "Leave the Outdoor Air Damper Wide Open." *ASHRAE Journal*, 1998, February, pp.58-60.
41. Spilter, J. D., Hittle, D.C., Johnson, D. L., Pedenson, C. O., 1987. "A Comparative Study of the Performance of Temperature-Based and Enthalpy-Based Economy Cycles." *ASHRAE Transactions*, Vol.93 part 2, pp.13-22.
42. Stoecker, W. F., 1976. *Procedures for Simulating the Performance of Components and Systems for Energy Calculations*. Third Edition.
43. Virk, G. S., and Loveday, D. L. 1991. "A comparison of predictive, PID, and On/Off techniques for energy management and control." *ASHRAE Transactions*, Vol.97, Part2, pp.3-10.
44. Wang, S., 1999. "Dynamic simulation of building VAV air-conditioning system and evaluation of EMCS on-line control strategies." *Building and Environment*, Vol.34, Iss.6, Nov.1999, pp 681-705.

45. Wong, S. P. W., Wang, S. K., 1989. "System simulation of the performance of a centrifugal chiller using a shell-and tube-type water-cooled condenser and R-11 as refrigerant." *ASHRAE Transactions*, Vol.95, Part1, pp 445-454.

46. Yang, I. H., Yeo, M. S., Kim, K. W., 2003. "Application of artificial neural network to predict the optimal start time for heating system in building." *Energy Conversion and Management* 44 (2003), pp 2791-2809.

47. Yuill, G. K., and Wray, C. P., 1990. "Overview of the ASHRAE TC 4.7 annotated guide to models and algorithms for energy calculation relating to HVAC equipment." *ASHRAE Transactions*, Vol.96, Part2.

48. Zaheer-uddin, M., 1986. "A two-component thermal model for a direct gain passive house with heated basement." *Building and Environment*, Vol.21.

49. Zaheer-uddin, M. and Goh, P. A. 1991. "Transient response of a closed-loop VAV system." *ASHRAE Transactions*, Vol.97, Part2.

50. Zaheer-uddin, M. and Zheng, G. R. 1994a. "A VAV system Model to Simulate Energy Management Control Functions: Off-normal Operation and Duty-cycling." *Energy Conversion & Management*, Vol.35, No.11, pp. 917-932.

51. Zaheer-uddin, M. and Zheng, G. R. 1994b. "A Dynamic Model of Multi-Zone VAV System for Control Analysis", *ASHRAE Transactions*, Vol. 100, Part 1, pp. 219-229.

52. Zaheer-uddin, M. and Zheng, G. R. 2001. "Multistage Optimal Operating Strategies for HVAC Systems." *ASHRAE Transactions*, Vol.107, Part2, pp.

53. Zhang, Z. L., 2001. "Temperature control strategies for radiant floor heating systems." Master Thesis, The Center for Building Studies, Concordia University, Montreal, Canada.

54. Zheng, G. R. 1997. "Dynamic modeling and global optimal operation of multizone variable air volume HVAC system." Ph.D Thesis, The Center for Building Studies, Concordia University, Montreal, Canada.